PLACE IN RETURN BOX to remove this checkout from your record. TO AVOID FINES return on or before date due.

DATE DUE	DATE DUE	DATE DUE

MSU Is An Affirmative Action/Equal Opportunity Institution

1

EX

SYNTHETIC DESIGN OF THE ELECTRONIC EXCITED STATES OF BINUCLEAR COMPLEXES

By

Joel Ivan Dulebohn

A DISSERTATION

Submitted to
Michigan State University
in partial fulfillment of the requirements
for the degree

DOCTOR OF PHILOSOPHY

Department of Chemistry

1990

ABSTRACT

SYNTHETIC DESIGN OF THE ELECTRONIC EXCITED STATES OF BINUCLEAR COMPLEXES

By

Joel Ivan Dulebohn

The usual excited state deactivation process for many binuclear metal complexes is photodegradation of the metal-metal bond. The metal-metal bond can be retained in the excited state by externally anchoring the metal together with a bidentate ligand. Alternatively, the metal-core may be preserved by internally anchoring the metals together with a multiple metal-metal bond. The synthetic chemistry aimed at designing excited states of externally and internally anchored binuclear complexes is described herein.

A novel homologous series of $Rh_2(0,0)$, $Rh_2(0,II)$, and $Rh_2(II,II)$ bis(difluorophosphino)methylamine complexes has been synthesized. These binuclear rhodium compounds are all prepared from the reaction of $[RhCl(PF_3)_2]_2$ with $CH_3N(PF_2)_2$. Under reducing conditions, $Rh_2[CH_3N(PF_2)_2]_3(PF_3)_2$, 1, is isolated. Conversely, reaction of $[RhCl(PF_3)_2]_2$ with $CH_3N(PF_2)_2$ in the presence of the oxidant $Cl_2IC_6H_5$ produces $Rh_2[CH_3N(PF_2)_2]_3Cl_4$, 3. In the absence of oxidants and

Rh₂(CH₃N(P separations of are consistent absorption is characteristic exhibit red, 1

sate parenta

The enshort-lived (short-lived (short-lived (short-lived (short-lived (short-lived))) and short-lived (short-lived). The short-lived (short-lived) acceptors. It bond cores of dimers [(C₄I Mo... Mo. se

consistent w

provides a n

reductants, the unsymmetrical mixed-valence $Rh_2[CH_3N(PF_2)_2]_3Cl_2(PF_3)$, 2, complex is obtained. The $Rh\cdots Rh$ separations of 2.841(2) Å, 2.785(1) Å, 2.707(1) Å in 1, 2, and 3, respectively, are consistent with the presence of a Rh-Rh single bond. Electronic absorption spectra are dominated by intense bands, which are characteristic of $\sigma \rightarrow d\sigma^*$ transitions. Crystalline solids of 1, 2, and 3 exhibit red, long-lived emissions, and is consistent with a $d\sigma^*$ excited state parentage of primarily triplet character.

The emission of quadruply bonded dimers is characteristically short-lived ($\tau \sim 100$ ns). An approach of increasing the excited state lifetime by energetically lowering a MLCT state below the $^1(\delta\delta^*)$ state is investigated. Th π -acid ligands 4,4'-dimethyl-2,2'-bypridine (dmbpy) and maleonitrile dithiolate mnt²⁻ can in principle give rise to lowest energy MLCT states. We have found, however, that the ligands are too strong π -acceptors. Introduction of these strong π -acid ligands to the quadruple bond cores of $Mo_2(O_2CCH_3)_4$ and $Mo_2Cl_4(CH_3CN)_4$ yields the $Mo_2(V,V)$ dimers $[(C_4H_9)N]_2[Mo_2(O)(S)(\mu-S)_2(mnt)_2]$ and $Mo_2O_4Cl_2(dmbpy)_2$. The $Mo\cdots Mo$ separation of 2.858(1) Å, and 2.562(2) Å, respectively, are consistent with the presence of a Mo-Mo single bond. This chemistry provides a new route to the preparation of $Mo_2(V,V)$ dimers.

Copyright by JOEL IVAN DULEBOHN 1990

To My Wife, and Son

Vicki and Matthew Dulebohn

unsel, a
University
cpportunti
to thank
Alexander

also would ray crystal I al:

finest rese in chemist distillation

who set no the question years of W To my wife

I m

to my son,
also send a

me throug!

ACKNOWLEDGEMENTS

I would like to thank Dr. Daniel G. Nocera for his inspiration, counsel, and friendship during my graduate study at Michigan State University. I have learned from Dr. Nocera to look at obstacles as opportunties, and to solve these obstalcles in different ways. I would like to thank Dr. Carl H. Brubaker for being my second reader, and Dr. Alexander Tulinsky and Dr. Eugene LeGoff for being on my committee. I also would like to thank Dr. Donald L. Ward for helping me solve my X-ray crystal structures.

I also want to thank the members of the group, who are one of the finest research groups in the country, for inspiring me into new heights in chemistry. A special thanks to Dr. Dunbar's group who has the best distillation stills in the midwest.

I must express my deepest gratitude to my family. To my parents who set no limitation on me, and instilled in me never to be afraid to ask the question WHY? To my sister and brother who had to put up with 18 years of WHY? and who only occasionally told me God wanted it that way. To my wife, Vicki who shares my dreams and helps me realize them, and to my son, Matthew who shows me much of the mystery of life. I want to also send a special thank-you to all my family and friends who supported me through these years with their friendship and their prayers.

LIST OF T

LIST OF F

I INTR

II. EXPE

A.

TABLE OF CONTENTS

				F	age
LIST	OF	TABLE	es		IX
LIST	OF	FIGUR	RES		KII
I	INT	RODU	CTION	T	1
II.	EXI	PERIME	ENTAI		3 0
	A.	Syntl	neses		31
		1.	Gene	ral Procedures	31
		2.	Synth	neses of Dirhodium Complexes	31
			a.	Starting Materials	31
			b.	$Rh_2[CH_3N(PF_2)_2]_3(PF_3)_2$, (1)	31
			c.	$Rh_2[CH_3N(PF_2)_2]_3Cl_2(PF_3), (2)$	32
			d.	$\label{eq:charge_preparation} \textbf{Preparation of Rh}_2[\textbf{CH}_3\textbf{N}(\textbf{PF}_2)_2]_3\textbf{Cl}_2(\textbf{PF}_3)$	
				from $Rh_3(\mu-Cl)_3[CH_3N(PF_2)_2]_3$	33
			e.	Rh ₂ [CH ₃ N(PF ₂) ₂] ₂ Cl ₄ , (3)	33
		3.	Synth	nesis of $Rh_3(\mu-Cl)_3[CH_3N(PF_2)_2]_3$, (4)	34
		4.	Synth	neses of Diiridium Complexes	35
			a.	Starting Materials	3 5
			b.	Attempt to Prepare	
				Ir ₂ [CH ₃ N(PF ₂) ₂] ₃ Cl ₂ (PF ₃), (5)	35
			c.	Attempt to Prepare $\rm Ir_2[CH_3N(PF_2)_2]_3Cl_4,$ (6) .	3 5
		5.	Synth	nesis of Dimolybdenum Complexes	3 6

				1	Page
			a.	Starting Materials	. 36
			b.	Mo ₂ Cl ₄ (dmbpy) ₂ , (7)	. 36
			c.	$[(C_4H_9)_4N)]_2$	
				${Mo_2(O)(S)(\mu-S)_2[S_2C_2(CN)_2]_2}, (8)$. 36
			d.	Mo ₂ Cl ₂ O ₂ (μ-O) ₂ (dmbpy) ₂ , (9)	37
			e.	Attempt to Prepare $Mo_2(dppm)_2(mnt)_2$, (10).	37
	B.	Instr	ument	ation and Methods	. 38
		1.	Absor	ption Spectroscopy	3 8
		2.	Infra	red Spectroscopy	3 8
		3.	Time-	-Resolved and Steady State Luminescence	3 9
		4.	Mass	Spectroscopy	39
		5.	Nucle	ar Magnetic Resonance Spectroscopy	39
	C.	Cryst	tal Str	ucture Determinations	40
		1.	Gene	ral Procedures	4 0
		2.	Meth	ods	40
			a.	$Rh_2[CH_3N(PF_2)_2]_3(PF_3)_2$, (1)	4 0
			b.	Rh ₂ [CH ₃ N(PF ₂) ₂] ₃ Cl ₂ (PF ₃), (2)	41
			c.	Rh ₂ [CH ₃ N(PF ₂) ₂] ₃ Cl ₄ , (3)	. 41
			d.	$\mathrm{Rh}_3(\mu\text{-Cl})_3[\mathrm{CH}_3\mathrm{N}(\mathrm{PF}_2)_2]_3$	
				in C2/c Space Group, (4)	42
			e.	$\mathrm{Rh}_{3}(\mu\text{-Cl})_{3}[\mathrm{CH}_{3}\mathrm{N}(\mathrm{PF}_{2})_{2}]_{3}$	
				in Pmna Space Group, (4')	4 3
			f.	$[(C_4H_9)_4N)]_2\{Mo_2(O)(S)(\mu\text{-}S)_2[S_2C_2(CN)_2]_2\}, \ (8)$. 43
			g.	$Mo_2Cl_2O_2(\mu-O)_2(dmbpy)_2$, (9)	44
III.	RHO	DIUM	FLUO	ROPHOSPHINE CHEMISTRY	46
	A.	Back	ground	l	4 6

				Page
	B.	Dirhodi	um Complexes	54
		1. R	esults	54
		a	. Synthesis of Dirhodium Complexes	54
		b	. Structural Interpretation	70
		C.	. Electronic Absorption and	
			Emission Spectra	91
		2. D	discussion	. 107
	C.	Trirhod	lium Complex	120
		1. R	esults and Discussion	120
		a	. Synthesis of $Rh_3(\mu-Cl)_3[CH_3N(PF_2)_2]_3$	1120
		b	. Structural Interpretation	. 120
		C	. Electronic Absorption and	
			Emission Spectra	. 129
IV.	PREF	PARATIC	ON OF DIMOLYBDENUM(V,V) DIMERS	133
	A.	Backgro	ound	133
	B.	Results	and Discussion	134
		1. R	eaction of Mnt ^{2–} with Quadruply Bonded Metal	
		C	omplexes	. 134
		2. R	eaction of Bipyridine with Quadruply Bonded	
		M	Ietal Complexes	. 156
APP	ENDIX	Nuclea	r Magnetic Resonance Spectra	173
REF	EREN	CES		. 193

1 Crystal Data Rh₂[CH₃N₁P

Rh₂[CH₃N

2 Atomic Posit

Parameters !

3 Atomic Posi

Parameters

Atomic Po

Paramete

Selected Rh₂[CH₃

Selected Bo

Rh2(CH3N)

LIST OF TABLES

	I	age
1	Crystal Data for $Rh_2[CH_3N(PF_2)_2]_3(PF_3)_2$ (1),	
	$Rh_{2}[CH_{3}N(PF_{2})_{2}]_{3}Cl_{2}(PF_{3})$ (2), and	
	Rh ₂ [CH ₃ N(PF ₂) ₂] ₃ Cl ₄ (3)	71
2	Atomic Positional and Isotropic Displacement (${\rm \AA}^2$)	
	Parameters for $Rh_2[CH_3N(PF_2)_2]_3(PF_3)_2$ (1)	. 72
3	Atomic Positional and Isotropic Displacement (${ m \AA}^2$)	
	Parameters for $Rh_2[CH_3N(PF_2)_2]_3Cl_2(PF_3)$ (2)	. 73
4	Atomic Positional and Isotropic Displacement (${ m \AA}^2$)	
	Parameters for $Rh_2[CH_3N(PF_2)_2]_3Cl_4$ (3)	. 74
5	Selected Bond Distances (Å) and Bond Angles (deg) for	
	Rh ₂ [CH ₃ N(PF ₂) ₂] ₃ (PF ₃) ₂ (1)	. 84
6	Selected Bond Distances (Å) and Bond Angles (deg) for	
	Rh ₂ [CH ₃ N(PF ₂) ₂] ₃ Cl ₂ (PF ₃) (2)	85,86

- Selected Bor Rh₂[CH₃N
- 8 Emission Sp
- 9 Calculated d
- D Crystal Data
- Atomic Posi:

 Parameters:

 Space Grou
- Atomic Pos Parameter Pnma Sy
 - Selected for Rh₃[
- Selected I
- Crystal Data

		Page
7	Selected Bond Distances (Å) and Bond Angles (deg) for	
	Rh ₂ [CH ₃ N(PF ₂) ₂] ₃ Cl ₄	87
8	Emission Spectral Data for Crystalline 1, 2, and 3 at 77 K	. 99
9	Calculated decay rate constants and energy gaps for	
	1, 2, and 3	. 106
10	Crystal Data for $Rh_3(\mu-Cl)_3[CH_3N(PF_2)_2]_3$	121
11	Atomic Positional and Isotropic Displacement (\mathring{A}^2)	
	Parameters for $Rh_3[CH_3N(PF_2)_2]_3Cl_3$ (4) in the C2/c	
	Space Group	122
12	Atomic Positional and Isotropic Displacement (\mathring{A}^2)	
	Parameters for $Rh_3(\mu-Cl)_3[CH_3N(PF_2)_2]_3$ (4') in the	
	Pnma Space Group	123
13	Selected Bond Distances (Å) and Bond Angles (deg)	
	for $Rh_3[CH_3N(PF_2)_2]_3(Cl)_3$ (4) in the C2/c space group	. 125
14	Selected Bond Distances (Å) and Bond Angles (deg)	
	for $Rh_3[CH_3N(PF_2)_2]_3(Cl)_3$ (4') in the Pnma space group	126
15	Crystal Data for $[Mo_2(O)(S)(\mu-S)_2(mnt)_2]^{2-}$ and	
	$Mo_2O_4Cl_4(dmbpy)_2$	144

16 Atomic

Param

II Atomi

Paran

B Selec

 $[\mathrm{Mo}_2$

19 Selec

[N(c)]

x Rele

(X,

Z Rel

(X,

2 Ato

 P_{a_1}

 $S_{\epsilon_{i}}$

23

 M_0

	Pa	age
16	Atomic Positional and Isotropic Displacement (\mathring{A}^2)	
	Parameters for $(Mo_2(O)(S)(\mu-S)_2(mnt)_2)^{2-}$	5
17	Atomic Positional and Isotropic Displacement ($Å^2$)	
	Parameters for the Tetrabutylammonium Ions 146,	147
18	Selected Bond Distances (Å) and Bond Angles (deg) for	
	$[Mo_2(O)S(\mu-S)_2(mnt)_2]^{2-}$	0
19	Selected Bond Distances (Å) and Bond Angles (deg) for	
	[N(C ₄ H ₉) ₄] ⁺ Ions	,152
20	Relevant angles for complexes with $Mo_2(\mu-S)_2XY$	
	(X, Y = O, S) cores	4
21	Relevant angles for complexes with $Mo_2(\mu-S)_2XY$	
	(X, Y = O, S) cores	5
22	Atomic Positional and Isotropic Displacement (\mathring{A}^2)	
	Parameters for $Mo_2(O)_2Cl_2(\mu-O)_2(dmbpy)_2$	4
23	Selected Bond Distances (Å) and bond Angles (deg) for	
	$Mo_2O_2Cl_2(\mu-O)_2(dmbpy)_2$	7

- Schematic r processes. k constants fo energy tran
- The structur
- The structur
- ⁴ Relative en∈
 - Relative ene:
 M₂ and in D₂
 M₂L₈ comp!
 - Production of Rh₂(bridge

LIST OF FIGURES

	Page
1	Schematic representation of excited state deactivation
	processes. k_{nr} , k_r , k_{sub} , k_{en} and k_{et} are the rate
	constants for nonradiative and radiative decay, substitution,
	energy transfer and electron transfer, respectively 3
2	The structure of triad that mimics the photosynthetic
	reaction center 6
3	The structure of $[Ru(me(bpy)-3DQ^{2+})(me(bpy)-PTZ)_2]^{4+}$
4	Relative energy diagram for $Mn_2(CO)_{10}$
5	Relative energies of the d-derived molecular orbitals in $D_{\infty h}$
	M_2 and in D_{4h} M_2L_8 complex. The ground state of the d^4 - d^4
	M_2L_8 complex is ${}^1A_{1g}(\sigma^2\pi^4\delta^2)$
6	Production of hydrogen from the irradiation of
	$[Rh_2(bridge)_4]^{2+}$ in acidic solution

Photo with

are i

8 Photacet

9 Illusin is pho

L Red

11 FA

12 FA

13 FA

Ios

ind

14

15 F.

F.A Pre

		Page
7	Photoinduced bimolecular reaction of $[Ir(COD)(\mu-pz)]_2$	
	with 1,2-dichloroethane and methylene chloride. Pyrazines	
	are indicated by bowed lines strapping the metal centers	. 22
8	Photoinduced catalytic conversion of isopropyl alcohol into	
	acetone and hydrogen by using Pt ₂ (pop) ^{4—} as a photocatalyst	. 25
9	Illustration of the potential energy diagram for reagent	
	in its photoexcited state and its photoproduct with the	
	photoproduct having an photoexcited state	. 28
10	Redox chemistry of Co ₂ [CH ₃ N(PF ₂) ₂] ₃ (CO) ₂	. 50
11	FAB mass spectrum of $Rh_2[CH_3N(PF_2)_2]_3(PF_3)_2$, 1	57
12	FAB mass spectrum of $Rh_2[CH_3N(PF_2)_2]_3(PF_3)Cl_2$, 2	
	prepared by method i of Section II.A.2.c	. 59
13	FAB mass spectrum of $Rh_2[CH_3N(PF_2)_2]_3Cl_4$, 3	61
14	Iostope peak-intensity pattern for ions containing the	
	indicated number of chlorine atoms (from ref. 123)	. 83
15	FAB mass spectrum of $Rh_2[CH_3N(PF_2)_2]_3(PF_3)Cl_2$, 2,	
	prepared by method ii of Section II.A.2.c	66

- FAB mass s
- Rh₂[CH₃N:] ellipsoids. I Selected bor

S ORTEP dra

- An ORTEP the number at the 50% 1 of clarity. T
- An ORTEP value of numbering sumbering sumberin
 - A skeletal vi (b) 2, and (a)

⁷ lists select

Structural fr nearly along

		Page
16	FAB mass spectrum of $Rh_2[CH_3N(PF_2)_2]_3(PF_3)Cl_2$, 2,	
	prepared by method ii of Section II.A.2.c	. 68
17	ORTEP drawing and numbering scheme of	
	$Rh_2[CH_3N(PF_2)_2]_3(PF_3)_2$,1 with 30% probability thermal	
	ellipsoids. For clarity hydrogen atoms are not shown.	
	Selected bond distances and angles are listed in Table 5	. 76
18	An ORTEP view of Rh ₂ [CH ₃ N(PF ₂) ₂] ₃ (PF ₃)Cl ₂ , 2, showing	
	the numbering scheme. Thermal parameters are shown	
	at the 50% level. Hydrogen atoms are omitted for the sake	
	of clarity. Table 6 lists selected bond distances and angles	7 8
19	An ORTEP view of Rh ₂ [CH ₃ N(PF ₂) ₂] ₃ Cl ₄ , 3, showing the	
	numbering scheme. Thermal ellipsoids are at the 50%	
	probability level; hydrogen atoms are not shown. Table	
	7 lists selected bond distances and angles	80
20	A skeletal view of the inner coordination spheres of (a) 1,	
	(b) 2, and (c) 3	. 82
21	Structural framework of (a) 1, (b) 2, and (c) 3 as viewed	
	nearly along the Rh-Rh axis. Axial ligands are omitted	. 90

2 Elect

spect

Elec CH₂

spec

24 Election C

spec

E Fit con

36 Fit

 $\infty_{
m D}$

Fit

27

28

con

 P_{r_0}

sta

 m_a

Þer

e]e

		Page
22	Electronic absorption spectrum () of 1 dissolved in	
	CH ₂ Cl ₂ at room temperature, and corrected emission	
	spectrum () of crystalline 1 at 77 K	. 93
23	Electronic absorption spectrum () of 2 dissolved in	
	CH ₂ Cl ₂ at room temperature, and corrected emission	
	spectrum () of crystalline 2 at 77 K	95
24	Electronic absorption spectrum () of 3 dissolved	
	in CH ₂ Cl ₂ at room temperature, and corrected emission	
	spectrum () of crystalline 3 at 77 K	97
25	Fit of the variation of the observed emission decay rate	
	constant to eq 16 of 1 in the 10 - 180 K temperature range	101
26	Fit of the variation of the observed emission decay rate	
	constant to eq 16 of 2 in the 10 - 200 K temperature range	103
27	Fit of the variation of the observed emission decay rate	
	constant to eq 16 of 3 in the 10 - 290 K temperature range	105
28	Proposed energy diagram of the lowest energy excited	
	states of the $Pt_2(III,III)L_2$ phosphates. The state	
	manifold is derived from the spin-orbit coupling	
	perturbation of the ³ E _u state arising from the one-	
	electron $3(d\pi^* \rightarrow d\sigma^*)$ promotion	. 111
		Page

29 Simp two C

to be

mini

the

30 Qua

dδ-s

sha

spli

isol syn

Rh

of t

are

 Q_{u}

31

ort

Rh

Th

rzs

Rh

int

an

29	Simple molecular orbital diagram for the interaction of	
	two C_{3v} Rh(0)P ₄ fragments. The $d\pi$ - and $d\delta$ -symmetry	
	orbitals are filled and indicated by the shaded box. To	
	minimize level congestion, the σ - σ * splitting is shown	
	to be small and its manifold is isolated from that of	
	the $d\pi$ and $d\delta$ orbitals	115

Page

2 A pe

Rh₃

ellip

hyd

3 Elec

CH

spe

34 Ele

dis

35 Mi

36 Mi

El

3,

[M

≆ Oi

th

sh

in

32	A perspective ORTEP view and labeling scheme of	
	$Rh_3(\mu-Cl)_3[CH_3N(PF_2)_2]_3$, 4, with the thermal	
	ellipsoids at the 50% probability level. For clarity	
	hydrogen atoms are not shown	128
33	Electronic absorption spectrum () of 4 dissolved in	
	CH2Cl2 at room temperature, and corrected emission	
	spectrum () of crystalline 4 at 77 K,	131
34	Electronic absorption spectrum of $[(C_4H_9)_4]_2Mo(mnt)_3$	
	dissolved in CH ₂ Cl ₂	136
35	Mid IR spectrum of [(C ₄ H ₉) ₄] ₂ Mo(mnt) ₃	138
36	Mid IR spectrum of $[(C_4H_9)N]_2[Mo_2(O)(S)(\mu-S)_2(mnt)_2]$	141
37	Electronic absorption spectrum of $[(C_4H_9)N]_2$	
•	[$Mo_2(O)(S)(\mu-S)_2(mnt)_2$] dissolved in CH_2Cl_2	143
3 8	ORTEP drawing and numbering scheme of	
	$[Mo_2(O)(S)(\mu-S)_2(mnt)_2]^{2-}$ with 50% probability	
	thermal ellipsoids. For clarity $(C_4H_9)_4N^+$ ions are not	
	shown. Selected bond distance and angles are listed	
	in Table 18	149

- Mid IR spe
 the reactio:
- 40 Far IR spec
- 4 Electronic a dissolved i
- ORTEP dra Mo₂O₂Cl₂() ellipsoids. shown. Se
 - listed in T
- Mid IR spe
- Electronic Mo₂O₂Cl₂0
- 5 31P(1H) N?
 NMR spec
- % 31P(1H) N. prepared)

39	Mid IR spectrum of the green compound isolated from	
	the reaction of Mo ₂ (Cl) ₄ (dppm) ₂ with Na ₂ (mnt)	158
40	Far IR spectrum of the green compound isolated from	
	the reaction of Mo ₂ (Cl) ₄ (dppm) ₂ with Na ₂ (mnt)	160
41	Electronic absorption spectrum of $Mo_2(dppm)_2(mnt)_2$	
	dissolved in CH ₂ Cl ₂	162
42	ORTEP drawing and numbering scheme of	
	$Mo_2O_2Cl_2(\mu-O)_2(dmbpy)_2$ with 50% probability	
	ellipsoids. For clarity hydrogen atoms are not	
	shown. Selected bonddistances and angles are	
	listed in Table 23	166
4 3	Mid IR spectrum of $Mo_2O_2Cl_2(\mu-O)_2(dmbpy)_2$	169
44	Electronic absorption spectrum of	
	Mo ₂ O ₂ Cl ₂ (μ-O) ₂ (dmbpy) ₂ dissolved in CH ₃ CN	171
4 5	$^{31}P\{^{1}H\}$ NMR spectrum of $Rh_{2}[CH_{3}N(PF_{2})_{2}]_{3}(PF_{3})_{2}$, 1.	
	NMR spectrum was not reference to an external standard	174
46	$^{31}\mathrm{P}^{1}\mathrm{H}$ NMR spectrum of $\mathrm{Rh_{2}[CH_{3}N(PF_{2})_{2}]_{3}(PF_{3})Cl_{2}}$, 2	
	prepared by method i of Section II.A.2.c	176

4 31P(1H) N

& 19F NMR s

9 19F NMR s; prepared b

19 NMR s

³¹ ¹⁹F(³¹P) XX prepared b

2 19F(31P) N3

prepared b

3 19_F(31_{P) N}

NMR spec

34 31P(1H) N

47	$^{31}P\{^{1}H\}$ NMR spectrum of $Rh_{2}[CH_{3}N(PF_{2})_{2}]_{3}Cl_{4}$, 3	178
48	$^{19}\mathrm{F}$ NMR spectrum of $\mathrm{Rh}_2[\mathrm{CH}_3\mathrm{N}(\mathrm{PF}_2)_2]_3(\mathrm{PF}_3)_2,1$	180
49	$^{19}\mathrm{F}$ NMR spectrum of $\mathrm{Rh_2[CH_3N(PF_2)_2]_3(PF_3)Cl_2}$, 2	
	prepared by method i of Section II.A.2.c	182
50	¹⁹ F NMR spectrum of Rh ₂ [CH ₃ N(PF ₂) ₂] ₃ Cl ₄ , 3	184
51	$^{19}\mathrm{F}(^{31}\mathrm{P})$ NMR spectrum of $\mathrm{Rh_2[CH_3N(PF_2)_2]_3(PF_3)Cl_2}$, 2	
	prepared by method i of Section II.A.2.c	186
52	$^{19}\mathrm{F}\{^{31}\mathrm{P}\}$ NMR spectrum of $\mathrm{Rh}_2[\mathrm{CH}_3\mathrm{N}(\mathrm{PF}_2)_2]_3(\mathrm{PF}_3)\mathrm{Cl}_2$, 2	
	prepared by method i of Section II.A.2.c	188
53	19 F(31 P) NMR spectrum of Rh ₂ [CH ₃ N(PF ₂) ₂] ₃ Cl ₄ , 3	
	NMR spectrum was not reference to an external standard	190
54	³¹ P(1H) NMR spectrum of Rh ₂ (μ-Cl) ₂ [CH ₂ N(PF ₂) ₂] ₃ , 1	192

CHAPTER I

Introduction

The absolute first act of plants act of plants and deactiful and deactif

electron tra

such as end such as end molecule ac chemistry of excited star reached with to undergo that catalyte electron tremphasis hexcited stat

One attransfer real The photoson (RCs) contacted center consi

transfer of r

The absorption of a visible or ultraviolet photon by a molecule is the first act of photochemistry. In the excited state, the molecule can undergo many deactivation processes. As shown in Figure 1, these include (1) emission of a lower energy photon (luminescence), (2) emission of heat, (3) photosubstitution, (4) energy transfer, and (5) electron transfer. Cases 1-3 are unimolecular transformations, with radiationless decay (cases 2 and 3) occurring at the expense of luminescence. Typically, long-lived luminescence is desirous because it is a signature that the excited molecule has sufficient lifetime to participate in energy transfer and/or electron transfer bimolecular transformations.

The utility of electronic excited states in many important processes such as energy conversion chemistry, molecular electronics, and small molecule activation chemistry are predicated on the oxidation-reduction chemistry of the electronically excited molecule. 1-10 In order for the excited state to be useful in an electron transfer reaction it must be reached with high efficiency following light absorption, last long enough to undergo electron transfer reaction, and exhibit appreciable stability so that catalytic cycles can be designed. There are many examples of one electron transfer reactions over the past two decades. Yet recent emphasis has turned to the multielectron chemistry of transition metal excited states because the most useful system will necessarily rely on the transfer of more than one electron. 12-15

One approach to a multielectron system is coupling one electron transfer reactions. The best example of this approach is found in nature. The photosynthetic eubacteria contains photochemical reaction centers (RCs) containing one or more chlorophyll molecules. ¹⁶ Each reaction center consists of a primary electron donor P (bacteriochlorophyll), an

Schematic representation of excited state deactivation processes. k_{nr} , k_{r} , k_{sub} , k_{en} and k_{et} are the rate constants for nonradiative and radiative decay, substitution, energy transfer and electron transfer, respectively.

 $ML_x + hv$

Eiectro

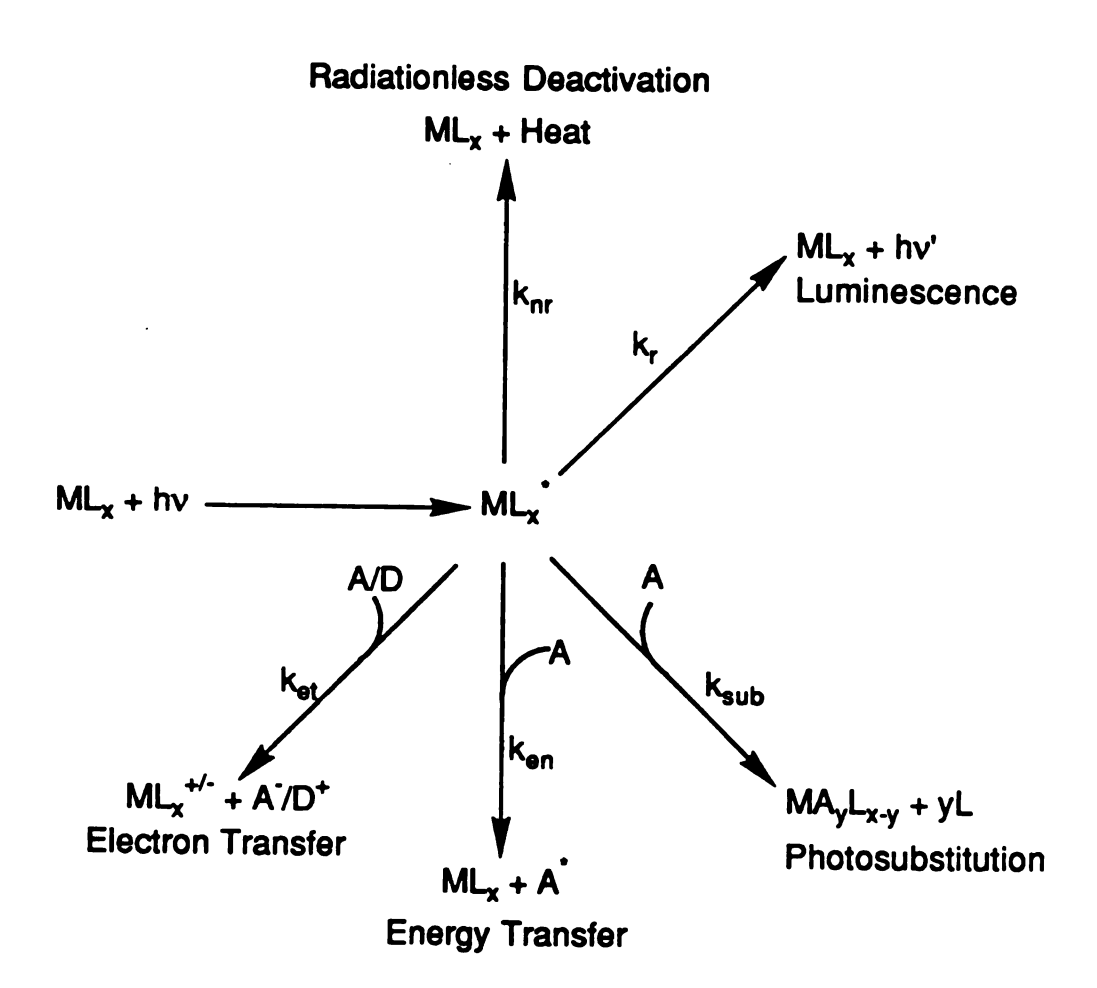


Figure 1

iI

an

Sc

in

DI

W)

P-

se;

SV.

ex

ele

3.

₫e

Pos

CO

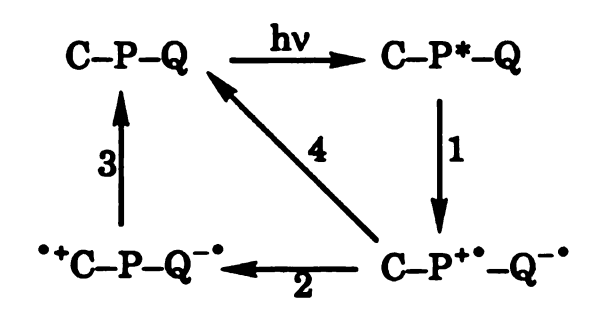
initial electron acceptor A (bacteriochlorophyll or bacteriopheophytin), and one or more secondary acceptors X (Fe-S center, quinones). Sometime a secondary electron donor D (Cyt c) is tightly bound to the RC.

The 'primary' chemical reaction sequence of photosynthesis occurs in the RC and is summarized by eq 1.

$$DPAX + hv \longrightarrow DP^+AX \longrightarrow DP^+A^-X \longrightarrow DP^+IX^- \longrightarrow D^+PAX^-$$
 (1)

When the RC is photoexcited, the primary donor P is excited to P*, which in turn transfers an electron to A. To prevent the back electron reaction to P*, an electron is transferred from A to secondary acceptor X and charge separation is stabilized.

Photochemically induced separation has been accomplished in synthetic molecules that contain a light absorber or chromophore, and electron donors and acceptors held in appropriate spatial array.¹⁷ Two examples based on the photosynthetic RC are illustrated in Figures 2 and 3. The former is based on the $\pi \to \pi^*$ chromophore of a porphyrin derivative.¹⁸ The molecular triad consists of a tetraarylporphyrin (P) covalently linked to both a carotenoid (C) and a quinone (Q). The postulated electron transfer reactions are shown in Scheme 1.¹⁹



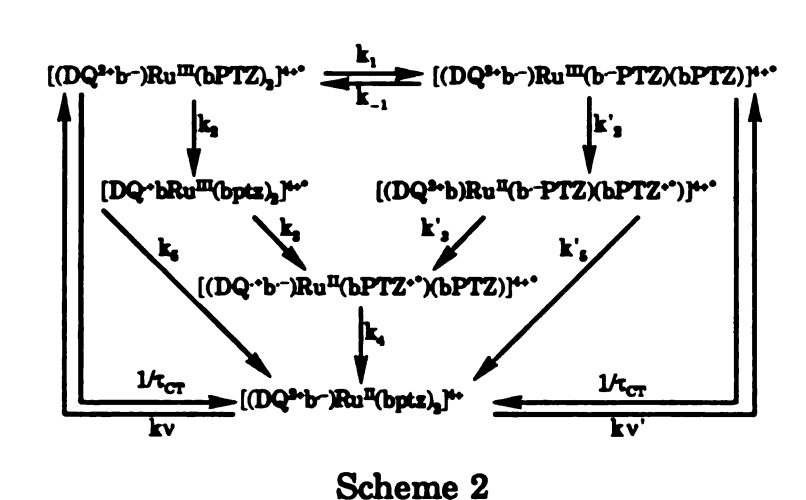
Scheme 1

The structure of triad that mimics the photosynthetic reaction center.

The structure of $[Ru(me(bpy)-3DQ^{2+})(me(bpy)-PTZ)_2]^{4+}$.

The excited P* undergoes electron transfer to yield $C-P^+-Q^{-\bullet}$ and subsequent electron transfer to the tetraarylporphyrin from the carotenoid yields a long-lived charge separated state $^{+\bullet}C-P-Q^{-\bullet}$ on the microsecond time scale. The charge separated state recombines to form the starting compound over 2 μ s. The yield of the charge separated species was low due to the recombination reaction indicated by step 4.

Figure 3 shows charge-separation based on MLCT excitation of [Ru(me(bpy)-3DQ²⁺)(me(bpy)-PTZ)₂]⁴⁺.²⁰ Two pathways are possible depending on the initial quenching act of the MLCT, and are illustrated in Scheme 2.



Irregardless of the initial pathway, the same charge-separated species $[(DQ^{\bullet+}b)Ru^{II}(bPTZ^{+*}) (bPTZ)]^{4+*}$ is ultimately produced. The charge separated species storage time is not very long (165 ns) due to the recombination reactions k_5 and k'_5 .

The successful realization of overall multielectron chemistry necessary relies on the integration of the charge separated states with multielectron catalytic sites. This has not yet been achieved for

un for

ha

R

m

of

unimolecular charge transfer, but limited success has been recognized for some bimolecular inorganic systems.²¹ The most prominent schemes have been predicated on $Ru(bpy)_3^{2+}.^{22,23}$ The electronically excited $Ru(bpy)_3^{2+}$ ion, $^*Ru(bpy)_3^{2+}$, can readily transfer one electron to methylviologen. The reduced viologen reacts with protons in the presence of colloidal platinum to produce hydrogen as described by the eqs 2-4.

$$Ru(bpy)_3^{2+} + hv \longrightarrow Ru(bpy)_3^{2+*}$$
 (2)

$$\text{Ru(bpy)}_3^{2+*} + \text{MV}^{2+} \longrightarrow \text{Ru(bpy)}_3^{3+} + \text{MV}^+$$
 (3)

$$MV^{+} + H^{+} + Pt \longrightarrow MV^{2+} + 1/2H_{2}$$
 (4)

The photogenerated Ru(bpy)₃³⁺ ion is a strong oxidant. It has been shown that Ru(bpy)₃³⁺ can react with water or hydroxide in the presence of a RuO₂ catalyst under suitable conditions to produce oxygen. Nevertheless, the overall efficiency of the Ru(bpy)₃²⁺ cycle is low, due to the fast back reactions between Ru(bpy)₃³⁺ and MV⁺. One approach to avoid these back reactions is to develop charge separated species of the type discussed in the context of Figures 2 and 3. Other approaches have appeared in recent years based on semiconductors,^{24,25} membranes,^{26,27} vesicles,^{26,28} and polymers.^{29,30}

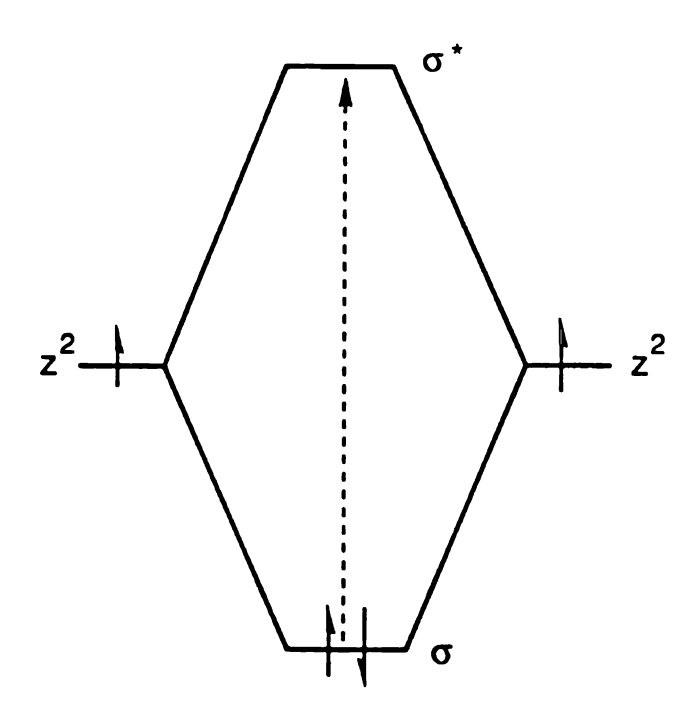
Our group has been interested in addressing the issue of multielectron photochemistry from a different conceptual basis. Charge separation is circumvented if the multielectron chemistry of the excited state occurs in single reaction sequence. This research has focussed on polynuclear metal cores where the redox activity of individual metal centers may be coupled in a discrete excited state molecule.

To date most effort has been directed towards coupling the redox activity of metal centers in a bimetallic core. A major obstacle in this chemistry is the photodegeneration of the bimetallic core along a dissociative pathway. An example of a predominate photocleavage pathway is that of $\mathrm{Mn_2(CO)_{10}}$ (Figure 4), which has a single bond between the metal atoms. ³¹⁻³⁴ Irradiation of the lowest-energy transition in this dimer promotes an electron from the σ bonding orbital to the antibonding metal-metal σ^* orbital. This excitation reduces the metal-metal bond order to zero yielding the ${}^{\bullet}\mathrm{Mn(CO)_{5}}$ radical fragment. Because the dissociative pathway for σ^* deactivation is very efficient, the electronically excited lifetimes for single metal bonded dimers are short. Luminescence from M-M complexes is extremely rare, and chemistry from the M-M complexes is typically free-radical based.

The photodegradation of M-M complexes can be circumvented by anchoring the two metal atoms together with the coordination of bidentate ligands across the metal-metal bond. This is dramatically illustrated by a comparison of $\text{Re}_2(\text{CO})_8\text{L}_2$ (L = CO, $\text{P(C}_6\text{H}_5)_3$) and $\text{Re}_2(\text{CO})_8(\stackrel{\frown}{P})$ ($\stackrel{\frown}{P}$ = bis(dimethylphosphino)methane) (dmpm) and bis(diphenylphosphino)methane) (dppm)) photochemistry. The $\text{Re}_2(\text{CO})_8\text{L}_2$ dimers undergo rapid and efficient metal-metal bond cleavage to produced ${}^{\bullet}\text{Re}(\text{CO})_4\text{L}$ radicals. Coordinating a $\stackrel{\frown}{P}$ bidentate ligand across the metal-metal bond circumvents photodegradation of the dimer, and a highly emissive long-lived $\sigma\sigma^*$ excited state is observed at low temperature. This emission is attributed to the bidentate ligand maintaining the metal atoms in a rigid and proximate geometry in the $\sigma\sigma^*$ excited state. There are other examples of d^7-d^7 species that also have σ^* luminescence. These include the $\text{Pt}_2(\text{III,III})$ pyrophosphate $\text{Pt}_2(\text{pop})_4\text{X}_2^{4-}$ (pop =

Relative energy diagram for $\mathrm{Mn_2(CO)_{10}}$.

$$Mn_2(CO)_{10} \xrightarrow{hv} 2 (CO)_5Mn$$



$$dπ$$
 $dδ$

$$(CO)_5Mn \cdot Mn_2(CO)_{10}$$

- Mn(CO)₅

Figure 4

 $(H_2OP)_2O$, X = halides),⁴¹ and the $Pt_2(III,III)$ phosphate $Pt_2(HPO_4)_4L^{2n-1}$ [L = H_2O , n= 2; L = Cl, Br, n = 4) complexes.⁴² The retention of the metalmetal core in the excited state is a necessary condition of $d\sigma^*$ luminescence in these complexes.

Another approach to prevent photofragmentation is to anchor the metal atoms with multiple bonds. In this manner, even if one net bond is annihilated, the remaining metal-metal interaction holds the binuclear core intact. Numerous quadruply bonded metal-metal complexes have been prepared. These complexes are comprised primarily of rhenium, chromium, molybdenum, and tungsten metal atoms coordinated by a variety of ligands.

Numerous theoretical 43-50 and experimental 51-67 investigations have led to the elucidation of L₄MML₄ electronic structure. A general molecular orbital diagram of the quadruply bonded metal dimer is shown in Figure 5.52 The L4MML4 quadruple bonded dimer is derived from an M_2 core ($D_{\infty h}$ symmetry) in which the z axis of a right handed cartesian coordinate system lies along the metal-metal bond. The linear combination of d_{z2} , (d_{xz}, d_{yz}) , and (d_{x2-y2}, d_{xy}) atomic orbitals on each metal forms the bonding and antibonding σ , π , and δ molecular orbitals, respectively. In the $D_{\infty h}$ point group the π and δ molecular orbitals are each doubly degenerate. The symmetry of the M-M core is lowered from $D_{\infty h}$ to D_{4h} when the eight ligand of L_4MML_4 is placed in equal position of the M-M core, and therefore, causes the splitting of the δ orbital degeneracy. By definition of the coordinate system in Figure 5, the ligands lie along the x and y axis, and the four metal-ligand bonds are generated by the overlap of the ligands orbitals with the metal d_x2_{-v}2 orbitals and the s, p_x, p_y orbitals (which are not shown in Figure 5). The

Relative energies of the d-derived molecular orbitals in $D_{\infty h}~M_2$ and in D_{4h} $M_{\,2}L_{\,8}$ complex. The ground state of the d^4 - d^4 $M_{\,2}L_{\,8}$ complex is $^1\!A_{1g}(\sigma^2\pi^4\delta^2).$

5

:

X

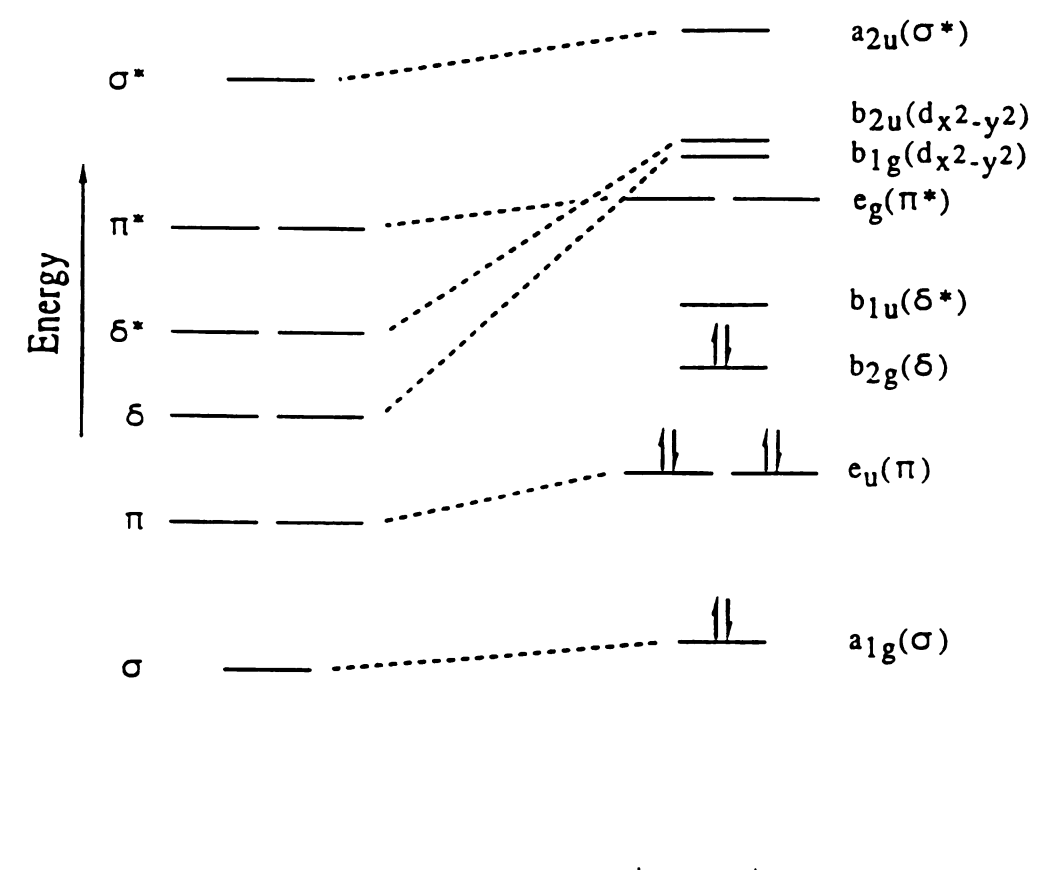


Figure 5

and thus cor

Re metal bo

dimetallic

Mult

there is n

properties

intensivel

respective

complexe

Promotion

the bondi

the exciv

Wexcited

 $Rh_2(br)$

 $\mathcal{M} = \mathcal{U}$

mpb (

2hq (2

One o

 $\mathbb{R}h_{2}($

shown Proto

yield

[Rh phot

dich

ep⁰²

and thus compete with the expected rapid recombination to reform the Re-Re metal bond.

Multielectron diradical chemistry has been also observed for dimetallic centers strapped by a bidentate ligand across a core in which there is no metal-metal bond. The spectroscopic and photochemical properties of $d^8-d^8 = 4^{1.72-78}$ and $d^{10}-d^{10} = 7^{9.80}$ complexes have been studied intensively. Simple molecular orbital arguments suggest that the respective ground state and excited state configuration of the binuclear complexes are represented as $(d_{z2})^2(d_{z2})^2$ and $(d_{z2})^2(d_{z2})^1(p_z)^1$. Promotion of an electron from the metal-metal antibonding framework to the bonding orbital results in an increase of the metal-metal interaction in the excited state.

With the structural integrity of the dimetal core preserved in d^8-d^8 excited states, a rich photooxidation chemistry of $Pt_2(pop)_4^{4-}$, 8^{1-85} [Rh₂(bridge)₄]²⁺ (bridge = 1,3-diisocyanopropane)^{86,87} and [M(COD)(μ -L)]₂ (M = Rh, Ir; COD = 1,5 cyclooctadiene; μ -L = hp (2-hydroxypyridinate), mhp (6-methyl-2-hydroxypyridinate), chp (6-chloro-2-hydroxypyridinate), 2hq (2-hydroxyquinolate), pz (pyrazolate)) has been observed. 11c,12a,25,88,89 One of the earlier examples is the reduction of H_2 by the irradiation of [Rh₂(bridge)₄]²⁺ in aqueous 12 M HCl solution. 86,87 The reaction steps are shown in Figure 6. In the reaction scheme [Rh₂(bridge)₄]²⁺ in 12 M HCl is protonated to [(Cl⁻)Rh^I---Rh^I(H⁺)]²⁺. Subsequent irradiation at λ > 530 nm yields H_2 and the two electron oxidative-addition product [Rh₂(bridge)₄Cl₂]²⁺. Another example of oxidative-addition photochemistry is the visible irradiation of [Ir(COD)(μ -pz)]₂ with 1,2-dichloroethane (DCE) or methylene chloride. The reaction scheme is shown in Figure 7. Irradiation (λ = 577 nm) of [Ir(COD)(μ -pz)]₂ with DCE

leads to the of [lr(COI electron o

Pt₂(pop)₄
into aceta
The elect
isopropa

the produndergo

dihydrid oxygen t

T

dimers

chemisi oxidati

demon

Mo₂(H triple t

The or

 $M_{0_2(I)}$

two ele

leads to the formation of ethylene and $[Ir(COD)(\mu-pz)Cl]_2$. The irradiation of $[Ir(COD)(\mu-pz)]_2$ in methylene chloride leads to the formation of a two-electron oxidative-addition product $[Ir(COD)(\mu-pz)]_2(ClCH_2)(Cl)$.

Other examples of bimetallic free radical chemistry include $Pt_2(pop)_4^{4-}$. This dimer can photocatalytically convert isopropyl alcohol into acetone and hydrogen by the reaction scheme shown in Figure 8.⁸⁵ The electronically excited $Pt_2(pop)_4^{4-*}$ abstracts the methine hydrogen of isopropanol to give $Pt_2(pop)_4^{4-*}$ and $(CH_3)_2COH^*$ radical. Subsequent reaction of this radical with another equivalent of $Pt_2(pop)_4^{4-}$ results in the production of $Pt_2(pop)_4^{4-*}$. The $Pt_2(II,III)$ mixed-valent $Pt_2(pop)_4^{4-*}$ undergoes disproportionation to give $Pt_2(pop)_4^{4-*}$ and $Pt_2(pop)_4^{4-*}$. The dihydride reacts with HCl to generate hydrogen and reacts rapidly with oxygen to give $Pt_2(pop)_4^{4-*}$.

The multielectron free radical chemistry of d^7 - d^7 , d^8 - d^8 , and d^{10} - d^{10} dimers is not paralleled by the quadruple bond dimers. In this case, the chemistry is dominated by electron transfer and discrete two electron oxidation-addition transformations. In our laboratory we have demonstrated the oxidation photochemistry of the quadruple bonded $Mo_2(HPO_4)_4^{4-}$ dimer in an acid medium to produce hydrogen and the triple bonded $Mo_2(HPO_4)_4^{4-}$. 14a

$$Mo_2(HPO_4)_4^{4-} + 2H^+ \xrightarrow{hv} Mo_2(HPO_4)_4^{2-} + H_2$$
 (5)

The overall reaction is composed of sequential one electron transfer to result in a formal oxidation change metal core from Mo₂(II,II) to Mo₂(III,III). Alternatively nonaqueous soluble phosphates promote the two electron reduction of halocarbons. ^{14b}

Production of hydrogen from the irradiation of $[Rh_2(bridge)_4]^{2+}$ in acidic solution.

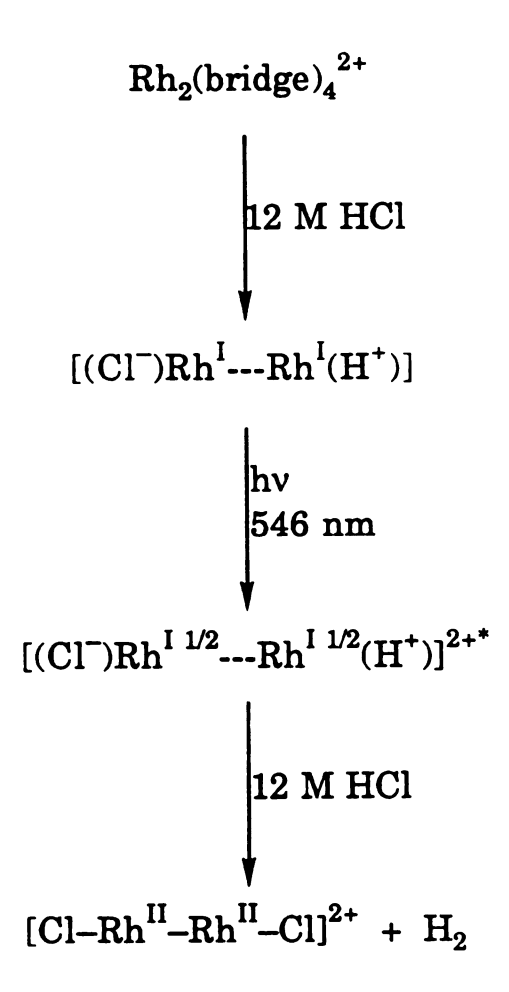


Figure 6

Photoinduced bimolecular reaction of $[Ir(COD)(\mu-pz)]_2$ with 1,2-dichloroethane and methylene chloride. Pyrazines are indicated by the bowed lines strapping the metal centers.

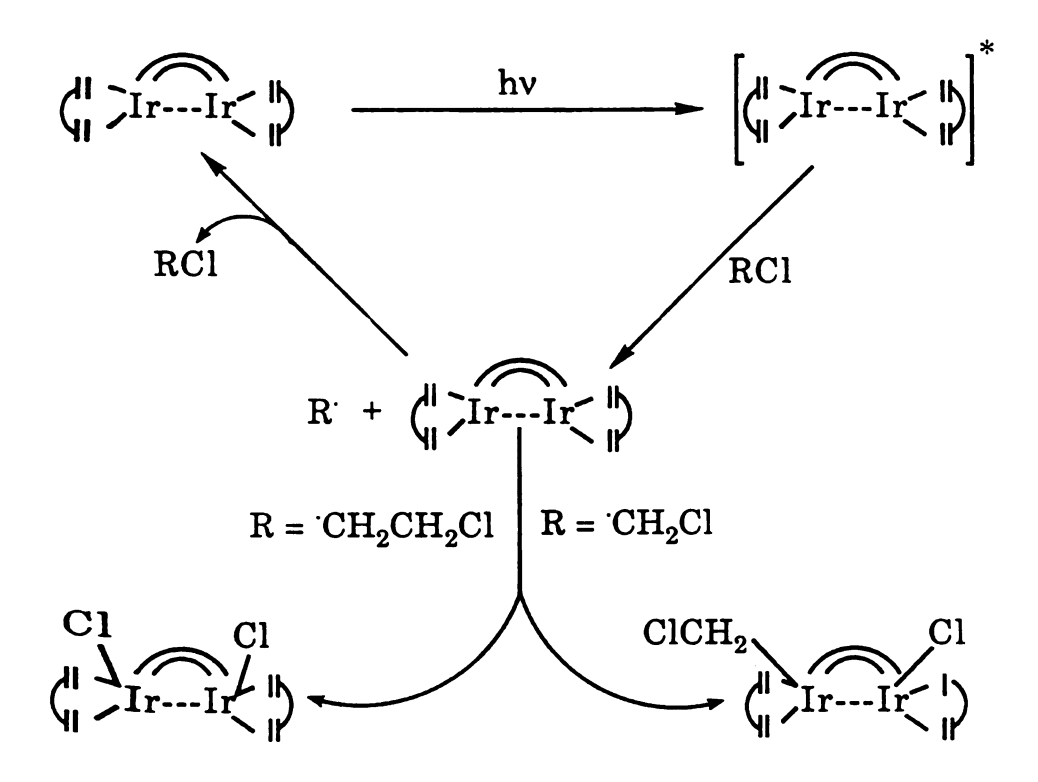


Figure 7

leads to th of [In(COD

electron or

Oth

Pt₂(pop)₄

into aceto

The electr isopropan

reaction o

the produc

undergoes

dihydride

oxidev ro

Tdimers;

chemis

oxidat

gem0:

 y_0 tripl

The c

result

102/111,

two electr

leads to the formation of ethylene and $[Ir(COD)(\mu-pz)Cl]_2$. The irradiation of $[Ir(COD)(\mu-pz)]_2$ in methylene chloride leads to the formation of a two-electron oxidative-addition product $[Ir(COD)(\mu-pz)]_2(ClCH_2)(Cl)$.

Other examples of bimetallic free radical chemistry include $Pt_2(pop)_4^{4-}$. This dimer can photocatalytically convert isopropyl alcohol into acetone and hydrogen by the reaction scheme shown in Figure 8.⁸⁵ The electronically excited $Pt_2(pop)_4^{4-*}$ abstracts the methine hydrogen of isopropanol to give $Pt_2(pop)_4^{4-*}$ and $(CH_3)_2COH^*$ radical. Subsequent reaction of this radical with another equivalent of $Pt_2(pop)_4^{4-}$ results in the production of $Pt_2(pop)_4^{4-}$. The $Pt_2(II,III)$ mixed-valent $Pt_2(pop)_4^{4-}$ undergoes disproportionation to give $Pt_2(pop)_4^{4-}$ and $Pt_2(pop)_4^{4-}$. The dihydride reacts with HCl to generate hydrogen and reacts rapidly with oxygen to give $Pt_2(pop)_4^{4-}$.

The multielectron free radical chemistry of d^7 - d^7 , d^8 - d^8 , and d^{10} - d^{10} dimers is not paralleled by the quadruple bond dimers. In this case, the chemistry is dominated by electron transfer and discrete two electron oxidation-addition transformations. In our laboratory we have demonstrated the oxidation photochemistry of the quadruple bonded $Mo_2(HPO_4)_4^{4-}$ dimer in an acid medium to produce hydrogen and the triple bonded $Mo_2(HPO_4)_4^{4-}$.

$$Mo_2(HPO_4)_4^{4-} + 2H^+ \xrightarrow{hv} Mo_2(HPO_4)_4^{2-} + H_2$$
 (5)

The overall reaction is composed of sequential one electron transfer to result in a formal oxidation change metal core from Mo₂(II,II) to Mo₂(III,III). Alternatively nonaqueous soluble phosphates promote the two electron reduction of halocarbons. 14b

Photoinduced catalytic conversion of isopropyl alcohol into acetone and hydrogen by using $Pt_2(pop)^{4-}$ as a photocatalyst.

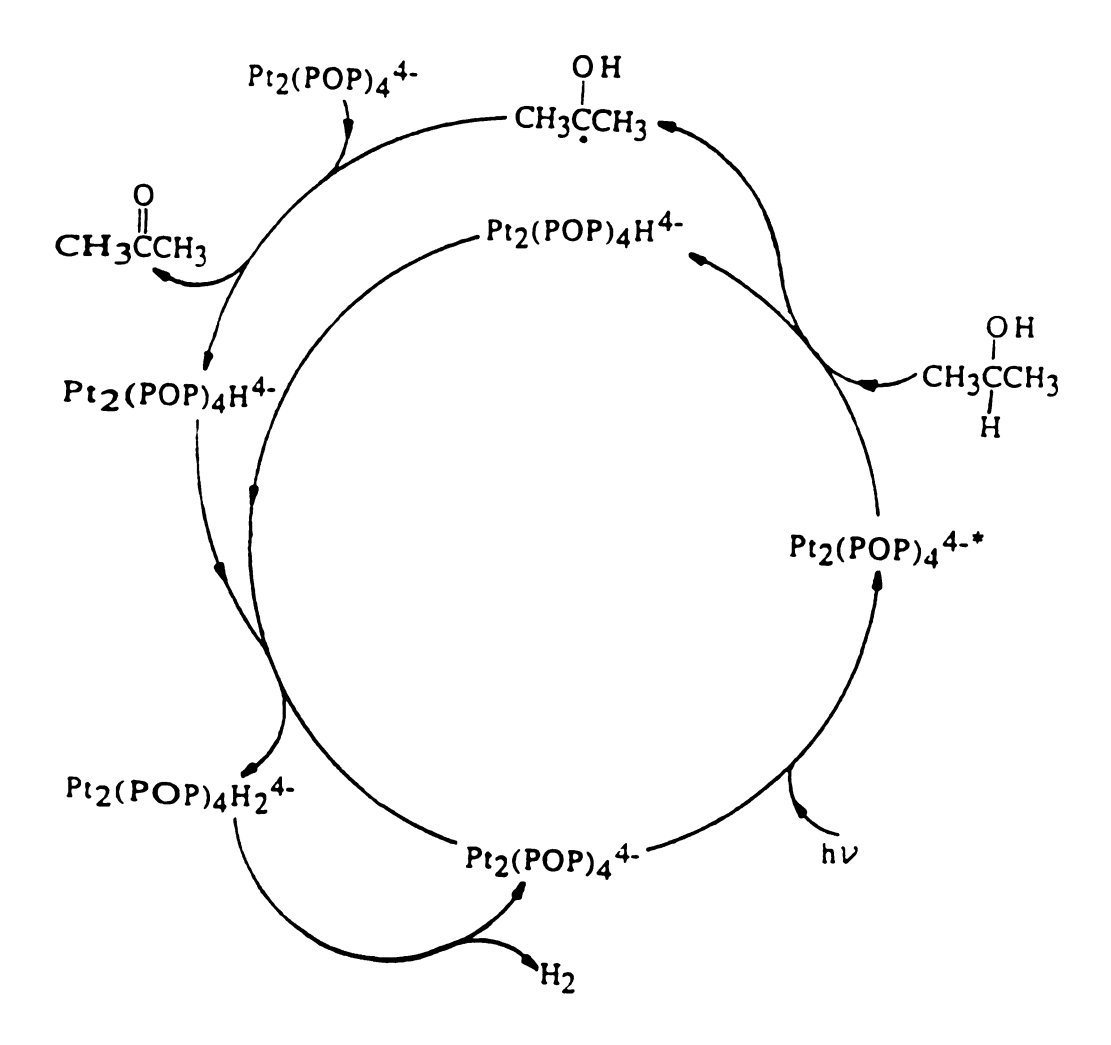


Figure 8

addition p

of the r

onstruc

of a seri

excited s

The pho

$$Mo_2(O_2P(OR)_2)_4 + ClCH_2CH_2Cl \xrightarrow{hv} Mo_2(O_2P(OR)_2)_4Cl_2 + C_2H_4$$
 (6)

When electron transfer from the metal core is avoided, concerted two electron reactions are observed. The visible irradiation of the quadruply bonded W₂(dppm)₂Cl₄ dimer in the presence of CH₃I yields the oxidative-addition product W₂(dppm)₂Cl₄(CH₃)(I), where CH₃I adds to the W-W bond in a discrete multielectron process. ^{14c}

$$W_2(dppm)_2Cl_4 + CH_3 \xrightarrow{hv} W_2(dppm)_2Cl_4(CH_3)(I)$$
 (7)

In this case also the formal oxidation state changed from $W_2(II,II)$ to $W_2(III,III)$.

As evidenced by the above discussion, guidelines for multielectron photoreactivity have begun to emerge. However, few photochemical schemes have been realized in which the initial multielectron photoreagent is regenerated. 90,91 As is the case for the photoreactant, the multielectron photoproduct typically resides in deep thermodynamic or kinetic wells that hinders its conversion back to the desired photoreactive state. It is not unreasonable to expect, therefore, that these kinetic or thermodynamic barriers of the photoproduct, in principle, can be surmounted by channeling the regenerative reaction via the excited state of the photoproduct. In this manner, photocatalytic schemes can be constructed. The success of this approach necessarily relies on the design of a series of multielectron reagents, each of which possesses a long-lived excited state. A scheme illustrating this strategy is shown in Figure 9. The photoreactant R is excited to R*, which has enough energy to

Illustration of the potential energy diagram for a reagent in its photoexcited state and its photoproduct with the photoproduct having an photoexcited state.

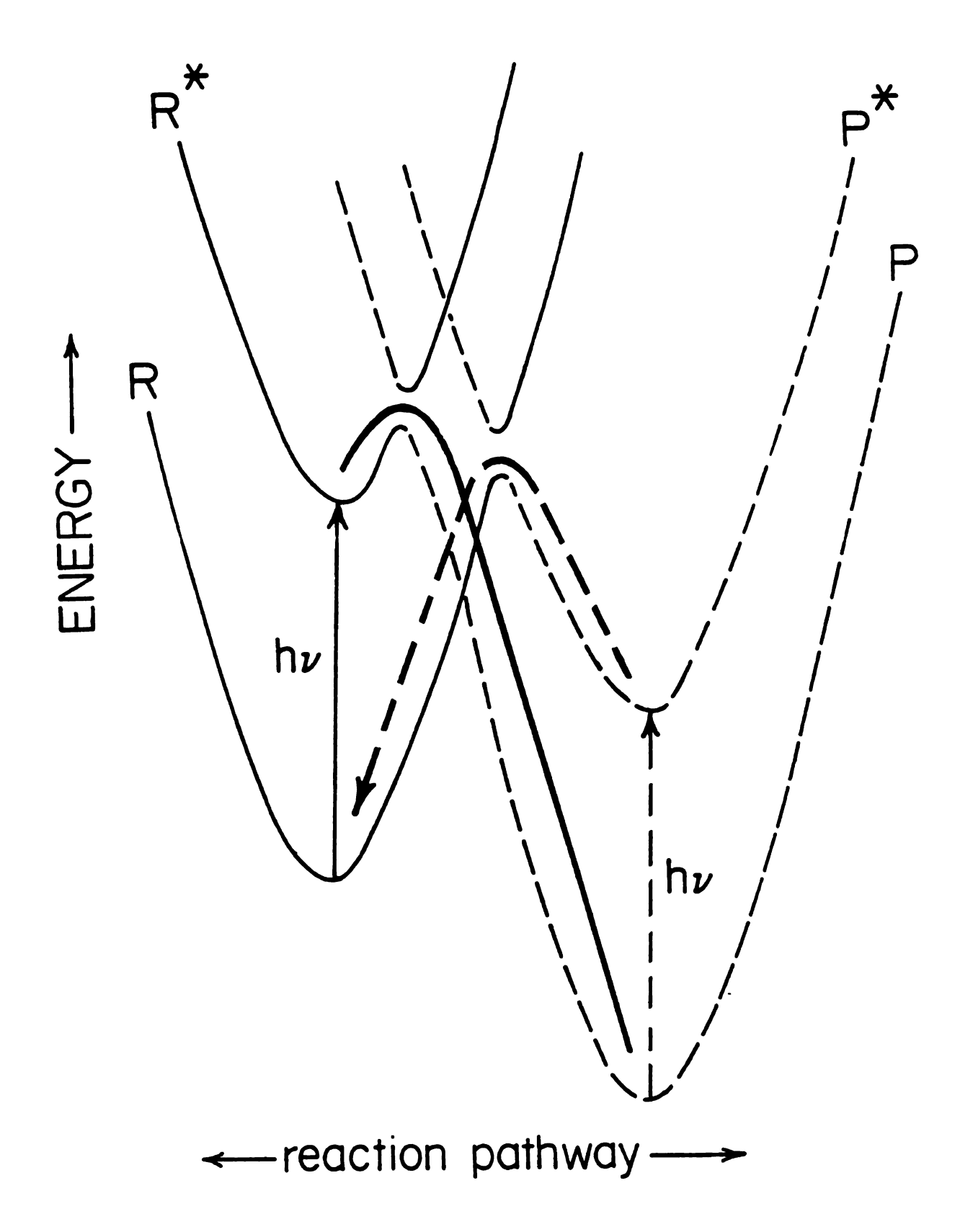


Figure 9

photopro photopro accomp barrier

bomolo
multie
emplo
cente
elect:

state and

and

lumi thes

demo

state

design a lon

invest comple

Na₂mr

monom

 $S)_2(mn$

overcome the thermodynamic and/or kinetic barrier to produce photoproduct P. If the system is designed such that the multielectron photoproduct possesses a long-lived excited state, regeneration of R can be accomplished in principle by using P* to overcome the thermodynamic barrier confronting the ground state.

To this end, we became interested in the possibility of synthesizing a homologous series of excited state complexes, which are interrelated by multielectron steps. Our strategy has depended primarily on the ability to employ a ligating coordination sphere capable of stabilizing metal redox centers in a variety of formal oxidation states while engendering electronic structural properties that are compatible with a rich excited-state redox chemistry. Chapter III reports the synthesis, and structural and spectroscopic characterization of a homologous Rh₂(0,0), Rh₂(0,II), and Rh₂(II,II) bis(difluorophosphino)methylamine series. Long lived luminescence characteristic of a do* excited state is observed for each of these novel binuclear complexes, and their interconversion is demonstrated.

Chapter IV describe the attempts to synthetically control the excited state in L_4MML_4 complexes. Our ultimate goal is to use excited state design of catalytic multielectron photochemistry with the goal of lowering a long-lived MLCT excited state below the $\delta\delta^*$ excited state. We investigated the chemistry of $Mo_2(II,II)$ quadruple bond starting complexes such as $Mo_2(O_2CCH_3)_4$ and $(NH_4)_2Mo_2Cl_9$ with π -acid ligands Na_2mnt and dmpby. The reaction of mnt^{2-} with $Mo_2(O_2CCH_3)_4$ yields the monomer $[(C_4H_9)_4]_2Mo(mnt)_3$ and the $Mo_2(V,V)$ dimer $[Mo_2(O)(S)(\mu-S)_2(mnt)_2]^{2-}$. In the reaction of dmbpy with $(NH_4)_2Mo_2Cl_9$ the complex

Y:2C (dm

Ma₂C. dmb

 $Mo_2Cl_4(dmbpy)_2$ is believed to be formed. The oxidation in air of $Mo_2Cl_4(dmbpy)_2$ also yields a $Mo_2(V,V)$ dimer $Mo_2O_4Cl_2(dmbpy)_2$.

CHAPTER II

Experimental

Th

red with

stirred f

that had

of cobalto

red solutio

^{oran}ge-bro

A. Syntheses

1. General Procedures

The synthesis of all complexes, unless otherwise stated, were performed under argon atmospheres by using standard Schlenk-line techniques. All solvents were dried and deoxygenated before use. Microanalyses were performed by Galbraith Laboratories, Inc., Knoxville, TN.

2. Syntheses of Dirhodium Complexes

- a. Starting Materials. The starting compounds [RhCl(PF₃)₂]₂, CH₃N(PF₂)₂, Rh₂(O₂CCH₃)₄, and Cl₂IC₆H₅ were prepared by literature methods. ⁹¹⁻⁹⁵ Phosphorus trifluoride (Ozark-Mahoning Company) and cobaltocene (Strem Chemical Company) were used as received.
- b. $\mathbf{Rh_2[CH_3N(PF_2)_2]_3(PF_3)_2}$. 1. A 15 mL dichloromethane solution containing 0.701 g of $[\mathbf{RhCl(PF_3)_2}]_2$ (1.12 mmol) was charged with 0.58 mL of $\mathbf{CH_3N(PF_2)_2}$ (0.83 g, 5.0 mmol) via syringe. The orange solution turned red with liberation of $\mathbf{PF_3}$. Upon cessation of $\mathbf{PF_3}$ liberation, 0.422 g of $\mathbf{Co(C_5H_5)_2}$ (2.23 mmol) was added from a side-arm. The mixture was stirred for 10 min under $\mathbf{PF_3}$ and then filtered to remove cobaltocenium that had formed. Addition of 10 mL of hexane led to further precipitation of cobaltocenium and excess cobaltocene. Filtration under argon yielded a red solution that was vacuum distilled to dryness to produce 0.691 g of an orange-brown precipitate. The solid was introduced onto a Florisil®

column
The fra
precipi

C₃H₉F₁

P, 28.0

diffract

Rh₂[CF

with h

mL of I solution the so

approx

of an o

25%).

(1.07); obtain

argon.

of a

 $\mathrm{CH_{3}N_{0}}$

orange-

under v

column and eluted with a hexane:dichloromethane (85%:15%) solution. The fraction was distilled to dryness under *vacuo* to give an orange-yellow precipitate. Yield 0.312 g (0.35 mmol, 32%). Anal. calcd (found) for C₃H₉F₁₈N₃P₈Rh₂: C, 4.08 (5.67); H 1.03 (1.40); F, 38.74 (33.02); N, 4.76 (6.17); P, 28.07 (25.49); Rh 23.32 (22.08). Orange crystals of 1, suitable for x-ray diffraction studies, were obtained from dichloromethane solution layered with hexane.

c. $Rh_2[CH_3N(PF_2)_2]_3Cl_2(PF_3)$, 2. The $Rh_2(II,0)$ complex $Rh_2[CH_3N(PF_2)_2]_3Cl_2(PF_3)$ was prepared by three methods:

Method i. To a solution of 0.300 g of $[RhCl(PF_3)_2]_2$ (0.477 mmol) in 15 mL of benzene, 0.24 g of CH₃N(PF₂)₂ (1.4 mmol) was added. The yellow solution turned red and PF₃ gas was liberated. After stirring for 20 min, the solution was filtered, and the filtrate volume was reduced to approximately 10 mL. Addition of 15 mL of hexane led to the precipitation of an orange solid, which was collected by filtration under an argon flow, washed with benzene, and dried in vacuo. Yield 0.102 g (0.118 mmol, 25%). Anal. calcd (found) for $C_3H_9Cl_2F_{15}N_3P_7Rh_2$: C, 4.16 (4.73); H, 1.05 (1.07); F, 30.14 (32.92); N, 4.68 (4.85). Red-orange crystals of 2 were obtained by layering a CH₂Cl₂ solution of the complex with hexane under argon. Method ii. $[RhCl(PF_3)_2]_2$ (0.201 g, 0.32 mmol) was dissolved in 5 mL of benzene. The solution was saturated with PF₃ and 1.8 mL of CH₃N(PF₂)₂ (0.27 g, 1.6 mmol) was added by syringe. The mixture was bubbled with PF₃ for 30 min during which a precipitate formed. The orange-red precipitate was filtered, washed with benzene, and dried under vacuo. Yield 0.184 g, (0.213 mmol, 67%).

(RhCl(P

M

2.4 mm

After a

#se he

100m

gigon

(0.33;

CI)₃

0.04

to fi

yield

mmo

PF₃ CH₃N

minut

side-an

refluxe

Washed

mmol, 5

H, 1.07 (

Method iii. To an orange solution containing 0.251 g of $[RhCl(PF_3)_2]_2$ (0.40 mmol) in 5 mL of benzene was added 0.28 mL (0.41 g, 2.4 mmol) of $CH_3N(PF_2)_2$. The solution turned red and PF_3 was liberated. After a few minutes of stirring, a precipitate began to form. The mixture was heated to reflux for 16 h under argon. The mixture was cooled to room temperature, and the red-orange precipitate was filtered under argon, washed with benzene, and dried under vacuum. Yield 0.290 g (0.335 mmol, 84%).

- d. Preparation of $Rh_2[CH_3N(PF_2)_2]_3Cl_2(PF_3)$ from $Rh_3(\mu-Cl)_3[CH_3N(PF_2)_2]_3$ (see Section II.A.3) was dissolved in 5 mL of a benzene solution saturated with PF₃. Addition of 0.040 mL of $CH_3N(PF_2)_2$ (0.34 mmol) with stirring prompted a precipitate to form after a few minutes. The suspension was refluxed for 4 h. The red-orange precipitate was filtered, collected, and dried under vacuum to yield 0.038 g of $Rh_2[CH_3N(PF_2)_2]_3Cl_2(PF_3)$ (0.044 mmol, 89%).
- e. Rh₂[CH₃N(PF₂)₂]₃Cl₄, 3. Crystalline [RhCl(PF₃)₂]₂ (0.394 g, 0.627 mmol) was dissolved in 15 mL of benzene. The solution turned dark and PF₃ was liberated immediately upon the addition of 0.44 mL (3.83 mmol) of CH₃N(PF₂)₂. The solution color lightened within seconds. After a few minutes of stirring, Cl₂I(C₆H₅) (0.700 g, 2.55 mmol) was added from a side-arm, causing the solution to turn yellow. The suspension was refluxed for 4 h and a yellow precipitate was filtered off under argon, washed with benzene, and dried under vacuum. Yield 0.315 g, (0.371 mmol, 59%). Anal. calcd (found) for C₃H₉Cl₄F₁₂N₃P₆Rh₂: C, 4.25 (4.73); H, 1.07 (1.11); Cl 16.71 (16.80); F, 26.87 (27.10); N, 4.95 (4.80); Rh, 24.25

(23.67). X-ray quality yellow crystals of 3 were prepared by diffusing ether into a THF solution of the complex while under argon.

Alternatively 3 can be prepared by adding 0.010 mL (0.11 g, 0.68 mmol) of CH₃N(PF₂)₂, and 195 µL of Me₃SiCl to a suspension of 0.151 g (0.344 mmol) Rh₂(O₂CCH₃)₄ in 20 mL of CH₂Cl₂. The suspension was refluxed for 12 h under argon, cooled, charged with an additional 130 µL (1.02 mmol) of Me₃SiCl and refluxed for an additional 20 h. The suspension was cooled again and an additional 0.010 mL (0.68 mmol) of CH₃N(PF₂)₂ and 165 µL (1.30 mmol) of Me₃SiCl was added. The suspension was brought to reflux for 24 h. After cooling the suspension, the solution was filtered to remove unreacted Rh₂(O₂CCH₃)₄ leaving a dark red filtrate. The volume of the solution was reduced to 10 mL by vacuum distillation and the resulting filtrate was placed in the refrigerator for 12 h. An orange-yellow precipitate was collected by filtration and dried under vacuo. Yield 0.0247 g (0.0291 mmol, 8.5%).

3. Synthesis of $Rh_3(\mu\text{-Cl})_3[CH_3N(PF_2)_2]_3$, 4

A 5.0 mL solution of benzene was charged with 0.225 g of [RhCl(PF₃)₂]₂ (0.36 mmol), and 0.050 mL of CH₃N(PF₂)₂ (0.43 mmol). The red solution was refluxed for 5 h under argon. The solution was cooled to room temperature and the solution volume was decreased by 2.0 mL by vacuum distillation. To the filtrate, 5.0 mL of hexane was added, and a red precipitate formed. The precipitate was filtered under argon, and dried under vacuum. Yield 0.0274 g (0.030 mmol, 8%). X-ray crystals of 4 were obtained by diffusing hexane into a CH₂Cl₂ solution of the complex

under a

groups (

4. Synt

metho

as rec

bubb of be

mLand

A s

filt

yel pre

0.2

 $[]_1$ bi

C)

0r

sa fro

under argon. This method yielded crystals with C2/c and Pnma space groups on separate preparations.

4. Syntheses of Diiridium Complexes

- a. Starting Materials. [IrCl(C₈H₁₄)₂]₂ was prepared by literature methods.⁹⁶ IrCl₃·H₂O and C₈H₁₄ were purchased from Aldrich and used as received.
- b. Attempt to Prepare $Ir_2[CH_3N(PF_2)_2]_3Cl_2(PF_3)$, 5. PF₃ was bubbled into a suspension of 0.401 g $[IrCl(C_8H_{14})_2]_2$ (0.447 mmol) in 10 mL of benzene until all the solid had dissolved. To this yellow solution, 0.26 mL (2.2 mmol) of $CH_3N(PF_2)_2$ was added. The solution turned orange, and then returned to yellow. PF₃ was passed into the solution for 30 min. A small amount of a grey-yellow precipitate was removed from solution by filtration and the filtrate was reduced to 4 mL by vacuum distillation. A yellow precipitate formed with the addition of 8 mL of hexane. The precipitate was collected by filtration and dried under vacuum. Yield 0.229 g of this product.
- c. Attempt to Prepare $Ir_2[CH_3N(PF_2)_2]_3Cl_4$, 6. 0.200 g of $[IrCl(C_8H_{14})_2]_2$ (0.223 mmol) was suspended in 10 mL of benzene. PF₃ was bubbled into the solution and after all of the solid had dissolved, 0.23 mL of $CH_3N(PF_2)_2$ (1.86 mmol) was added. The yellow solution turned to light orange for a few seconds, and then back to yellow. The solution was saturated with PF₃ and 0.303 g of $Cl_2I(C_6H_5)$ (1.10 mmol) was delivered from a side-arm. The solution was heated to reflux under argon for 2 h.

The argo prec

und

5. \$

Mo by

disc

dip

pre

in (N)

sol:

dri

Mo.

gree the

gree

The yellow solution was cooled to room temperature and filtered under argon. Hexane was added to the yellow filtrate and a light yellow precipitate formed. The solution was filtered, and the solid was dried under *vacuo*. Yield 0.0764 g of this product.

5. Syntheses of Dimolybdenum Complexes

- a. Starting Materials. The starting compounds $(NH_4)_5Mo_2Cl_9\cdot H_2O$, disodium 1,2-dicyanoethylene-2,2-dithiolate (Na_2nmt) , $Mo_2(O_2CCH_3)_4$, and $Mo_2Cl_4(dppm)_2$ [dppm = bis(diphenylphosphino)methane] were prepared by literature methods. $^{97-100}$ $(C_4H_9)_4NBr$ (Aldrich) and 4,4'-dimethyl-2,2'-dipyridyl (dmpby) (Aldrich) were used as received.
- b. $Mo_2Cl_4(dmbpy)_2$, 7. This preparation was modified from the preparation of $Mo_2Cl_4(bpy)_2^{14}$. 2.00 g (10.9 mmol) of dmbpy was dissolved in 30 mL of methanol. With the subsequent addition of 0.500 g of $(NH_4)_5Mo_2Cl_9\cdot H_20$ (0.826 mmol), the solution was stirred for 90 min and a solid formed. The product was filtered, washed with one 10 mL portion of water, and methanol, and three 10 mL portions of ether. The solid was dried in vacuum. Yield 0.406 g (0.578 mmol, 70%).
- c. $[(C_4H_9)_4N)]_2[Mo_2(O)(S)(\mu-S)_2[S_2C_2(CN)_2]_2]$, 8. A suspension of $Mo_2(O_2CCH_3)_4$ (0.604 g, 1.41 mmol) in 50 mL of dry methanol was charged with 1.06 g of Na_2 mnt (5.67 mmol). The yellow suspension turned dark green. After 5 h of stirring, the mixture was filtered and the volume of the green filtrated was reduced to 35 mL by rotary evaporation. To the green solution, 1.81 g (5.62 mmol) of $(C_4H_9)_4NBr$ was added. The flask

was c

forme

Upon

precip was f

0.278

44.91

X-ray

with

ident

Yield

C, 52

(10.56

mmo

for 5

filter form

vacu

Yielo

C₂₄H

(23.4)

evapo

susper

was cooled for 12 h in a dry ice-acetone bath and a green precipitate formed. The precipitate was filtered in air and washed with methanol. Upon dissolution of this precipitate in boiling methanol, the green precipitate dissolved and a red precipitate remained. The red precipitate was filtered and recrystallized from hot methanol and acetone. Yield 0.278 g (0.264 mmol, 19%). Anal. calcd (found) for $C_{40}H_{72}Mo_2N_6O_1S_7$: C, 44.91 (45.38); H, 6.78 (6.86); N, 7.86 (7.60); S, 20.98, (20.35); Mo, 17.98 (18.19). X-ray quality crystals of 8 were grown from a solution of CH_2Cl_2 layered with hexane. Green crystals, grown from the green filtrate, were identified by IR and absorption spectrum to be $[(C_4H_9)_4N]_2Mo(mnt)_3$. Yield 0.500 g (0.494 mmol, 35%). Anal. calcd (found) for $C_{40}H_{72}MoN_6S_4$: C, 52.77 (55.38); H, 7.25 (7.89); N, 11.19 (10.61); S, 19.21 (16.20); Mo, 9.85 (10.56).

- d. Mo₂Cl₂O₂(μ-O₂)(dmbpy)₂, 9. A suspension of 0.384 g (0.547 mmol) Mo₂Cl₄(dmbpy)₂ in 50 mL of o-dichlorobenzene was heated to reflux for 5 h under air. The suspension was cooled to room temperature, and filtered. Hexane was added to the red filtrate and a red precipitate formed. The precipitate was filtered, washed with ether, and dried under vacuum. The precipitate was recrystallized from CH₂Cl₂ and hexane. Yield 0.080 g (0.115 mmol, 21%). Anal. calcd (found) for C₂₄H₂₄C₁₄Mo₂N₄O₂: C, 41.46 (36.06); H, 3.48 (3.30); N, 8.06 (6.43); Cl 10.20 (23.46); Mo, 27.60 (23.54). X-ray quality crystals of 9 were grown from slow evaporation of CH₃CN solution.
- e. Attempt to Prepare Mo₂(dppm)₂(mnt)₂, 10. To a green suspension of Mo₂Cl₄(dppm)₂ (0.210 g, 0.190 mmol) in 30 mL of acetone,

Na₂

100

filt

an

Wa

m

14. (s

B.

l

\$0

sp of

2.

59

Na₂mnt (0.0694 g, 0.380 mmol) was added. The suspension turned dark green, and was refluxed for 3 h under argon. The solution was cooled to room temperature and stirred for an additional 2 h. The suspension was filtered, the filtrate volume was reduced to 10 mL by vacuum distillation, and 20 mL of hexane was added. The solution was cooled to 10 °C for 12 h and a dark green precipitate (10) formed. The precipitate was filtered, washed with hexane, and dried under vacuum. Yield 0.0761 g (0.0613 mmol, 32%) based on $Mo_2(dppm)_2(mnt)_2$. IR (KBr pellet) 2207 (s, C=N); 1482 (m), 1152 (s), (C=C stretch); 797 (m), 737 (s) (out-of-plane c-h bend); 688 (s out-of-plane ring C=C bend).

B. Instrumentation and Methods

1. Absorption Spectroscopy

Electronic absorption spectra were recorded on dichloromethane solutions (HPLC grade) of the compounds with a Cary 17 spectrophotometer. Extinction coefficients, which were determined by use of 1-cm quartz cuvette, were calculated from the Beer-Lambert equation.

2. Infrared Spectroscopy

Infrared spectra were obtained as KBr pellets on a Perkin Elmer 599 and a Nicolet 740 FT IR spectrophotometer.

3. Time-Resolved and Steady State Luminescence

Time-resolved and steady-state luminescence spectra were recorded on previously described Nd:YAG pulsed laser system ($\lambda_{\rm exc} = 355$ nm, fwhm = 8 ns) and high-resolution emission spectrometer ($\lambda_{\rm exc} = 365$ nm) respectively, 102,103 constructed at Michigan State University. All luminescence spectra were corrected for the instrument response function. Variable temperature luminescence and lifetime measurements were recorded on a sample cooled with an Air Product closed-cycle cryogenic system by methods described elsewhere. 102

4. Mass Spectroscopy

The mass spectra were taken at the NIH/MSU Mass Spectrometry Facility. The mass spectra were measured on a double focusing (EB geometry) JEOL HX-110 mass spectrometer. The acceleration potential used for this work was 10 kV. All data were acquired, stored, and processed on a JEOL DA5000 data system. Fast Atom Bombardment (FAB) ionization was preformed with a 6 kV neutral beam of xenon atoms impinging on a o-nitrobenzyl alcohol (NBA) matrix.

5. Nuclear Magnetic Resonance Spectroscopy

NMR spectra were performed at the Max T. Roger NMR Facility at Michigan State University. The ³¹P{¹H} NMR spectra were recorded at 202.334 MHz and 121.421 MHz with a Varian VXR-500S and a Varian VXR-300S, respectively. The ¹⁹F, and ¹⁹F{³¹P} NMR spectra were recorded at 470.268 MHz on the VXR-500S spectrometer. ³¹P{¹H} chemical shifts

were i H₃PC

¹⁹F N

reco

Lab

Lab

1.

C.

1

1

ca SI

2]

a. A

para

refine

was fo

were reported in parts per million (δ-scale), and measured relative to 85% H₃PO₄. Positive chemical shifts are downfield from the standard. The ¹⁹F NMR were referenced to an external standard of CFCl₃ with positive chemical shifts downfield from the standard. All NMR spectra were recorded at 25 °C. Deuteriochloroform (99.8%, Cambridge Isotope Laboratories) and deuterioacetonitrile (99%, Cambridge Isotope Laboratories) solvents were used as received.

C. Crystal Structure Determinations

1. General Procedures

Crystal structure determinations were performed by Dr. Donald L. Ward of the X-ray Crystal Structure Facility at Michigan State University. The diffraction data were collected on a Nicolet P3F diffractometer using graphite-monochromated MoKa (λ = 0.71073 Å) radiation. All calculations were performed on a VAX 11/750 computer using SDP/VAX.¹⁰⁴

2. Methods

a. $\mathbf{Rh_2[CH_3N(PF_2)_2]_3(PF_3)_2}$, 1. An orange irregularly shaped crystal of 1 (dimensions $0.14 \times 0.32 \times 0.44$ mm) was mounted on a glass fiber. The cell parameters and orientation matrix were obtained from least-squares refinement of 25 reflections in the range $15 < 20 < 24^\circ$. The space group was found to be $P\overline{1}$.

and

ever

sy coo

co

Ü

t

;

Þ

aı stı

place The

We.

diffe

c. R

dime

A total of 4552 reflections was collected, of which 4172 were unique and not systematically absent. Three standard reflections were measured ery 93 reflections and indicated a decrease of intensity of 15.2%; a decay rection was applied.

The structure was solved by Patterson heavy-atom methods. The ordination sphere was completed by a series of difference Fourier ntheses. The hydrogen atoms were placed in idealized positions and estrained to ride on the carbon atoms. Anisotropic refinements were ed to give R = 0.067 and $R_W = 0.078$. The largest shift-to-error was 0.11σ , and the largest peak in the final difference map was $1.01(18) \text{ e/Å}^3$.

 $Rh_2[CH_3N(PF_2)_2]_3Cl_2(PF_3)$, 2. An irregular shaped red-orange crystal 2 (dimensions 0.36 x 0.45 x 0.56 mm) was mounted in a glass capillary a random orientation. The cell constants and orientation matrix were tained from least-square refinement of 15 reflections in the range 20 < < 25°. From systematic absences and from refinement, the space group as determined to be $P2_12_12_1$.

A total of 9542 reflections were collected, of which 4889 were unique and not systematically absent. Corrections were applied and the ructure was solved as described for 1 above. The nonhydrogen atoms are refined with anisotropic parameters, and hydrogen atoms were acced in idealized positions and constrained to ride on the carbon atoms. The largest shift-to-error was 0.15σ , and the largest peak in the final afterence map was 0.57 (7) e/Å³.

 $Rh_2[CH_3N(PF_2)_2]_3Cl_4$, 3. A yellow transparent needle of 3 (crystal mensions 0.04 x 0.10 x 0.42 mm) was mounted with Paratone-N oil and

cool orie refl froi an ato ato cai ax ato 0.1 d. pr gla go fro

> Fr der

> > and str

> > wer wer

fact

cooled with a nitrogen gas stream to -70°C. The cell constants and an orientation matrix were obtained from least-square refinement of 23 reflections in the range 15 < 20 < 20°. From the systematic absences and from refinement, the space group was determined to be C2/c.

A total of 2957 reflections were collected. Corrections were applied and the structure was solved as described above for 1. The nonhydrogen atoms were refined with anisotropic thermal parameters, and hydrogen atoms were placed in idealized positions and constrained to ride on the carbon atoms. Atoms N(1) and C(1) lie along a crystallographic two-fold axis that passes midway between the two rhodium atoms; only half of the atoms are crystallographically unique. The largest shift-to-error was 0.14 σ , and the largest peak in the final difference map was 0.68(8) e/Å³.

d. $Rh_3(\mu\text{-Cl})_3[CH_3N(PF_2)_2]_3$ in C2/c Space Group, 4. A dark red-orange prism crystal of 4 (dimensions 0.40 x 0.52 x 0.82 mm), was mounted in a glass capillary with its long axis roughly parallel to the phi axis of the goniometer. The cell constants and orientation matrix were obtained from least-square refinement of 19 reflections in the range 15 < 20 < 20°. From systematic absences and from refinement, the space group was determined to be C2/c.

A total of 8658 reflections were collected, of which 8058 were unique and not systematically absent. Corrections were applied and the structure was solved as described for 1 above. The nonhydrogen atoms were refined with anisotropic thermal parameters. The hydrogens atoms were calculated in two disordered sets of positions, assigned occupation factors of 0.5, and were included in the refinement but restrained to ride

on the

0.030, s

irregul

mounte

orienta

reflection

refinem

A

and not

every 9;

decay co

T SHELY

remain

synthe

on the

lie o

cryst

were and

large

£ [(C4.

dimens

random (

on the atom to which they are bonded. The largest shift-to-error was 0.03σ , and the largest peak in the final difference map was 0.91(9) e/Å³.

e. $\mathbf{Rh_3}(\mu\text{-Cl})_3[\mathbf{CH_3N(PF_2)_2}]_3$, in Pmna space group 4'. A deep red irregular shaped crystal of 4 (dimensions 0.20 x 0.36 x 0.56 mm) was mounted on a fiber in a random orientation. The cell constants and orientation matrix were obtained from least-square refinement of 25 reflections in the range $20 < 20 < 25^\circ$. From systematic absences and from refinement, the space group was determined to be Pmna.

A total of 2952 reflections were collected, of which 2679 were unique and not systematically absent. Three standard reflections were measured every 93 reflection and indicated an increase of intensity of 2.6%; a linear decay correction was applied.

The structure was solved using the direct methods program SHELXS86. A total of 17 atoms were located from an E-map; the remaining atoms were located in succeeding difference Fourier syntheses. The hydrogen atoms were included in the refinement to ride on the atom to which they are bonded. Atoms Rh(2), Cl(3), N(3), and C(3) lie on a crystallographic mirror plane; only half of the atoms are crystallographically unique. P(2), F(2a), and F(2b) are disordered and were refined in two sets of 0.5 occupancy positions [P(2a), F(2aa), F(2ab); and P(2b), F(2bb), F(2ba)]. The largest shift-to-error was 0.26σ, and the largest peak in the final difference map was 0.53(9) e/Å³.

f. $[(C_4H_9)_4N)]_2[Mo_2(O)(S)(\mu-S)_2[S_2C_2(CN)_2]_2]$, 8. A red crystal platelet of 8 (dimensions 0.11 x 0.30 x 0.50 mm) was mounted on a glass fiber in a random orientation. The cell parameters and orientation matrix were

obtaine

28 < 20

and n

nonhyo

The hy

ride on

0.20σ, ε

g. Mog dimens

orienta

least-so

syster

detern

and i

anis

A to

Were

atoms

are bon

passes b

obtained from least-square refinement of 21 reflections in the range 15 < 20 < 20°. The space group was determined to be P2₁/c.

A total of 7767 reflections were collected, of which 7168 were unique and not systematically absent. Corrections were applied and the structure was solved as described for 4 (see Section II. C. 2e) above. The nonhydrogen atoms were refined with anisotropic thermal parameters. The hydrogens atoms were included in the refinement but restrained to ride on the atom to which they are bonded. The largest shift-to-error was 0.20σ , and the largest peak in the final difference map was 0.83(7) e/Å³.

g. $Mo_2Cl_2O_2(\mu-O_2)(dmbpy)_2$, 9. A clear red diamond shape crystal of 9 (dimensions 0.10 x 0.15 x 0.20 mm) was mounted on a fiber in a random orientation. The cell constants and orientation matrix were obtained from least-square refinement of 12 reflections in the range $15 < 2\theta < 20^\circ$. From systematic absences and from refinement, the space group was determined to be $P3_121$.

A total of 9353 reflections were collected, of which 2109 were unique and not systematically absent. Three standard reflections were measured every 93 reflection and indicated an increase of intensity of 16.5%; an anisotropic decay correction was applied.

The structure was solved using the Patterson heavy-atom methods. A total of 17 atoms were located from an E-map; the remaining atoms were located in succeeding difference fourier syntheses. The hydrogen atoms were included in the refinement to ride on the atom to which they are bonded. Complex 9 possesses a crystallographic two-fold axis that passes between the Mo(1), Mo(1)' atoms; only half of the atoms are

cryst

large

crystallographically unique. The largest shift-to-error was 0.01σ , and the largest peak in the final difference map was 1.13(12) e/Å³.

CHAPTER III

Rhodium Fluorophosphine Chemistry

A. I

syn

the me

eng rich

to 1

acco

cent

the

can

This

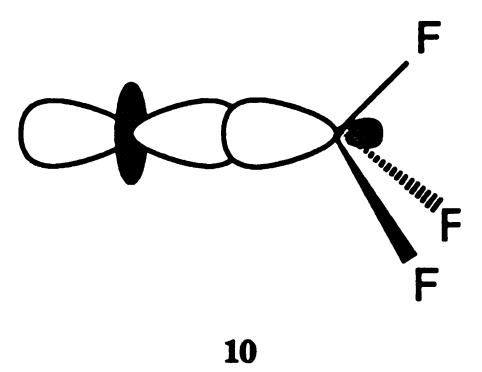
fluor

acce

frame

A. Background

Our interest in developing multielectron schemes is centered on synthesizing a homologous series of excited state complexes, which are interrelated by multielectron steps. The strategy depends primarily on the ability to employ a ligating coordination sphere capable of stabilizing metal redox centers in a variety of formal oxidation states while engendering electronic structural properties that are compatible with a rich excited-state chemistry. For these reasons, we turned our attention to the chemistry of fluorophosphine metal complexes. The good π -accepting and moderate σ -donating ability $^{105-110}$ of bidentate fluorophosphine ligands is manifested in their ability to stabilize metal centers in low and high oxidation states, respectively. As illustrated by the schematic represented by 10 for PF₃, phosphorus lone pair electrons can be donated to the metal σ orbital.



This σ -donor ability of the phosphorus will stabilize metals in high oxidation states. Conversely, the π -accepting properties of fluorophosphines will stabilize metals in low oxidation states. The π -accepting properties of PF₃ can be understood within two bonding frameworks. The low-lying 3d orbitals of phosphorus can accept electron

pic

der

Mo

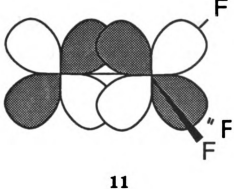
res Thi

sho

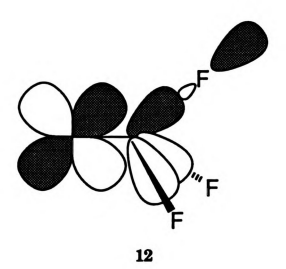
The other

fluor

density from the metal $d\pi$ orbitals by the conventional π -back bonding picture illustrated by 11.



More recently Marynick has suggested orbitals with σ* symmetry with respect to the P-F bond axis can accept electron density from the metal. 106 This accepting orbital is formed from the P-F σ^* bonding interaction shown in 12.



There are several reasons for the enhanced π -accepting ability of PF₃ over other phosphines like PH3 and PR3 (R = alkyl). Firstly, phosphorusfluorine bonds are highly polar bonds, and these characteristically have low-lying σ^* accepting orbitals. Secondly, because the σ P-F bond is highly polar toward F, the σ^* orbital must necessarily be highly polar toward P, therefore, increasing the σ^* -metal $d\pi$ overlap.

On the basis of these arguments, we became intrigued with the bidentate bis(difluorophosphino)alkyl/arylamines, $RN(PF_2)_2$, (R = methyl, phenyl) owing to the studies of King and coworkers, 112 which establish the precedence for this ligand to give rise to a diverse redox chemistry of bimetallic cores. The unique redox properties of metal coordinated by this ligand is best exemplified by the cobalt complex $Co_2[CH_3N(PF_2)_2]_3(CO)_2$, (see Figure 10) which upon treatment with Br₂, gives the Co₂(II,II) derivative Co₂[CH₃N(PF₂)₂]₃(CO)₂Br₄, ¹¹³ and upon its electrochemical reduction yields the Co₂(-I,-I) anion, Co₂[CH₃N(PF₂)₂]₃(CO)₂^{2-.114} In this system, the bis(difluorophosphino)methylamine ligand has stabilized the metal core to an overall six electron change in formal oxidation state! Moreover, the cobalt complex illustrates the ability of the $\mathrm{RN}(\mathrm{PF}_2)_2$ ligand to coordinate across singly bonded metal-metal (M-M) cores while accommodating very different coordination geometries about the metal center. 115,116 For instance, the binuclear compound Fe₂[CH₃N(PF₂)]₂(CO)₆ 13, has a square-pyramidal geometry rather than the usual trigonal-bipyramidal for five-coordinated iron (0) atoms. 115

Redox chemistry of $Co_2[CH_3N(PF_2)_2]_3(CO)_2$.

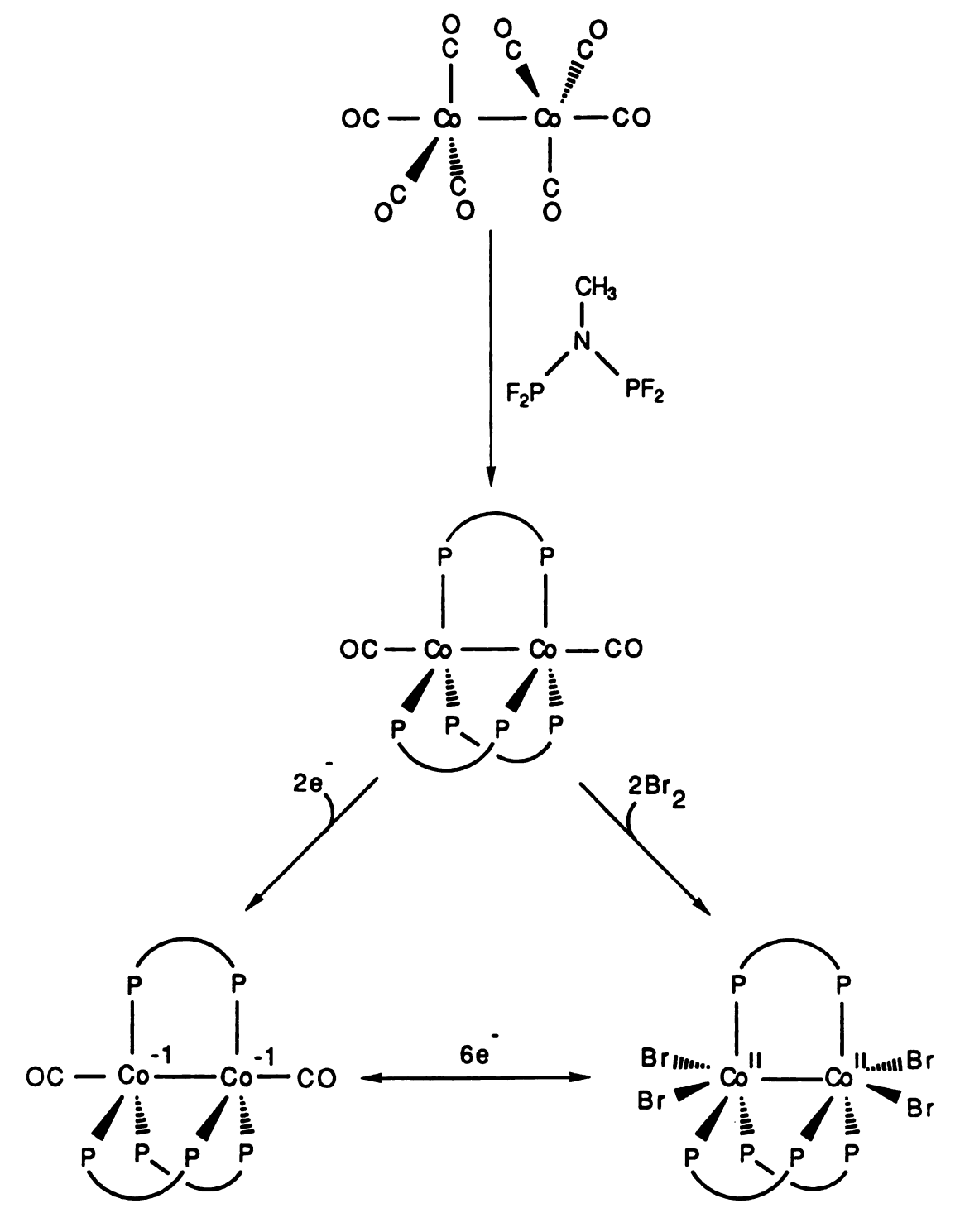


Figure 10

Ş

tł

Be

ch

Subsequent loss of CO from 13 forms $Fe_2[CH_3N(PF_2)]_2(CO)_5$ 14, which possesses a geometry about each iron atom that can be considered as either a distorted octahedron or distorted trigonal bipyramid depending if the metal-metal bond is considered as a coordination position.¹¹⁶

Because multielectron transformations usually prompt a significant change in structure of the coordination sphere of a metal, the ability of the

p

CO

Pi

H

01

uorophosphine ligand to permit different geometries could be important a the design of multielectron schemes.

Studies were initiated with group VIII metals because of Kruck and coworkers reported 117 that UV photolysis of HIr(PF₃)₄ yields Ir₂(PF₃)₈ and H₂. The Ir₂(PF₃)₈ photoproduct was subsequently observed to react ith water to regenerate HIr(PF₃)₄. The fate of oxygen is unknown. This eaction is important because (1) the photochemical reaction is at least a two electron process; and (2) the photochemical reaction represents half of the water splitting cycle with implied oxygen activation.

The photochemical reaction of HIr(PF₃)₄ may proceed by three ausible mechanisms: radical, acid-base, or oxidative addition/reduction imination. A radical mechanism is shown by eqs 8-11,

$$HIr(PF_3)_4 + hv \longrightarrow H + Ir(PF_3)_4$$
 (8)

$$\cdot \mathbf{H} + \cdot \mathbf{H} \longrightarrow \mathbf{H}_2 \tag{10}$$

radiation produces the ·H and ·Ir(PF₃)₄ radicals as primary hotoproducts. Simple recombination of products will not be instructive. However, combination radical crossover yields the observed roducts. Alternatively, excitation could significantly change the pK_a of $Ir(PF_3)_4$ producing H⁺ and $Ir(PF_3)_4$. Nucleophilic attack of $Ir(PF_3)_4$ HIr(PF₃)₄ will yield H₂ and the observed dimer.

$$HIr(PF_3)_4 + hv \longrightarrow HIr(PF_3)_3)_4^*$$
 (11)

$$HIr(PF_3)_4^* \longrightarrow H^+ + Ir(PF_3)_4^-$$
 (12)

$$HIr(PF_3)_4 + Ir(PF_3)_4^- \longrightarrow Ir_2(PF_3)_8 + H^-$$
 (13)

$$H^+ + H^- \longrightarrow H_2 \tag{14}$$

th

re

CO

Wi

Finally and perhaps most reasonably is the intermolecular reductive elimination show by equations 15-17.119

$$HIr(PF_3)_4 + hv \longrightarrow HIr(PF_3)_3 + PF_3$$
 (15)

$$HIr(PF_3)_4 + HIr(PF_3)_3 \longrightarrow (PF_3)_3 Ir ---Ir(PF_3)_4$$
 (16)

$$HIr(PF_{3})_{4} + HIr(PF_{3})_{3} \xrightarrow{H} (PF_{3})_{3} I\dot{r} ---Ir(PF_{3})_{4}$$

$$(PF_{3})_{3} I\dot{r} ---Ir(PF_{3})_{4} + PF_{3} \xrightarrow{H} H_{2} + Ir_{2}(PF_{3})_{8}$$

$$(17)$$

Excitation causes PF₃ to photodissociate from the metal center to produce a vacant coordinated site. 120 Reaction of the coordinatively unsaturated HIr(PF₃)₃ with HIr(PF₃)₄ yields the binuclear hydride intermediate which can undergo subsequent reductive elimination to produce H2 and $Ir_2(PF_3)_8$.

Irregardless of the particular mechanism, it is necessary to bring together monomeric iridium centers to ultimately yield products. Certainly, the low photoreaction yield of the reaction is consistent with a rate determining step for hydrogen production involving a bimolecular reaction between monomeric iridium species. These observations suggest that binuclear iridium (and rhodium) complexes with bidentate CH₃N(PF₂)₂ ligands may retain the interesting multielectron chemistry, while exhibiting an increased quantum yield for photoreactivity. Because the observed photochemistry of the $M_2(PF_3)_8$ (M= Rh, Ir) establishes reactive excited state chemistry for Group VIII fluorophosphines complexes, we decided to explore the chemistry of $CH_3N(PF_2)_2$ beginning with bimetallic rhodium complexes.

in

ро

ex.

syl

B. Dirhodium Complexes

1. Results

a. Synthesis of Dirhodium Complexes. The $[RhCl(PF_3)_2]_2$ dimer reacts smoothly with bis(difluorophosphino)methylamine to yield $Rh_2[CH_3N(PF_2)_2]_3Cl_2(PF_3)$, 2, and under reducing and oxidizing conditions to yield $Rh_2[CH_3N(PF_2)_2]_3(PF_3)_2$, 1 and $Rh_2[CH_3N(PF_2)_2]_3Cl_4$, 3, respectively. The formation of 2 corresponds to an intramolecular disproportionation of the $Rh_2(I,I)$ starting material. However, the intimate mechanism, appears to be more complicated owing to our isolation and characterization from reaction mixtures of the recently reported trimer, $Rh_3(\mu-Cl)_3[CH_3N(PF_2)_2]_3$. We have observed that reaction of this trimetallic complex with excess ligand leads to 2 in good yields.

The unsymmetrical binuclear complex can be viewed as a synthon for 1 and 3. The former is derived from the reduction of the Rh(0) center of 2 with subsequent trapping by PF₃, whereas 3 can be envisaged to form from the oxidation of the Rh(0) center by chlorine. Indeed, although 1 and 3 are prepared from the aforementioned [RhCl(PF₃)₂]₂ starting compound in high yields, we have been able to directly convert among 1, 2, and 3 with the appropriate choice of oxidizing and reducing conditions. For instance, oxidation of 1 by Cl₂IC₆H₅ readily affords 3. Conversely, sodium borohydride reduction of 3 produces 1, but admittedly in low yields. As expected, both 1 and 3 can directly be obtained from 2. The ability to synthetically interconvert among these Rh₂ complexes underscores the

i S

> fr 07

ca

(a .

pa

who

and the

the

fluorophosphine ligand's capacity to readily accommodate metal cores in a variety of formal oxidation states.

The complexes 1, 2, and 3 where characterized by elemental analysis, mass spectroscopy, and x-ray crystallography. The elemental analysis was not reliable; even samples from which crystals were chosen for x-ray structural determination yielded poor analysis.

A more reliable method for routine analysis was mass spectroscopy. The mass spectrum of 1, 2, and 3 were recorded by employing Fast Atom Bombardment (FAB) methods. The FAB mass spectra of 1, 2, and 3 are shown in Figures 11 - 13. The molecular ion observed for 1 occurs at a m/z of 882.95 and is labeled P in Figure 11. Loss of one and two PF₃ is indicated by a m/z of 794.95 and 706.96, respectively. Unknown fragments at m/z of 755, 688, and 609 are labeled with an U. The mass spectra of 2 and 3 differ from 1 in that fragmenation peaks display isotope peak-intensity patterns owing to the presence of chlorines. Figure 14 shows the peak intensity pattern for different numbers of chlorine atoms. This pattern was calculated from the binomial expansion 122

$$(a+b)^n = a^n + nb^{(n-1)}b + n(n-1)a^{(n-2)}b^2/2! + n(n-1)(n-2)a^{(n-3)}b^3/3! + ..(18)$$

where a represents the relative intensity of the first isotope (assumed to be one), b represents the relative intensity of the next highest mass isotope, and n is the number of isotope atoms present to determine the magnitude of the abundance contribution for a given isotope. Comparison of Figure 14 to the mass spectrum of 2 and 3 shows that the correct chlorine isotope

FAB mass spectrum of $\rm Rh_2[CH_3N(PF_2)_2]_3(PF_3)_2,\, 1.$

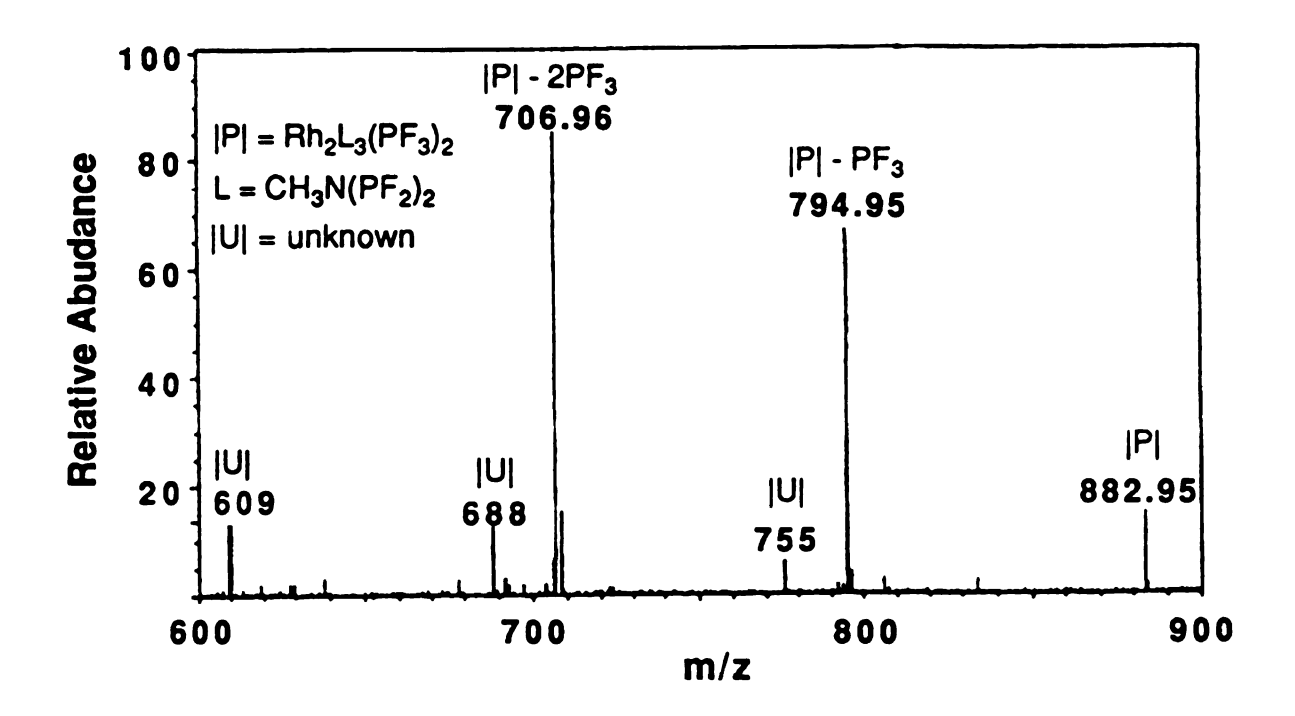


Figure 11

FAB mass spectrum of $Rh_2[CH_3N(PF_2)_2]_3(PF_3)Cl_2$, 2 prepared by method i of Section II.A.2c.

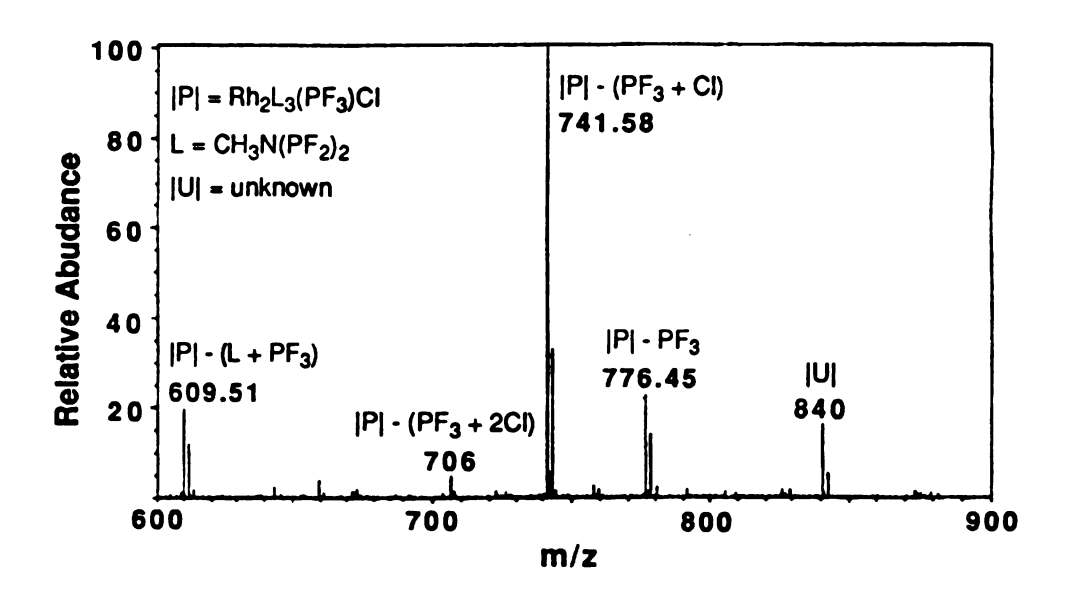


Figure 12

FAB mass spectrum of $Rh_2[CH_3N(PF_2)_2]_3Cl_4$, 3.

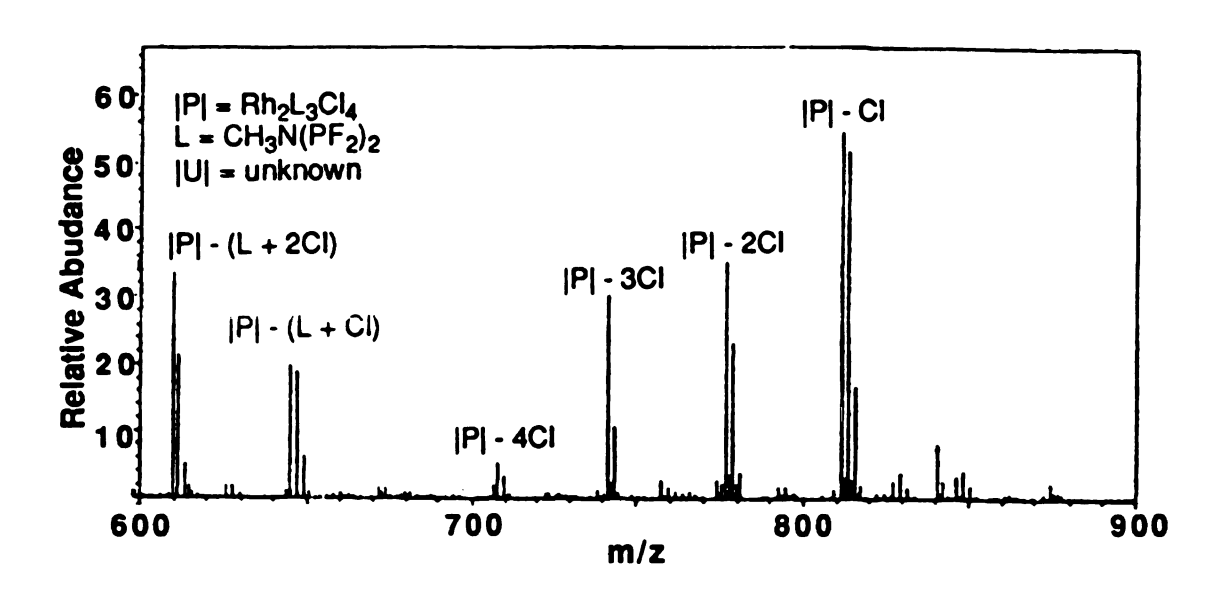


Figure 13

Isotope peak-intensity pattern for ions containing the indicated number of chlorine atoms (from ref. 123).

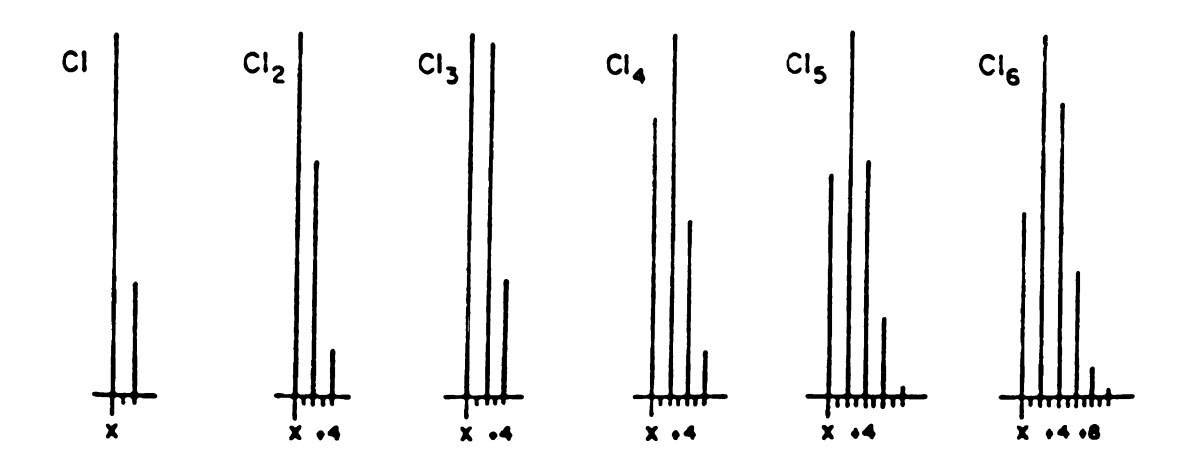


Figure 14

peak intensity pattern is observed. Molecular ions were not observed for 2 and 3. The mass spectrum of 2 shows fragments due to the loss of PF₃ at m/z of 776.45 and the loss of chlorines from the fragments at m/z of 741.50 and 706.48, respectively. Also the fragment due to the loss of $CH_3N(PF_2)_2$ and a PF₃ ligand is observed at m/z of 609.51. For 3 the FAB mass spectrum clearly shows the successive loss of chlorines (m/z of 811.46, 776.54, 741.65, and 707.66). Fragments due to the loss of $CH_3N(PF_2)_2$ and chlorine, and $CH_3N(PF_2)_2$ and two chlorines (m/z of 644.57, and 605.59, respectively) are also apparent.

In 2 and 3 unknown peaks at a m/z of 874 and 840 are observed. The peak at m/z of 874 show no chlorine isotope pattern, and the peak at m/z of 840 indicates one chlorine atom is present. However no other fragments arising from this ion were detected. It is likely that these unknown peaks arise from matrix contributions.

The mass spectral analysis provides a convenient analytical tool for assessing the optimal conditions for the preparation of compounds 1-3. To prepare 2 in good yield, a mole ratio of $[RhCl(PF_3)_2]_2$ to $CH_3N(PF_2)_2$ of at least 1:5 was needed (Section II.A.2.c). If the ratio is approximately 1:2, a mixture of 2 and $Rh_3(\mu-Cl)_3[\mu-CH_3N(PF_2)_2]_3$ (see Section II.A.3) was obtained. Several attempts were made to purify 2 by column chromatography, but decomposition on Florisil® or silica gel was observed. Pure 2 could only be obtained by several recrystallizations from CH_2Cl_2 /hexane mixtures. The FAB mass spectra of 2 prepared by methods ii and iii are shown in Figures 15 and 16. The mass spectra of product 2 prepared by these alternative methods are similar to those obtained for compound prepared by method i

FAB mass spectrum of $\mathrm{Rh_2[CH_3N(PF_2)_2]_3(PF_3)Cl_2}$, 2, prepared by method ii of Section II.A.2.c.

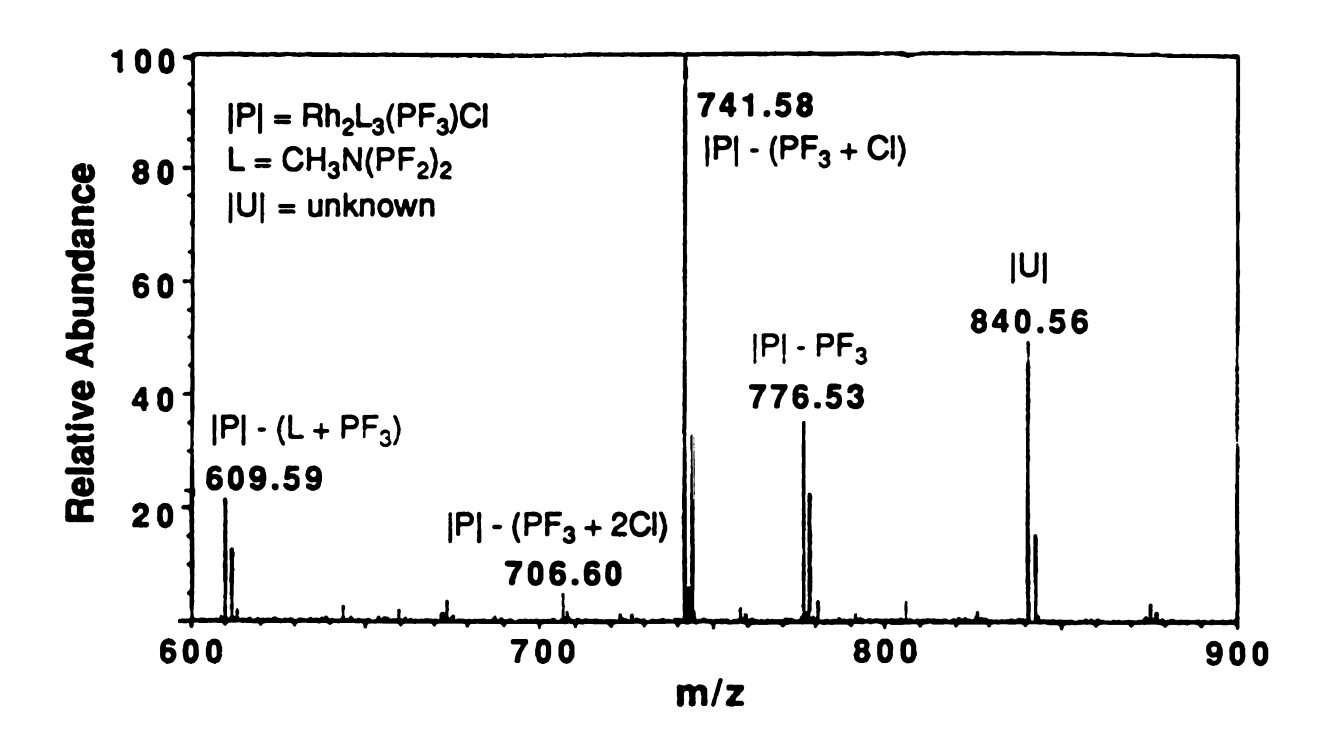


Figure 15

FAB mass spectrum of $\mathrm{Rh_2[CH_3N(PF_2)_2]_3(PF_3)Cl_2}$, 2, prepared by method iii of Section II.A.2.c.

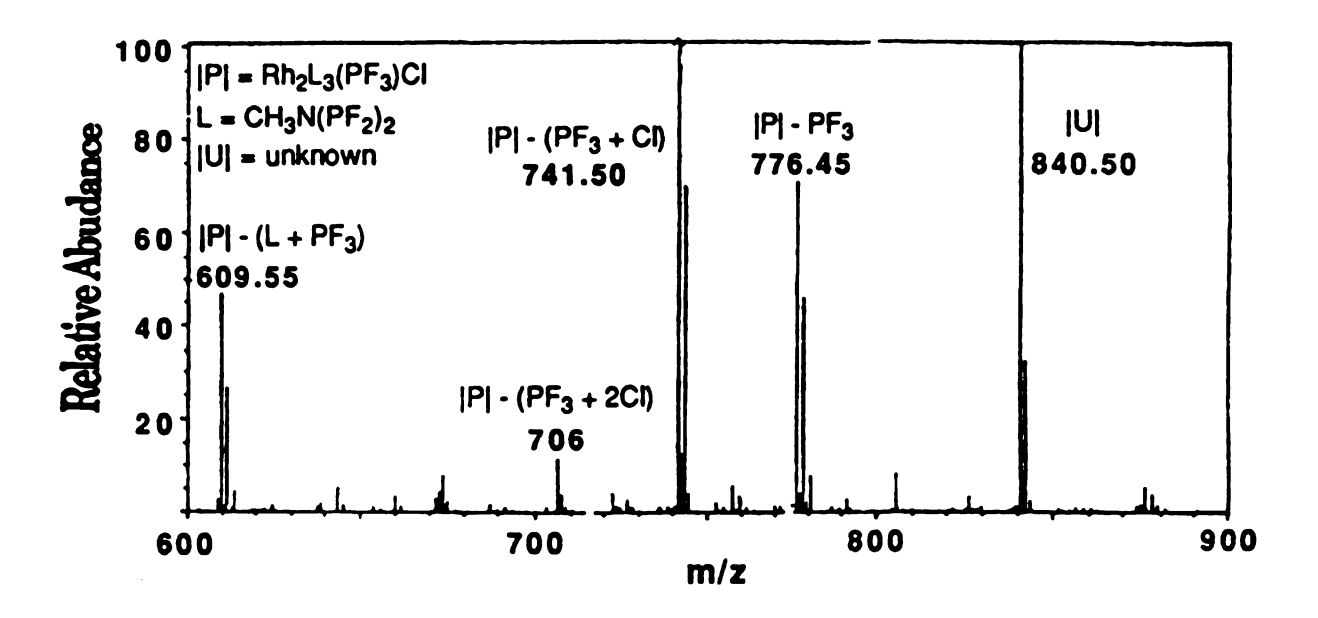


Figure 16

A series of reducing reactions from higher valent Rh₂ complexes were employed in an attempt to increase the yield of 1. In early attempts, 2 was used as the starting material with sodium borohydride (NaBH₄) as the reducing agent in the presence of PF₃. The product was 1, as determined by absorption spectroscopy, but only oils could be isolated. The same result was obtained by reducing 3 with NaBH₄ in ethanol. In benzene, no reaction took place with NaBH₄ or butyllithium [CH₃(CH₂)₃Li] as the reducing agents. With sodium amalgam (NaHg) as the reducing agent in THF at 0°C, a sticky purple precipitate formed when the solvent was removed under vacuum. The precipitate was not identified. The reducing agent tetrabutylammonium iodide (Bu₄NI) was alsoused under various conditions. The solvent for all reactions was CH₂Cl₂ and solutions of $[RhCl(PF_3)_2]_2$, $CH_3N(PF_2)_2$, and Bu_4NI at a mole ratio of 1:6:2 were stirred under PF₃, refluxed under argon, or heated to 43 °C for 12 h in the presence of PF₃. An unknown red precipitate or a red oil was typically obtained from these various reactions. The result was the same when the reaction was performed in benzene contained in a high pressure vessel heated to 65 °C for 12 h under PF₃. Alternatively sodium acenaphthylenide (NaAc) reduced solutions of $[RhCl(PF_3)_2]_2$ in the presence of PF₃ and CH₃N(PF₂)₂ in THF. A brown precipitate obtained from this reaction. The electronic absorption spectrum from this reaction indicated the brown precipitate to be a mixture of 2, NaAc, and presumably 1 indicated by a shoulder at 310 nm in the electronic absorption spectrum. The mixture could not be seperated by column chromatography.

The most convenient way to prepare 3 was to oxidize 2 with a slight excess of the oxidizing agent Cl₂IC₆H₅. The complex can also be prepared

by starting with Rh₂(O₂CCH₃)₄. Me₃SiCl is used to remove the carboxyl group, and as a source of chloride ligands. The absorption spectrum of the product from this method was the same as 3, but the yield was much lower. An unsuccessful attempt to prepare 3 was undertaken when Cl₂ gas was bubbled into a solution of 1.

b. Structural Interpretation. The crystal parameters and details of intensity collection for 1, 2, and 3 are listed in Table 1. Positional parameter for 1, 2, and 3 are listed in Table 2 - 4, respectively. The molecular structures adopted by 1, 2, and 3 are unique for dirhodium chemistry; they are represented by the ORTEP diagrams reproduced in Figures 17, 18, and 19. The presence of three bidentate fluorophosphine ligands in these structures is unusual and in contrast to the trans coordination of two bidendate ligands of the ubiquitous A-frame structures for dirhodium complexes. 124,125 Complexes 1, 2, and 3 are structurally distinguished among themselves by their rhodium coordination environments of which there are two basic types. illustrated by the inner coordination spheres depicted in Figure 20, trigonal bypyrimidal and octahedral coordination gives rise to the symmetrical structures of 1 and 3, respectively, and to the unsymmetrical structure of 2. In the case of 1, the coordination geometry about each Rh(0) is nearly an ideal trigonal bipyramid whose equatorial plane is comprised of three phosphorus atoms from each of the bridging fluorophosphine ligands, and whose apices are capped by the phosphorus of a terminal trifluorophosphine and by the neighboring Rh(0) of the The trigonal bipyramidal coordination of the Rh(0) binuclear core. centers is contrasted by the pseudooctahedral ligation sphere of Rh(II). In 3, the three phosphorus atoms of the individual fluorophosphine

Table 1. Crystal Data for $Rh_2[CH_3N(PF_2)_2]_3(PF_3)_2$ (1), $Rh_2[CH_3N(PF_2)_2]_3Cl_2(PF_3)$ (2), and $Rh_2[CH_3N(PF_2)_2]_3Cl_4(3)$

	1	8	8
formula	RhoF 12PaN2C3Ho	RhoF 1 CloP, NaCaHo	RhoF, CIAP N.C. Ho
formula weight	882.70	865.64	848.57
crystal dimensions, mm	$0.14 \times 0.32 \times 0.44$	$0.36 \times 0.45 \times 0.56$	$0.04 \times 0.10 \times 0.42$
crystal system	triclinic	orthorhombic	monoclinic
space group	P 1	P 2,2,2,	C 2/c
unit cell parameters		i i	
a, A	10.021(4)	9.620(2)	15.462(2)
b, A	10.139(4)	12.755(2)	10.999(2)
c, A	14.299(7)	19.564(3)	14.256(2)
α,deg	74.95(3)	8	06
g, deg	76.79(3)	6 6	107.52(1)
S,deg	62.17(3)	8	6
V, Å3	1230.9(9)	2400.6(6)	2312.0(6)
, 2	8	4	7
Pealed, g/cm 3	2.38	2.40	2.44
μ(Mo Kα), cm ⁻¹	19.7	21.5	23.8
radiation (λ, Å)	Mo Ka(0.71073)	Mo Ka(0.71073)	Mo Ka(0.71073)
temp, °C	23(1)	27(1)	-70(3)
scan method	0 - 20	0 - 20	θ - 2θ
scan rate, deg min ⁻¹	4	4	4
no. of unique data, total			
with $F_c^2 > 3\sigma(F_c^2)$	4172, 3149	4889, 3880	2560, 1623
no. of parameters refined	307	8 80	137
transmission factors, min, max	0.759, 1.363	0.465, 0.547	0.789, 1.153
8 H	0.067	0.026	0.042
R. D	0.078	0.025	0.045
GÖF°	3.14	1.20	2.54
	9 1 9	6	6

 ${}^{\mathbf{a}}R = \Sigma | |F_{o}| - |F_{e}| |/\Sigma |F_{o}|. \ {}^{\mathbf{b}}R_{\mathbf{w}} = [\Sigma w (|F_{o}| - |F_{e}|)^{2}/\Sigma w |F_{o}|^{2}]^{1/2}; w = 1/\sigma^{2}(|F_{o}|). \ {}^{\mathbf{c}} \operatorname{Goodness\ of\ fit} = [\Sigma w (|F_{o}| - |F_{e}|)^{2}/(N_{\mathrm{obsd}} - N_{\mathrm{parameters}})]^{1/2}.$

Table 2. Atomic Positional and Isotropic Displacement (Å 2) Parameters for $\mathbb{R}h_2[CH_3N(PF_2)_2]_3(PF_3)_2$ (1) ^a

Atom	x	y	z	$B/ ext{\AA}^2$
I Rh(1)	0.1433(1)	0.7525(1)	0.72377(8)	4.19(3)
R h(2)	0.2718(1)	0.9001(1)	0.79385(8)	4.12(3)
P (1)	0.2870(5)	0.7771(5)	0.5849(3)	6.4(1)
P (2)	0.4753(4)	0.7929(5)	0.6908(3)	5.5(1)
P (3)	-0.0786(4)	0.9434(5)	0.7599(3)	5.1(1)
P(4)	0.0807(5)	1.1139(4)	0.7367(3)	5.0(1)
P (5)	0.2357(4)	0.5608(4)	0.8454(3)	5.1(1)
P (6)	0.2353(4)	0.7682(4)	0.9400(3)	4.9(1)
P (7)	0.0472(5)	0.6428(5)	0.6695(4)	6.9(1)
P (8)	0.3708(5)	1.0138(5)	0.8463(4)	6.6(1)
F (1)	0.334(1)	0.665(1)	0.5174(8)	10.9(4)
$\mathbf{F}(2)$	0.223(1)	0.923(1)	0.5013(8)	11.1(5)
F (3)	0.581(1)	0.875(1)	0.6520(9)	9.1(3)
F (4)	0.605(1)	0.628(1)	0.7260(9)	9.1(4)
F (5)	-0.214(1)	0.978(1)	0.7059(8)	8.3(3)
F (6)	-0.170(1)	0.937(1)	0.8620(7)	7.9(3)
F (7)	0.030(1)	1.2552(9)	0.7847(8)	8.2(3)
F (8)	0.098(1)	1.199(1)	0.6290(7)	7.7(3)
F (9)	0.150(1)	0.463(1)	0.8860(8)	8.3(3)
F (10)	0.392(1)	0.425(1)	0.8320(8)	8.4(4)
F (11)	0.351(1)	0.726(1)	1.0128(7)	8.5(3)
F (12)	0.092(1)	0.838(1)	1.0133(7)	8.5(4)
F (13)	0.147(1)	0.478(1)	0.6463(9)	11.1(4)
F (14)	-0.0807(9)	0.608(1)	0.7324(9)	8.9(3)
F (15)	-0.028(1)	0.716(1)	0.5756(8)	13.2(4)
F (16)	0.411(1)	1.136(1)	0.7778(9)	9.8(4)
F (17)	0.524(1)	0.921(1)	0.884(1)	11.4(4)
F (18)	0.278(1)	1.107(1)	0.9268(8)	9.6(3)
N (1)	0.453(1)	0.777(1)	0.584(1)	6.3(4)
N(2)	-0.088(1)	1.113(1)	0.7419(8)	5.3(3)
N(3)	0.240(1)	0.600(1)	0.9514(9)	5.4(3)
C (1)	0.580(2)	0.742(2)	0.504(1)	10.2(7)
C (2)	-0.233(2)	1.259(2)	0.735(1)	7.6(5)
C (3)	0.257(2)	0.489(2)	1.045(1)	8.6(7)

^a Anisotropically refined atoms are given in the form of the isotropic equivalent displacement parameter defined as $4/3[a^2B_{11}+b^2B_{22}+c^2B_{33}+ab(\cos\gamma)B_{12}+ac(\cos\beta)B_{13}+bc(\cos\alpha)B_{23}]$.

Table 3. Atomic Positional and Isotropic Displacement (Å 2) Parameters for $\mathbf{Rh}_2[\mathrm{CH}_3\mathrm{N}(\mathrm{PF}_2)_2]_3\mathrm{Cl}_2(\mathrm{PF}_3)$ (2) ^a

Atom	x	y	z	$B/ ext{\AA}^2$
Rh(1)	0.27066(5)	0.00685(4)	0.07903(3)	3.020(7)
Rh(2)	0.10328(5)	0.07458(4)	0.18646(2)	2.934(7)
C l(1)	0.4119(2)	-0.0632(2)	-0.0133(1)	5.75(4)
C l(2)	0.4552(2)	0.1142(2)	0.1206(1)	4.36(4)
P(1)	0.1040(2)	-0.0907(2)	0.0379(1)	4.25(4)
P(2)	-0.0719(2)	-0.0123(2)	0.14032(9)	3.32(3)
P (3)	0.3668(2)	-0.1162(2)	0.1473(1)	4.61(4)
P (4)	0.2632(2)	0.0029(2)	0.25600(9)	4.17(4)
P (5)	0.2086(2)	0.1511(2)	0.0202(1)	3.98(4)
P (6)	0.1393(2)	0.2383(1)	0.1468(1)	3.41(3)
P (7)	-0.0261(3)	0.1256(2)	0.2709(1)	5.12(5)
F (1)	0.0737(6)	-0.0770(5)	-0.0388(2)	8.0(1)
$\mathbf{F}(2)$	0.1319(6)	-0.2101(4)	0.0360(4)	7.9(1)
F (3)	-0.2015(5)	0.0526(4)	0.1190(3)	6.4(1)
F (4)	-0.1563(5)	-0.0903(4)	0.1855(3)	6.4(1)
F (5)	0.3211(7)	-0.2324(4)	0.1391(3)	7.4(2)
F (6)	0.5224(5)	-0.1346(5)	0.1350(4)	8.3(2)
F (7)	0.2082(6)	-0.0451(4)	0.3241(2)	6.4(1)
F (8)	0.3748(6)	0.0732(5)	0.2911(3)	7.0(1)
F (9)	0.0881(7)	0.1439(5)	-0.0310(3)	7.7(1)
F (10)	0.3184(7)	0.1906(4)	-0.0307(3)	7.0(1)
F (11)	0.0138(5)	0.3143(4)	0.1539(3)	5.5(1)
F(12)	0.2456(5)	0.3147(3)	0.1805(3)	5.4(1)
F (13)	-0.1496(8)	0.1924(7)	0.2555(4)	14.7(2)
F(14)	-0.0945(7)	0.0494(5)	0.3182(3)	9.7(2)
F(15)	0.0331(9)	0.1919(6)	0.3257(3)	12.3(2)
N(1)	-0.0524(6)	-0.0831(5)	0.0701(3)	3.9(1)
N(2)	0.3614(7)	-0.0963(6)	0.2291(4)	5.2(2)
N(3)	0.1749(6)	0.2571(5)	0.0646(3)	3.8(1)
C (1)	-0.1715(8)	-0.1436(7)	0.0391(5)	5.8(2)
C(2)	0.449(1)	-0.159(1)	0.2783(6)	9.7(3)
C (3)	0.186(1)	0.3651(6)	0.0349(5)	5.6(2)

^a Anisotropically refined atoms are given in the form of the isotropic equivalent displacement parameter defined as $4/3[a^2B_{11}+b^2B_{22}+c^2B_{33}+ab(\cos\gamma)B_{12}+ac(\cos\beta)B_{13}+bc(\cos\alpha)B_{23}]$.

Table 4. Atomic Positional and Isotropic Displacement (Å 2) Parameters for ${\rm IRh_2[CH_3N(PF_2)_2]_3Cl_4}$ (3) a

Atom	x	у	z	$B/ ext{\AA}^2$
Rh(1)	0.03788(4)	0.25217(7)	0.17586(4)	1.824(9)
Cl(1)	0.0943(1)	0.2502(3)	0.0352(1)	3.18(4)
Cl(2)	0.1755(1)	0.1618(2)	0.2759(2)	3.25(5)
P(1)	-0.0044(2)	0.0537(2)	0.1500(2)	2.61(4)
P(3)	-0.0846(2)	0.3444(2)	0.0873(2)	2.71(4)
P(4)	-0.1147(2)	0.4203(2)	0.2637(2)	3.01(5)
F (1)	0.0586(4)	-0.0229(5)	0.1078(3)	3.4(1)
F(2)	-0.0952(4)	0.0165(5)	0.0756(4)	3.7(1)
F(5)	-0.0708(4)	0.4334(5)	0.0092(4)	3.9(1)
F (6)	-0.1588(3)	0.2650(6)	0.0166(4)	4.2(1)
F(7)	0.0747(4)	0.5480(5)	0.1973(4)	4.5(1)
F(8)	0.2071(4)	0.4332(6)	0.2189(4)	4.8(1)
N(1)	0.000	-0.0257(9)	0.250	3.0(2)
N(2)	-0.1389(4)	0.4340(7)	0.1439(5)	2.7(1)
C(1)	0.000	-0.163(1)	0.250	6.3(5)
C(2)	-0.2091(6)	0.5243(9)	0.0866(8)	4.0(2)

^a Anisotropically refined atoms are given in the form of the isotropic equivalent displacement parameter defined as $4/3[a^2B_{11}+b^2B_{22}+c^2B_{33}+ab(\cos\gamma)B_{12}+ac(\cos\beta)B_{13}+bc(\cos\alpha)B_{23}]$.

ORTEP drawing and numbering scheme of $Rh_2[CH_3N(PF_2)_2]_3(PF_3)_2$, 1 with 30% probability thermal ellipsoids. For clarity hydrogen atoms are not shown. Selected bond distances and angles are listed in Table 5.

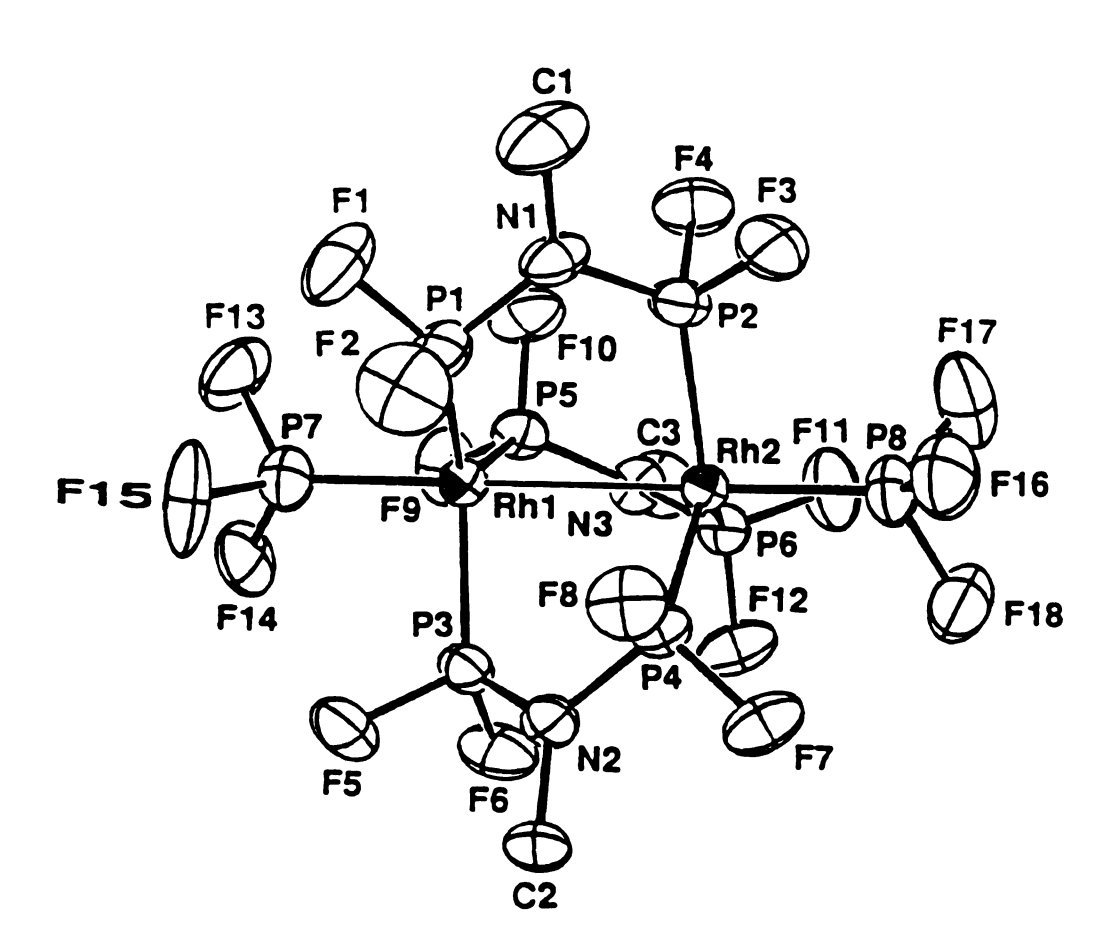


Figure 17

An ORTEP view of $Rh_2[CH_3N(PF_2)_2]_3(PF_3)Cl_2$, 2, showing the numbering scheme. Thermal parameters are shown at the 50% level. Hydrogen atoms are omitted for the sake of clarity. Table 6 lists selected bond distances and angles.

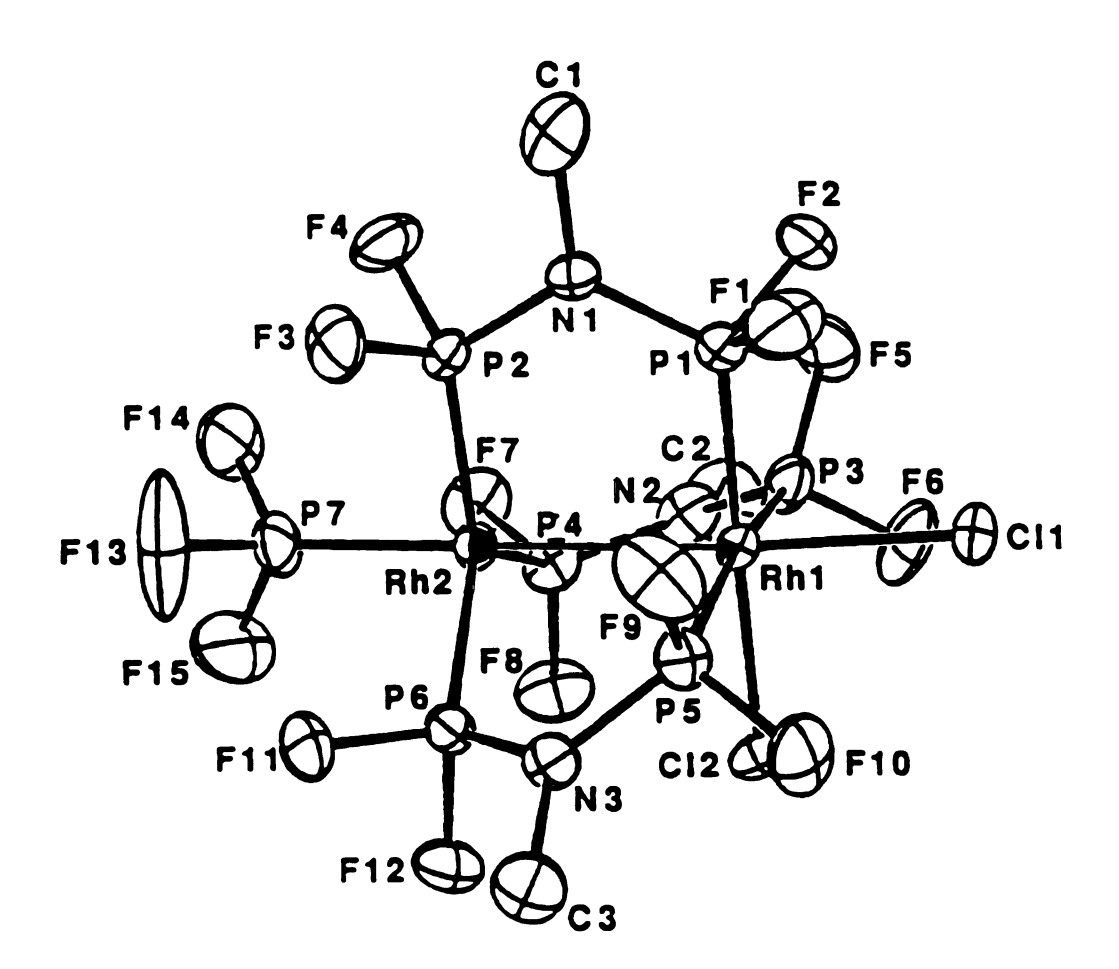


Figure 18

An ORTEP view of $Rh_2[CH_3N(PF_2)_2]_3Cl_4$, 3, showing the numbering scheme. Thermal ellipsoids are at the 50% probability level; hydrogen atoms are not shown. Table 7 lists selected bond distances and angles.

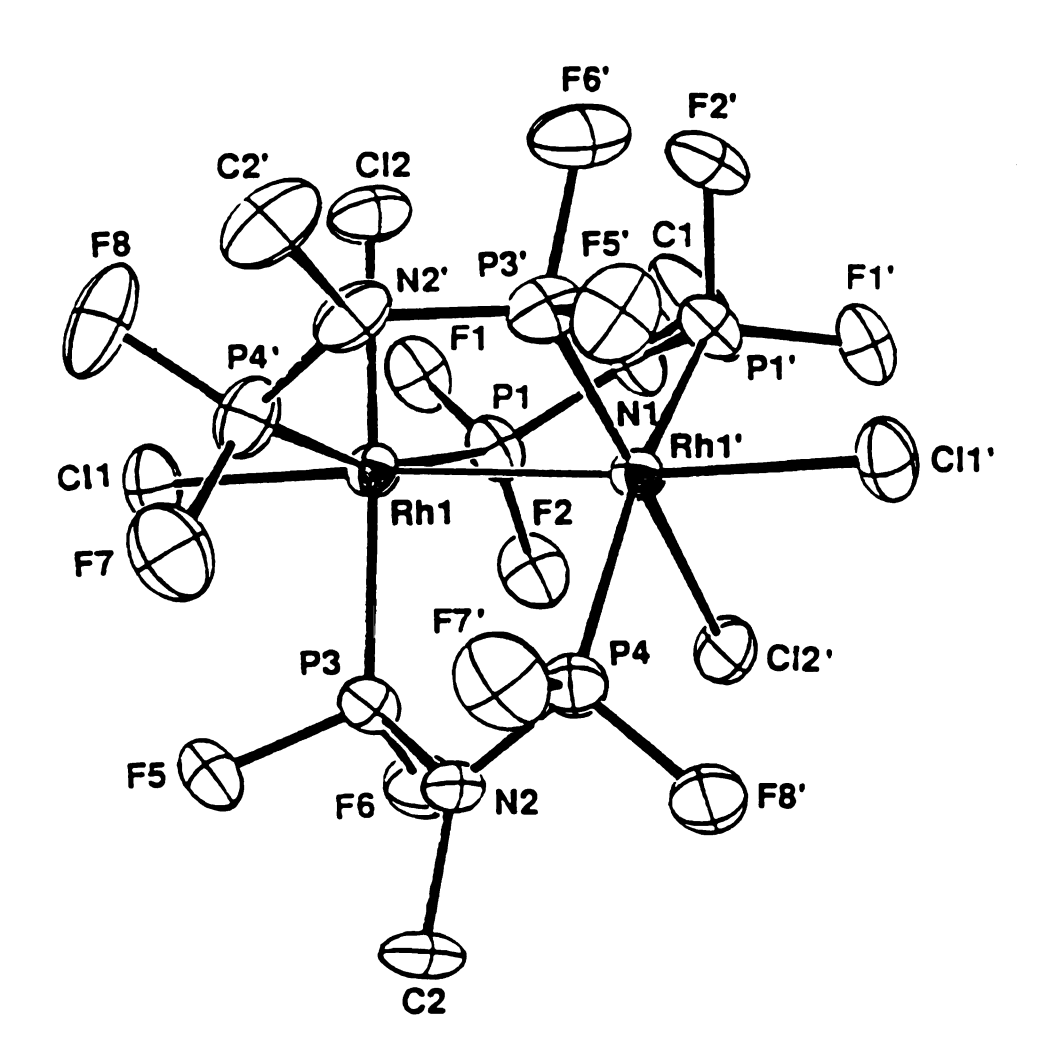


Figure 19

A skeletal view of the inner coordination spheres of (a) 1, (b) 2, and (c) 3.

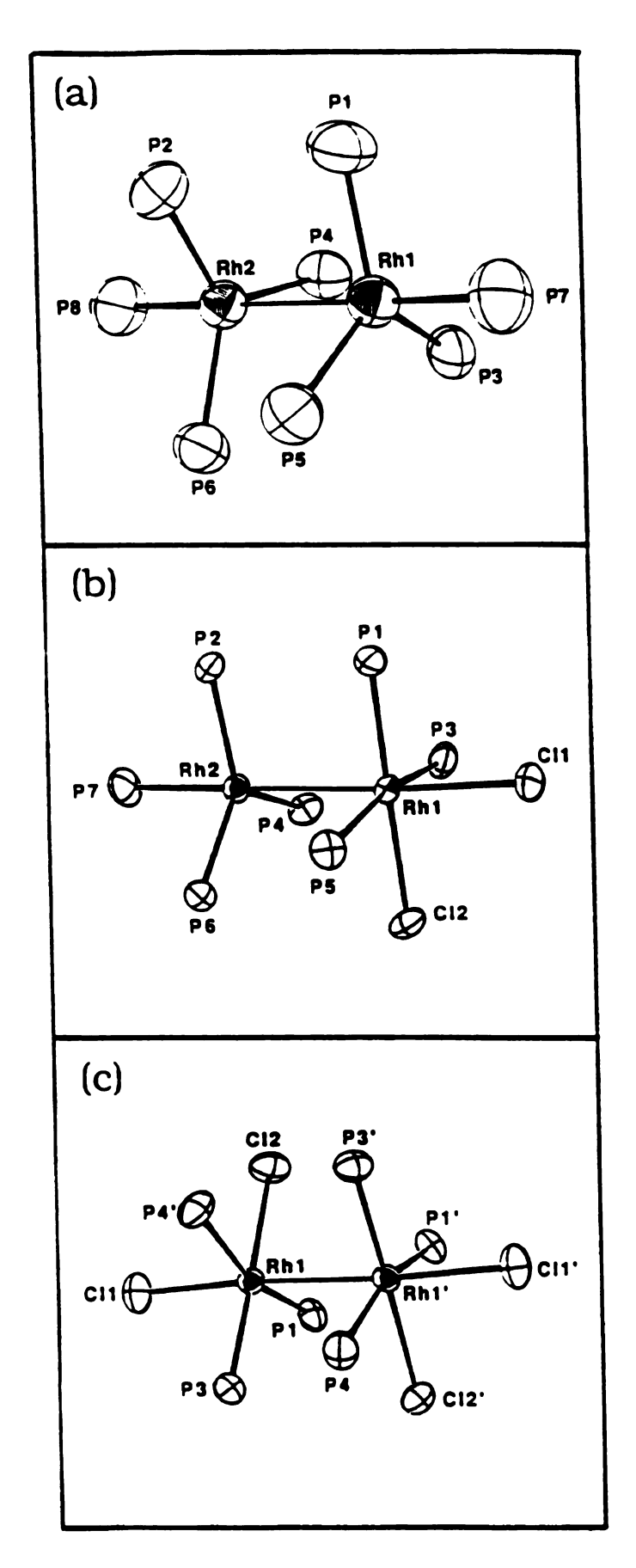


Figure 20

ligands adopt a meridional arrangement with a chlorine atom occupying the fourth site of the equatorial coordination plane. The pseudooctahedron about the Rh(II) is completed with the axial coordination of a chlorine atom and a Rh(II). The mutually trans arrangement of chlorines on adjacent Rh(II) centers has previously been postulated to be present in trans-Rh₂Cl₂(CO)₂(dmpm)₂ (dmpm = bis(dimethylphosphino)methane) and indeed observed for its chlorine oxidation product, trans-Rh₂Cl₂(CO)₂(dmpm)₂. With 1 and 3 as structural benchmarks, we see that the unsymmetrical congener, 2, is simply a structural composite of the Rh₂(0,0) and Rh₂(II,II) complexes in which the trigonal bipyramidal coordination about Rh(0) and octahedral coordination about Rh(II) is preserved.

Inspection of the selected bond angles and distances of 1, 2, and 3 listed in Tables 5 - 7 reveals several interesting trends. It is noteworthy that the Rh-Cl bonds trans to the rhodium-rhodium axis in 2 (d(Rh-Cl_{ax}) = 2.431(2) Å) and 3 (d(Rh-Cl_{ax}) = 2.416(2) Å) are significantly longer than the Rh-Cl bonds cis $(d(Rh-Cl_{eq}) = 2.385(2) \text{ Å in 2 and } d(Rh-Cl_{eq}) =$ 2.392(2) Å in 3) to it. Long axial Rh-Cl bonds have previously been attributed to the trans influence of the metal-metal bond. 127,128 However, in the case of 2 and 3, it is not that the Rh-Clax bonds are unusually long but rather that the Rh-Cl_{eq} bonds are short. These observations are congruent with simple bonding considerations. The good π -accepting ability of the fluorophosphine ligands should selectively enhance π donation from trans chlorine atoms. Accordingly, the π -backbonding between the rhodium and chlorine will be strengthened thereby resulting in a shortening of the Rh-Cl_{eq} bond. This simple bonding model is further supported by comparison of Rh-P distances. The resulting

Table 5. Selected Bond Distances (Å) and Bond Angles (deg) for Rh₂[CH₃N(PF₂)₂]₃(PF₃)₂ (1)

	distance ⁸	2.214(4)	2.225(3)	2.224(4)	2.176(6)			angle ^a	85.2(2)	85.4(2)	86.0(2)	179.5(1)	118.6(2)	119.7(1)	94.5(2)	119.9(1)	94.5(2)	94.5(2)		angle ^a	-30.39(17)	-32.29(16)	-29.07(16)
	n 2		_	_				atom 3	P(2)	P(4)	P(6)	P(8)	P(4)	P(6)	P(8)	P(6)	P(8)	P(8)					
	atom 2	P(2)	P(4	P(6)	P(8)			atom 2	Rh(2)	Rh(2)	Rh(2)	Rh(2)	Rh(2)	Rh(2)	Rh(2)	Rh(2)	Rh(2)	Rh(2)		atom 4	P(2)	P(4)	P(6)
Bond Distances	atom 1	Rh(2)	Rh(2)	Rh(2)	Rh(2)		Bond Angles	atom 1	Rh(1)	Rh(1)	Rh(1)	Rh(1)	P(2)	P(2)	P(2)	P(4)	P(4)	P(6)	Torsional Bond Angles	atom 3	Rh(2)	Rh(2)	Rh(2)
Во	distance ^a	2.841(2)	2.203(4)	2.222(3)	2.227(4)	2.134(7)		angle a	86.0(2)	85.4(2)	86.4(2)	179.4(1)	120.6(2)	121.2(1)	93.4(2)	116.8(1)	94.7(2)	94.1(2)	Torsio	m 2	1(1)	(1)	1(1)
	n 2	(2)	≏	≅	23	2		atom 3	P(1)	P(3)	P(5)	P(7)	P(3)	P(5)	P(7)	P(5)	P(7)	P(7)		atom	Rh(8	R
	atom 2	Rh	2	PC	P	P(7)		atom 2	Rh(1)	Rh(1)	Rh(1)	Rh(1)	Rh(1)	Rh(1)	Rh(1)	Rh(1)	Rh(1)	Rh(1)		atom 1	P(1)	P(3)	P(5)
	atom 1	Rh(1)	Rh(1)	Rh(1)	Rh(1)	Rh(1)		atom 1	Rh(2)	Rh(2)	Rh(2)	Rh(2)	P(1)	P(1)	P(1)	P(3)	P(3)	P(5)					

a Numbers in parentheses are estimated standard deviations in the least significant digits.

Table 6. Selected Bond Distances (Å) and Bond Angles (deg) for Rh₂[CH₃N(PF₂)₂]₃Cl₂(PF₃) (2)

Table 6 (cont.)

Torsional Bond Angles

atom 1	atom 2	atom 3	atom 4	angle ^a
P(1)	Rh(1)	Rh(2)	P(2)	-4.81(8)
P(3)	Rh(1)	Rh(2)	P(4)	22.76(8)
P(5)	Rh(1)	Rh(2)	P(6)	-26.43(7)

a Numbers in parentheses are estimated standard deviations in the least significant digits.

Table 7. Selected Bond Distances (Å) and Bond Angles (deg) for $\mathrm{Rh}_2[\mathrm{CH}_3\mathrm{N}(\mathrm{PF}_2)_2]_3\mathrm{Cl}_4$

			Bond Distances	tances			
atom 1	atom 2		distance ^b	atom 1	atom 2	m 2	distance ^b
Rh(1) Rh(1) Rh(1)	Rh(1)' Cl(1) Cl(2)		2.707(1) 2.416(2) 2.392(2)	Rh(1) Rh(1) Rh(1)	7	P(1) P(4)' P(3)	2.277(2) 2.226(2) 2.184(2)
			Bond Angles	Angles			
atom 1	atom 2	atom 3	angle ^b	atom 1	atom 2	atom 3	angle ^b
Rh(1)'	Rh(1)	Cl(1)	175.75(5)	Cl(1)	Rh(1)	P(4)'	92.56(6)
Rh(1)'	Rh(1)	CI(2)	92.94(6)	CI(2)	Rh(1)	P(1)	81.86(8)
Rh(1)'	Rh(1)	P(1)	87.48(7)	CI(2)	Rh(1)	P(3)	176.86(9)
Rh(1)'	Rh(1)	P(3)	87.01(7)	CI(2)	Rh(1)	P(4),	80.75(6)
Rh(1).	Rh(1)	P(4)'	90.21(2)	P(1)	Rh(1)	P(3)	101.28(9)
CI(1)	Rh(1)	CI(2)	90.69(8)	P(1)	Rh(1)	P(4)'	162.31(6)
Cl(1)	Rh(1)	P(1)	90.85(9)	P(3)	Rh(1)	P(4)′	96.11(7)
CI(1)	Rh(1)	P(3)	89.49(9)				
			Torsional Bond Angles	nd Angles			
	atom 1	atom 2	atom 3		atom 4	angle ^b	
	P(1) P(3)	Rh(1) Rh(1)	Rh(1)' Rh(1)');	P(1)' P(4)	32.61 -28.43	

^a Atoms designated by the prime () symbol are at: -x, +y, $\frac{1}{2}-z$. ^b Numbers in parentheses are estimated standard deviations in the least significant digits.

synergism established between the π -donating chlorine and the π -accepting fluorophosphine should not only strengthen the Rh–Cl_{eq} bond but should also be manifested in increased π -backbonding interactions between rhodium and the phosphorus trans to chlorine. This appears to be the case. As observed in Tables 6 and 7, the Rh–P distances for phosphorus trans to chlorine (d(Rh–P_{t,Cl}) = 2.183(2) Å in 2, d(Rh–P_{t,Cl}) = 2.184(2) Å in 3) are at least 0.07 Å shorter than those for phosphorus trans to another phosphorus (d(Rh–P_{t,P})_{av} = 2.255(2) Å in 2, d(Rh–P_{t,P})_{av} = 2.252(25) Å in 3). The latter distances are more typical of normal Rh(II)–P bonds. ^{126,129,130}

As a concluding issue, we consider the Rh…Rh bond distances. Separations of 2.841(2) Å, 2.785(1) Å, 2.707(1) Å in 1, 2, and 3, respectively, are indicative of a normal Rh-Rh single bond. The decrease along the series $Rh_2(0,0) > Rh_2(0,II) > Rh_2(II,II)$ is expected in view of the larger atomic radii of Rh(0) as compared to Rh(II). Although the Rh-Rh distances are considerably longer than those observed for rhodium carboxylates, 131-133 they are typical of Rh-Rh cores ligated by bidentate phosphines containing one bridgehead atom. 126,134-136, The presence of a single bond in 1, 2, and 3 induces significant rotation of the bridging fluorophosphine ligands away from an eclipsed conformation. The view along the nearly linear L-Rh-Rh-L' (L, L' = Cl or PF₃) bond axis of 1, 2, and 3 (Figure 21) clearly reveals a twisted conformation of the bidentate ligands. An average torsional angle $\chi_{av} = 30.6^{\circ}$ for 1 is comparable to the 33.3° twist angle reported for the bis(difluorophosphino)methylamine ligands in Co₂[CH₃N(PF₂)₂]₃(CO)₂, ¹⁴⁵ and is virtually identical to 3's average torsional angle of 30.5°. This remarkable flexibility of the bis(difluorophosphino)methylamine ligand allows the coordination

Structural framework of (a) 1, (b) 2, and (c) 3 as viewed nearly along the Rh-Rh axis. Axial ligands are omitted.

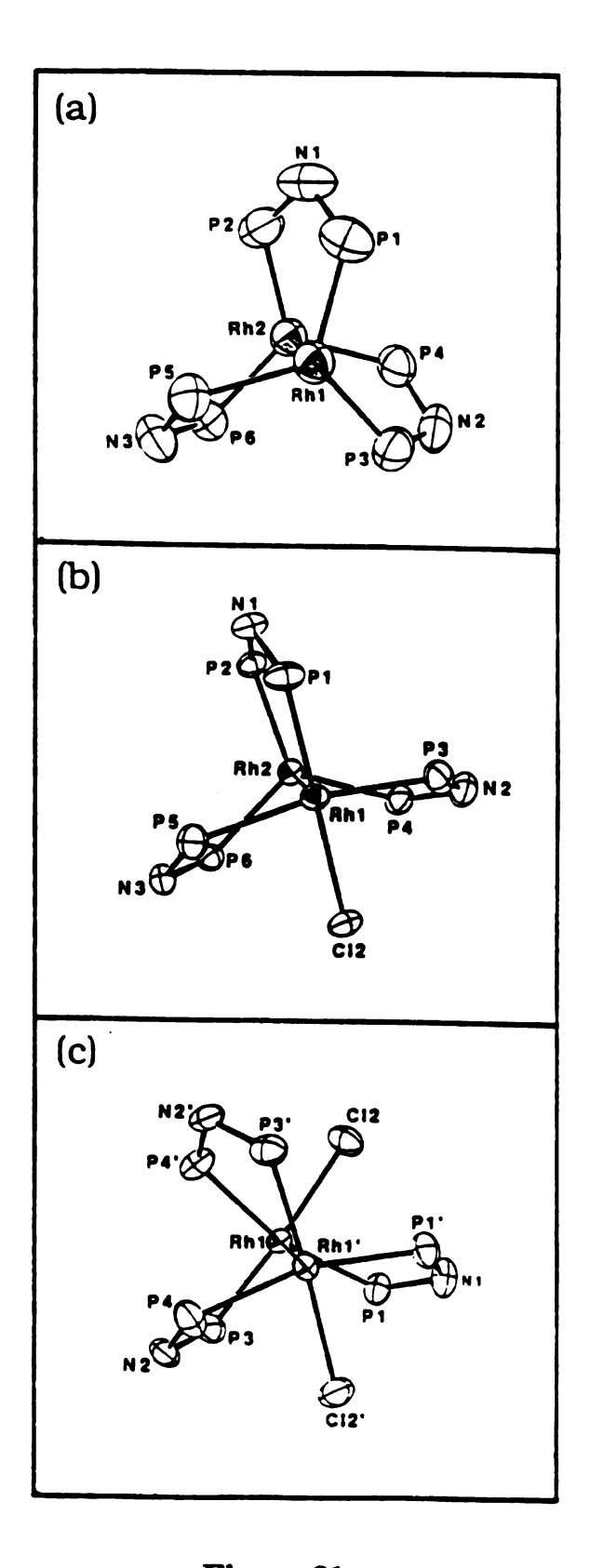


Figure 21

asymmetry about the dirhodium core in 2 to be accommodated with facility and, indeed, undoubtedly plays a crucial role in the stabilization of the unusual mixed-valence Rh₂(0,II) core.

c. Electronic Absorption and Emission Spectra. The electronic absorption spectra of the dirhodium fluorophosphine complexes 1, 2, and 3 are shown in Figures 22 - 24. The spectra exhibit pronounced absorptions in the ultraviolet spectral region with less intense absorption bands in the visible. The electronic absorption spectrum of 2 by methods ii and iii (Section A. 2. c) are similar to method i except that the former do not exhibt the low energy band at 570 cm⁻¹. Red luminescence is observed from solids and low temperature glasses of 1, 2, and 3 upon excitation with frequencies coincident with absorption manifold. In Figures 22 - 24 we show the emission spectra recorded on crystalline solids of 1, 2, and 3 at 77 K. Each displays an intense band in the red spectral region, and 1 and 3 feature an additional emission to higher The intensity of the emissions monotonically decrease with increasing temperature. Although luminescence from 3, which is the brightest lumophore of the series, can be detected to room temperature, the luminescence from 1 and 2 reach the limits of our instrumentation by ~ 220 K. This temperature dependence in emission intensity is accompanied by an extreme temperature sensitivity of the emission halfwidth, increasing by approximately 1000 - 1500 cm⁻¹ from 77 K to the highest temperatures at which emission can be detected. spectra are vibrationally featureless, and remain so to temperatures as low as 10 K. The emission maximum of 2 by methods i, ii and iii vary from 780, 750, and 730 nm, respectively. The reason for the variations are

Electronic absorption spectrum (——) of 1 dissolved in CH_2Cl_2 at room temperature, and corrected emission spectrum (- - -) of crystalline 1 at 77 K.

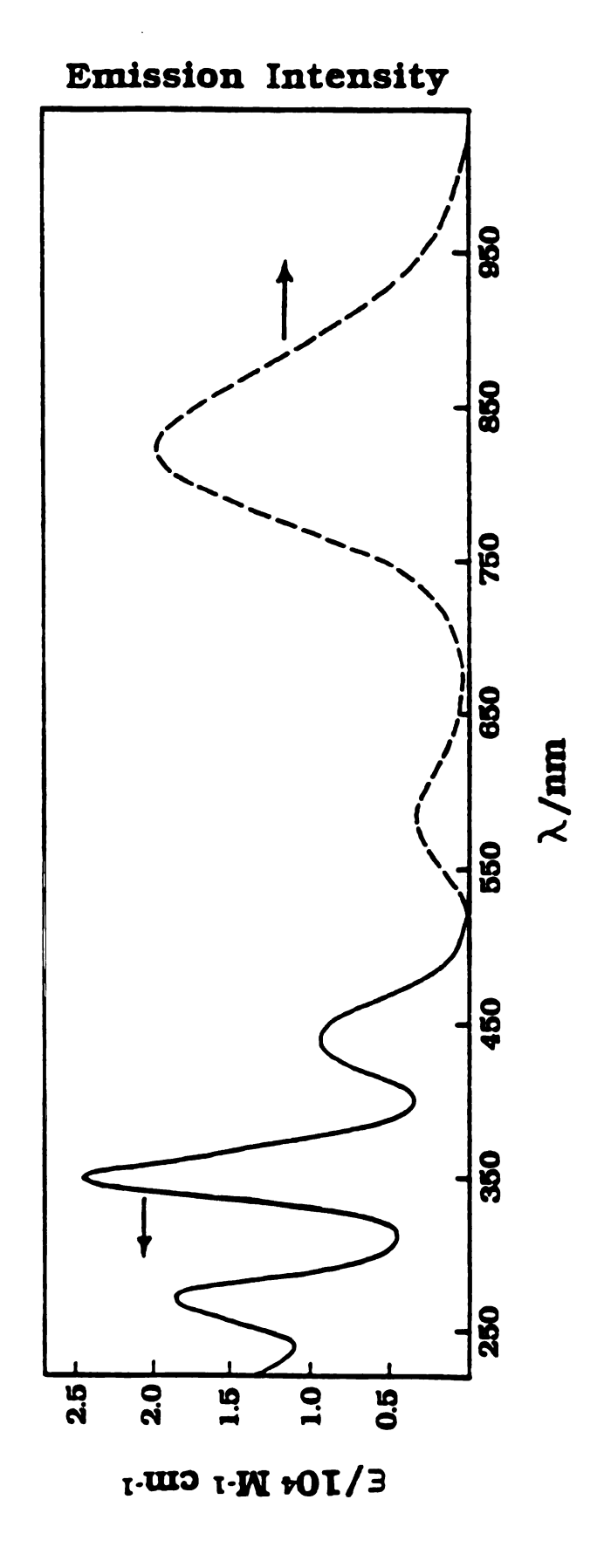


Figure 22

Electronic absorption spectrum (——) of 2 dissolved in CH_2Cl_2 at room temperature, and corrected emission spectrum (- - -) of crystalline 2 at 77 K.

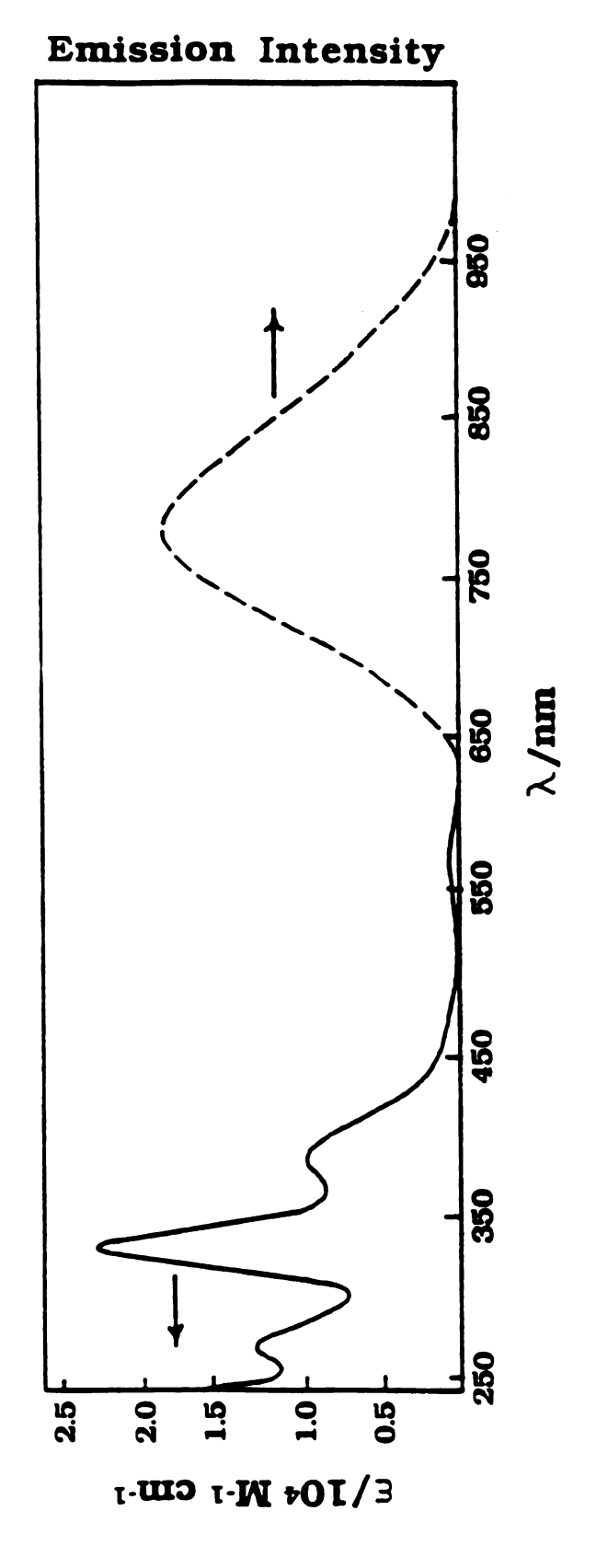


Figure 23

Electronic absorption spectrum (——) of 3 dissolved in CH_2Cl_2 at room temperature, and corrected emission spectrum (- - -) of crystalline 3 at 77 K.

Emission Intensity

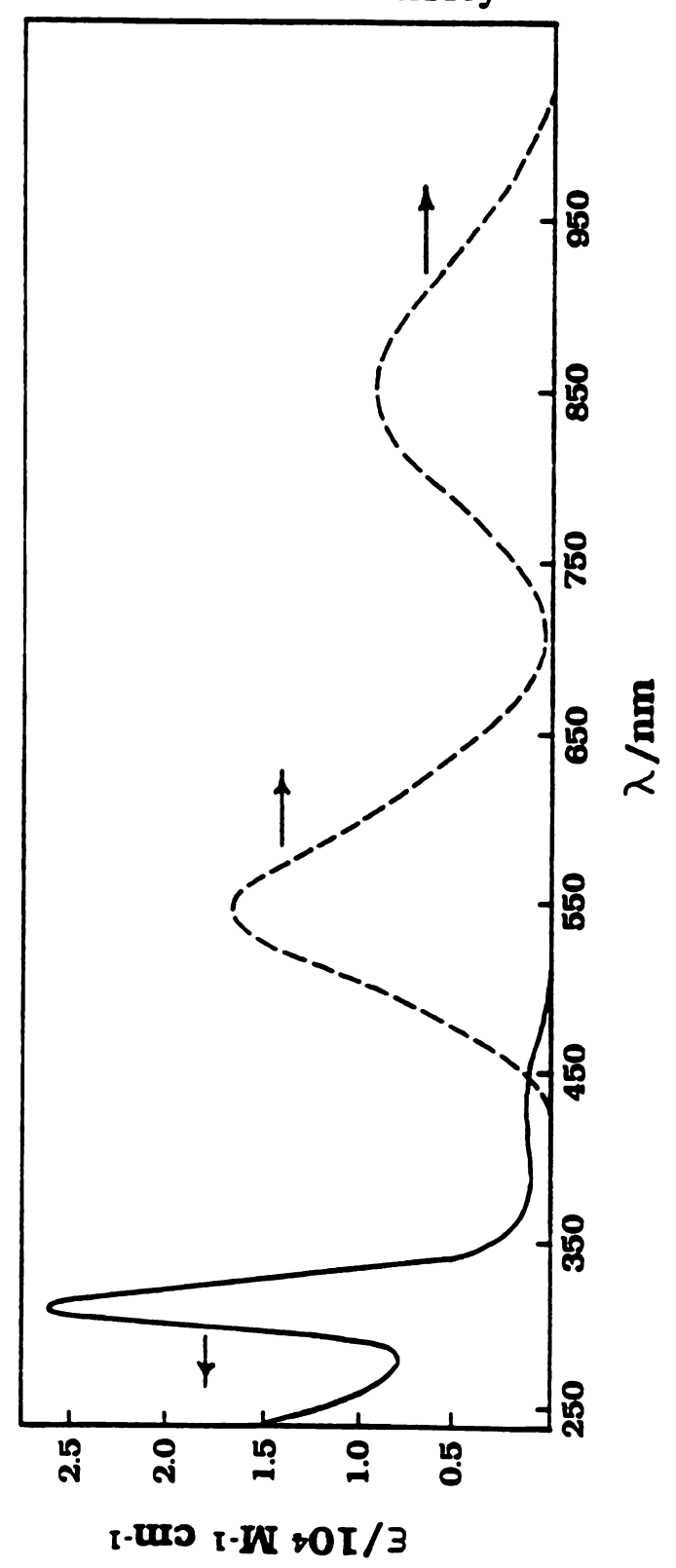


Figure 24

not understood. Luminescence was not detected from fluid solutions of any of the dirhodium complexes.

Insight into the nature of luminescence comes from time-resolved spectroscopic measurements. The red emissions from 1, 2, and 3 display similar behavior in that the lifetime decays are monoexponential and long. Microsecond lifetimes for 1, 2, and 3 (Table 8) are a signature of phosphorescence. Conversely, the decay of the higher energy emissions of 1 and 3 within the 8-ns temporal profile of the 355-nm excitation pulse from a Nd:YAG laser suggests to us that the red phosphorescence is accompanied by companion fluorescence. Interestingly, fluorescence from 2 could not be detected even at our instrument's highest sensitivity. In regard to the phosphorescence, the observed lifetime exhibits a pronounced attenuation of emission from 1, 2, and 3 with increasing temperature. Figures 25 - 27 display the temperature dependences of the excited state decay rate constant of 1, 2, and 3, respectively. In each case there is a low temperature regime in which the decay rate constant exhibits little variance then is followed by a sharp monotonic increase of the rate with increasing temperature. The observed rates for 1 - 3 are fit well (see Figures 25 - 27) by an expression for the decay constant based on a two-state Boltzmann distribution, ¹³⁸

$$k_{obs} = \frac{k_1 + k_2 \exp(-\Delta E/k_B T)}{1 + \exp(-\Delta E/k_B T)}$$
 (16)

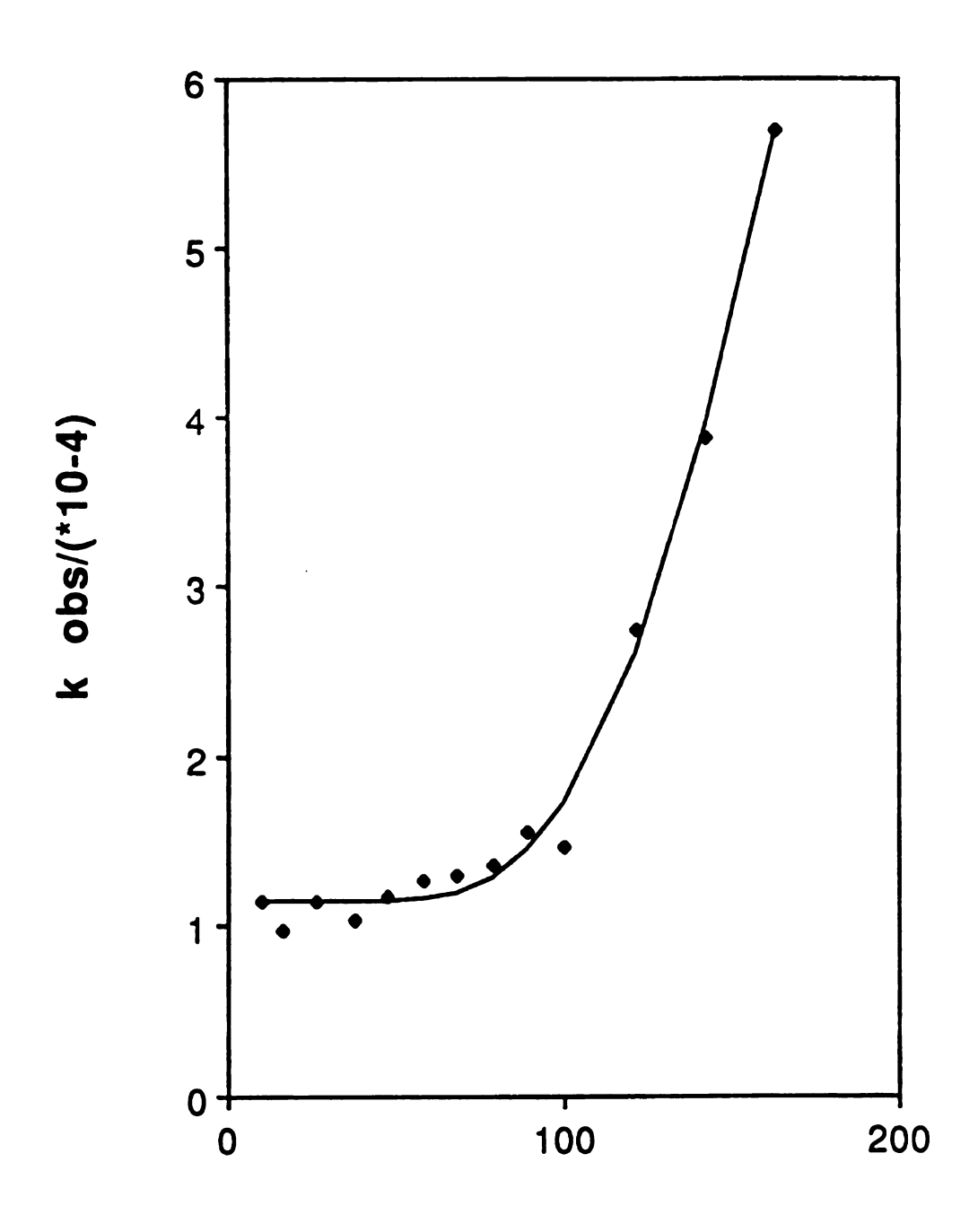
where k_1 and k_2 are the decay constants for the two states in thermal equilibrium separated by an energy gap ΔE . The calculated rate constant for and the energy gaps are summarized in Table 9.

Table 8. Emission Spectral Data for Crystalline 1, 2, and 3 at 77 K

λ _{max} , nm	τ, ns	λ _{max} , nm	τ, μ8
540	<8	840	5 3
		780	7 9
580	<8	820	287
	540 	540 < 8	540 < 8 840 780

^{*} No fluorescence is detected from solids of this compound.

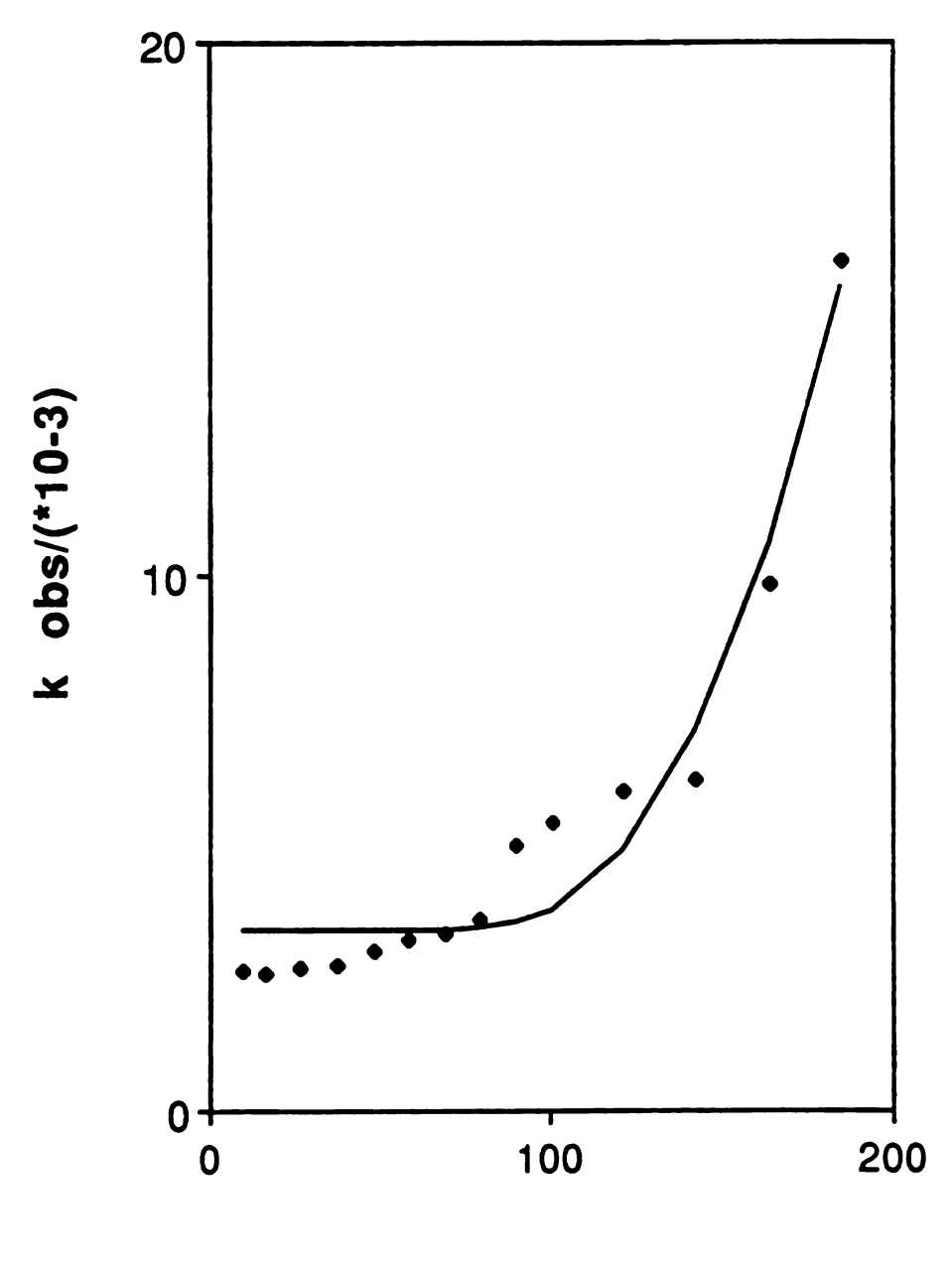
Fit of the variation of the observed emission decay rate constant to eq 16 of 1 in the 10 - 180 K temperature range.



TEMPERATURE (K)

Figure 25

Fit of the variation of the observed emission decay rate constant to eq 16 of 2 in the 10 - 200 K temperature range.



TEMPERATURE (K)

Figure 26

Fit of the variation of the observed emission decay rate constant to eq 16 of 3 in the 10 - 290 K temperature range.

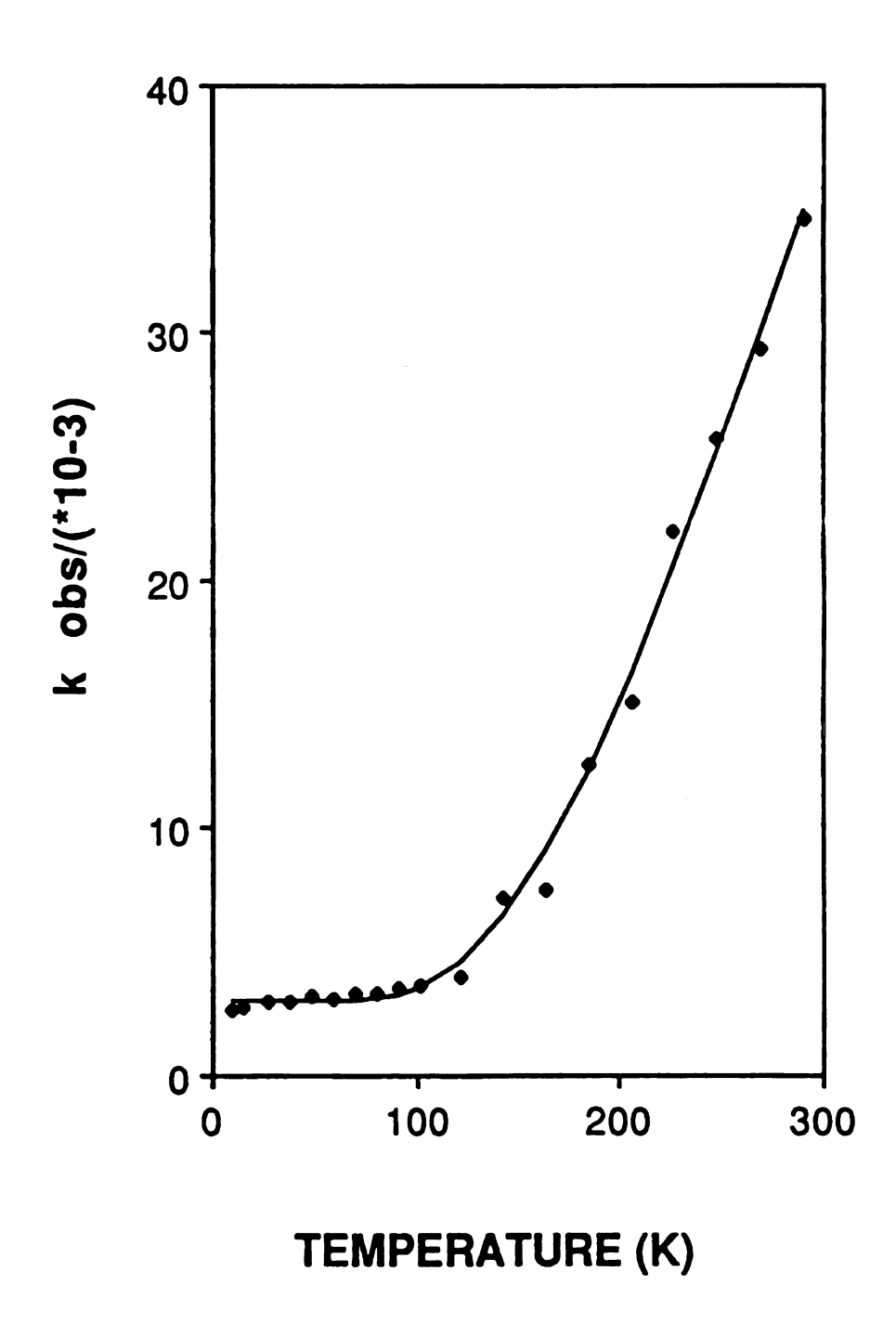


Figure 27

Table 9. Calculated decay rate constants and energy gaps for 1, 2, and 3

Complex	k ₁ /s ⁻¹	k_2/s^{-1}	ΔE / cm ⁻¹
1	1.1 x 10 ⁴	1.1×10^6	903
2	3.5×10^3	6.6×10^6	1258
3	3.0×10^3	2.8×10^5	1070

2. Discussion

Although cursory inspection of 1, 2, and 3 suggests disparate molecular and electronic structures, closer examination shows these complexes to be quite similar. Trigonal bipyramidal and octahedral coordination geometries, which are exclusively determined by the formal oxidation state of the rhodium metal centers, are preserved almost identically among the three complexes. Moreover, each of the binuclear complexes possesses a rhodium-rhodium single bond; and it is this bimetallic core and its associated axial ligands that appear to determine the electronic structure of this homologous series of complexes.

Absorption bands characteristic of the allowed transitions for M-M complexes dominate the electronic spectra of each of the dirhodium complexes. The absorption spectrum of 1, typical of most single bonded metal-metal dimers, 138,139 is dominated by an intense isolated band in the ultraviolet that is flanked by a broader less intense band to lower energy. The intensity, bandwidth, and position of the 305-nm band are signatures of a $\sigma \rightarrow d\sigma^*$ transition. The significant mixing of the metal-metal $d\sigma \rightarrow$ dσ* transition with axial ligand-to-metal charge transfer (LMCT) transition, $L\sigma \rightarrow d\sigma^*$, which has previously been observed for a variety of metal complexes containing L-M-M-L (M = Rh, Ir, Pt; L = halide, SCN, OH) cores,¹⁴⁰ is not likely significant in 1 owing to the much higher lone pair ionization potential of trifluorophosphine as compared to halides and pseudohalides. Consequently, the $\sigma \rightarrow d\sigma^*$ transition of 1 should be of relatively pure metal character. The lower energy, less intense absorption is analogous to the $d\pi^* \rightarrow d\sigma^*$ transitions of a variety of M-M complexes including Pt₂(III,III) sulfates¹³⁹ and pyrophosphites, 140a

Rh₂(II,II) acetates and isocyanides, ^{140b} and dimanganese and dirhenium carbonyls. ¹⁴⁰⁻¹⁴⁴

The absorption profiles of 2 and 3 are more complicated. Because the complexes are structurally unique, reliable assignment of the spectral features in Figures 24 and 25 is difficult without undertaking detailed spectroscopic measurements. Nevertheless, the spectra do display some useful qualitative information. Transitions arising from the ligand based σ-orbitals of the axial chloride ligands, in addition to the primarily metal center $\sigma \to d\sigma^*$ band, should be present. Inspection of Figures 24 and 25 indicates this to be the case; uv-absorptions possessing band shapes and energies consistent with σ transitions are observed. The appearance of bands between 270 - 350 nm in the spectra of 2 and 3 is compatible to the location of ligand-based and configurationally mixed metal-ligand transitions of Pt₂(III,III)Cl₂ and Rh₂(II,II)Cl₂ complexes. ¹⁴⁰ Moreover, the shift of $\sigma \rightarrow d\sigma^*$ transitions to lower energies upon metal-ligand mixing has been observed to increase the absorptivity of the $d\pi^* \rightarrow d\sigma^*$ transition via intensity stealing mechanisms. 140 The larger intensity of the absorption bands lying in the spectral region in which $d\pi^* \rightarrow d\sigma^*$ transitions typically occur (400 - 450 nm) for complexes 2 and 3 as compared to 1 is certainly consistent with the operation of similar $\sigma \rightarrow$ $d\pi^*$ intensity stealing mechanisms.

Our observation that electronic absorption is governed by the σ M-M framework of 1, 2, and 3 is complemented by the luminescence properties of these complexes. The pronounced narrowing of the emission bands at lower temperatures is characteristic for luminescence of $d\sigma^*$ parentage. Moreover, the invariance of the emission lifetime at low temperatures followed by a monotonic decrease with increasing

temperature is a trend previously observed by our group for the $d\sigma^{\boldsymbol{*}}$ emission from $Pt_2(III,III)L_2$ (L = Cl, Br, and H_2O) tetraphosphates.⁴² An excited stated model proposed for $Pt_2(III,III)L_2$ (L = Cl, Br, and H_2O) tetraphosphates, and consistent with the observed temperature dependance of the Rh₂ complexes, is shown in Figure 28. Photophysical analysis of these Pt2 complexes have revealed that the emissive excited state results from promotion of an electron from the $d\pi^*$ level to the $d\sigma^*$ level. In this case the lowest energy excited state is $^3(d\pi^*d\sigma^*)$ (3E_n), which is split to yield a lowest energy (B_{1u}, B_{2u}) spin-orbit component. The temperature dependence arises from the thermal population of a higher energy deactivating state corresponding to the E_u(³E_u) spin-orbit component. Similar behavior for the observed lifetime of the Pt₂(III,III)L₂ (L = Cl, Br, and I) pyrophosphites has been observed as well, and indeed, nonradiative deactivation by Boltzmann population within the $^3(d\pi^* \rightarrow$ $d\sigma^*$) spin-orbit manifold appears to be an emerging trend of $d\sigma^*$ luminescence for many M-M complexes. In the case of the dirhodium series, measured energy gaps of 1,200 cm⁻¹ shown in Table 9 conform well with those experimentally determined for the (B_{1u}, B_{2u}) - E_u gap of Pt₂(III,III)L₂ complexes and are in agreement with the 1000 cm⁻¹ splittings predicted from first-order spin-orbit coupling calculations. 42 Finally, our observation that luminescence is not detected from solutions of 1, 2, and 3 at temperatures equivalent to those at which the crystalline solids emit is consistent with recent photophysical studies demonstrating the importance of medium rigidity as a crucial controlling factor of do* luminescence. 41,141

Insight into the structural and spectroscopic properties of dirhodium complexes is provided by analysis of their electronic structure.

Proposed energy diagram of the lowest energy excited states of the $Pt_2(III,III)L_2 \ phosphates. \ The state manifold is derived from the spin-orbit coupling perturbation of the <math display="inline">^3E_u$ state arising from the one-electron $^3(d\pi^* \ \rightarrow \ d\sigma^*) \ promotion.$

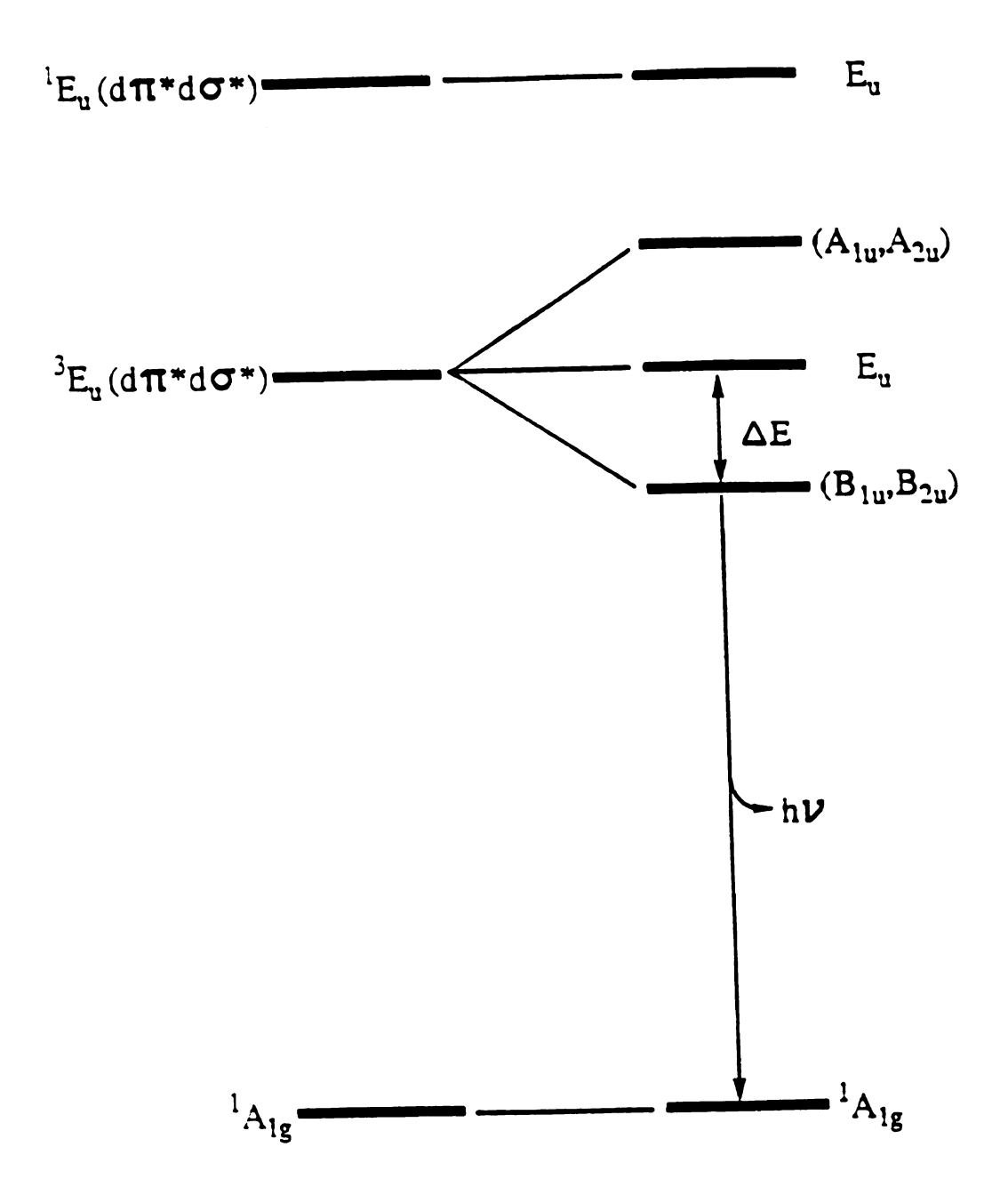


Figure 28

We begin by considering the level structure of the C_{3v} Rh(0) P_4 and C_{4v} Rh(II)P3Cl2 fragments. Molecular orbital treatments 145,146 suggest that eight electrons of the d⁹ Rh(0)P₄ fragment reside in orbitals of $\pi(d_{xz}, d_{yz})$ and $\delta(d_{xy}, d_{x^2-y^2})$ symmetry with the remaining electron occupying the $\sigma(d_{z^2})$ orbital. In the case of the d^7 Rh(II)P₃Cl₂ fragment, the $d_{x^2-y^2}$ level is displaced to very high energies owing to the destabilizing σ^* interactions of the metal with the ligands in the equatorial plane. Consequently, the odd electron of the d⁷ Rh(II)P₃Cl₂ fragment, as was the case for Rh(0)P₄, resides in the $\sigma(d_{z2})$ orbital with the remaining six electrons residing in the lower energy $\pi(d_{xy}, d_{x^2-y^2})$ and $\delta(d_{xy})$ orbitals; low symmetry splittings within the π orbitals have been ignored. Construction of the level diagrams for 1, 2, and 3 is achieved by the orbital mixing of the appropriate rhodium fragments. These results are shown in Figures 29 - 31. The orbitals that will interact most strongly are those that extend perpendicularly from the equatorial plane of the fragments, namely the spatially directed $\sigma(d_{z^2})$ orbitals. To a lesser extent the filled π -symmetry orbitals will interact and negligible overlap will occur between the d-orbitals, which are aligned parallel to each other. In each case, formation of a Rh-Rh single bond results from the pairing of the d_{z2} electrons of the individual fragments in the σ orbital. To this end, the delectron configurations of 1, 2, and 3 are best represented as $(d^8)d^1-d^1(d^8)$, $(d^8)d^1-d^1(d^6)$, and $(d^6)d^1-d^1(d^6)$, respectively. Within this framework, we see that 1 and 3 are isoelectronic with the M-M prototypes Co₂(CO)₈¹⁴⁷ and Mn₂(CO)₁₀,¹⁴⁸ respectively, and the existence of 2 formally completes the Rh-Rh single bonded series.

On the basis of this molecular orbital model, our observation of lowest energy excited states derived from the Rh-Rh core is not surprising. The lowest energy allowed transitions are predicted to be $d\sigma \to d\sigma^*$ and $d\pi^* \to d\sigma^*$, and for 2 and 3 $\sigma(Cl) \to d\sigma^*$. Although the $d\sigma$ manifold is purposely isolated from the levels of π - and δ -symmetries to minimize congestion in Figures 29 - 31, absorption spectra of the Rh₂ complexes clearly suggest a σ -splitting of considerable magnitude such that the lowest energy allowed transition in 1, 2, and 3 is $d\pi^* \to d\sigma^*$. In accordance with these considerations, our observation of emission from $\sigma^*(d\pi^* \to d\sigma^*)$ states follows directly from the level diagrams illustrated in Figures 29 - 31. Thus the similarity of the electronic absorption and emission properties of the seemingly disparate Rh₂ complexes is easily understood by the electronic structure models described in Figures 29 - 31.

The homologous series presented herein provides a basis for the synthetic design of luminescent multielectron congeners. With the twoelectron mixed-valence Rh₂(0,II) complex as a benchmark, the preparation of its multielectron $Rh_2(0,0)$ and $Rh_2(II,II)$ counterparts can be achieved such that a long-lived emissive $d\sigma^*$ excited state can be preserved. As is explicitly shown in Figures 29 and 30, conversion of the octahedral Rh(II) center of 2 to the trigonal bipyramidal Rh(0) center of 1 stabilizes a formally highly energetic level that can accommodate the addition of two electrons to the metal core. In this manner, the overall electronic structure necessary for do* luminescence is preserved. Furthermore, two-electron oxidation of the Rh(0) center of 2 does not significantly perturb the σ -framework because the formation of an octahedral coordination geometry destabilizes the formally occupied dδ orbital. This strategy should be completely general for several M-M systems contingent upon the successful preparation of the appropriate mixed-valence intermediate. We believe that the torsional flexibility and

Simple molecular orbital diagram for the interaction of two C_{3v} Rh(0)P₄ fragments. The d π - and d δ -symmetry orbitals are filled and indicated by the shaded box. To minimize level congestion, the σ - σ * splitting is shown to be small and its manifold is isolated from that of the d π and d δ orbitals.

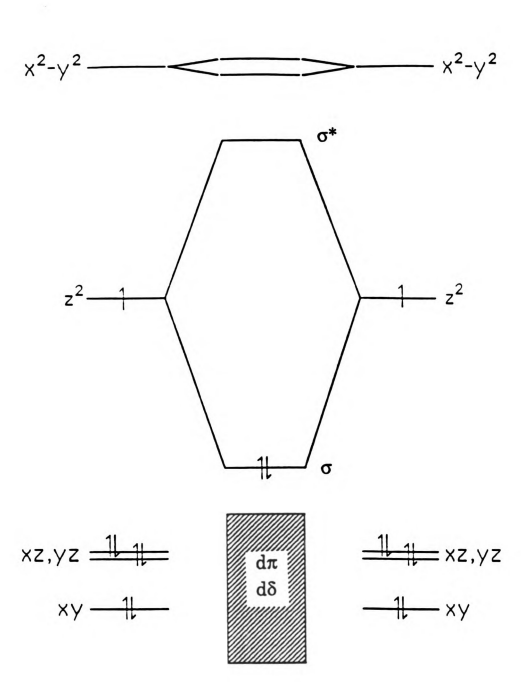


Figure 29

Qualitative level diagram for the interaction between C_{3v} Rh(0)P₄ and C_{4v} Rh(II)P₃Cl₂ fragments. The d π - and d δ -symmetry orbitals are filled and indicated by the shaded box. To minimize level congestion, the σ - σ * splitting is shown to be small and the σ -manifold is isolated from that of the d π and d δ orbitals. Low symmetry splitting within the d π level of the C_{4v} Rh(II)P₃Cl₂ fragment is not considered; interactions of the d σ and d σ * levels with the L σ and L σ * orbitals are also not considered.

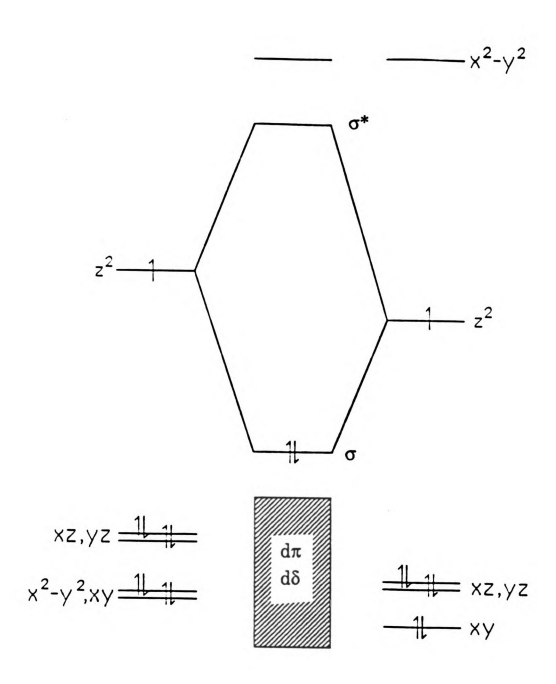


Figure 30

Qualitative level diagram for the interaction of two C_{4v} Rh(II) P_3Cl_2 fragments. The $d\pi$ - and $d\delta$ -symmetry orbitals are filled and indicated by the shaded box. The σ - σ^* splitting is shown to be small. Low symmetry splittings within the $d\pi$ levels of the C_{4v} Rh(II) P_3Cl_2 fragments are not considered; also the interactions of the $d\sigma$ and $d\sigma^*$ levels with the L σ and L σ^* orbitals are not considered.

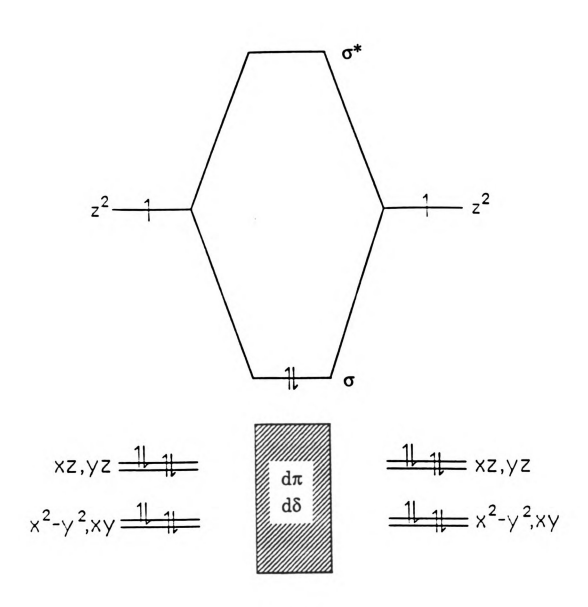


Figure 31

the electronic properties of the bis(difluorophosphino)-alkylamine ligand is crucial to our success in isolating the unusual Rh₂ mixed-valence dimer.

C. Trirhodium Complex

1. Results and Discussion

- a. Synthesis of $Rh_3(\mu\text{-Cl})_3[CH_3N(PF_2)_2]_3$. We observed in the preparation of 2, the formation of small amounts of $Rh_3(\mu\text{-Cl})_3[CH_3N(PF_2)_2]_3$, 4, when the reaction was not preformed in a large excess of the ligand $CH_3N(PF_2)_2^{121}$. Pure $Rh_3(\mu\text{-Cl})_3[CH_3N(PF_2)_2]_3$ is obtained with a $[RhCl(PF_3)_2]_2:CH_3N(PF_2)_2$ ratio of 1:1, but the yield from this reaction is low and unreacted $[RhCl(PF_3)_2]_2$ is recovered. In 4, the formal oxidation state of the rhodium atoms is Rh(I) and thus reaction from the $[RhCl(PF_3)_2]_2$ does not involve a formal change in oxidation state of the Rh_3 core. During our studies the formation of 4 was reported by reaction of $CH_3N(PF_2)_2$ with $[RhCl(CO)_2]_2$ with a mole ratio of 1:2. 121
- b. Structural Interpretation. The $Rh_3(\mu-Cl)_3[CH_3N(PF_2)_2]_3$ crystallizes in two different forms, one being in the space group C2/c, and the other in the space group Pnma. Mague's crystal structure of $Rh_3(\mu-Cl)_3[CH_3N(PF_2)_2]_3$ was for the monoclinic space group C2/c. In our solution of 4 in the Pnma space group, P(2)and F(2) atoms were modeled in two different sets of position with each disordered atom assigned an occupation of 0.5. The crystal parameters and detail of intensity for $Rh_3(\mu-Cl)_3[CH_3N(PF_2)_2]_3$ in the two different space groups are listed in Table 10. The positional parameters for 4 are listed in Table 11 and 12 (C2/c and

Table 10. Crystal Data for $Rh_3(\mu\text{-Cl})_3[CH_3N(PF_2)_2]_3$

	4	4'
formula	$Rh_3F_{12}P_6N_3C_3H_9$	$Rh_3F_{12}P_6N_3C_3H_9$
formula weight	916.02	916.02
crystal dimensions, mm	$0.40 \times 0.52 \times 0.82$	$0.20 \times 0.36 \times 0.56$
crystal system	monoclinic	orthorhombic
space group	C 2/ c	Pnma
unit cell parameters	17 000(0)	10.022(1)
a, A	17.339(2) 11.028(1)	10.055(1) 17.167(2)
b, Å c, Å	23.264(4)	13.010(3)
α, deg	90	90
β, deg	93.00(1)	90
γ, deg	90	90
V , $Å^3$	4442.3(10)	2245.7(6)
\boldsymbol{z}	8	4
$\rho_{\rm calcd}$, g/cm ³	2.77	2.71
μ(Mo Kα), cm ⁻¹	15.3	30.3
radiation (λ, Å)	Mo Kα(0.71073)	Mo Ka(0.71073)
temp, °C	24 (1)	24(1)
scan method	ω	θ - 2θ
scan rate, deg min ⁻¹ no. of unique data, total	4	2
with $F_0^2 > 3\sigma(F_0^2)$	8085, 6369	2679, 2188
no. of parameters refined	272	170
trans. factors, min, max	0.275, 0.722	0.934, 0.996
$R^{\mathbf{a}}$	0.041	0.026
$R_{\mathbf{w}}^{\mathbf{b}}$	0.046	0.027
GOF °	2.79	1.86

 $^{{}^{}a}R = \sum ||F_{o}| - |F_{c}|| / S |F_{o}|. \quad {}^{b}R_{w} = [\sum w(|F_{o}| - |F_{c}|)^{2} / \sum w |F_{o}|^{2}]^{1/2}; w = 1/\sigma^{2}(|F_{o}|). \quad {}^{c} \text{ Goodness of fit} = [\sum w(|F_{o}| - |F_{c}|)^{2} / (N_{obsd} - N_{parameters})]^{1/2}.$

Table 11. Atomic Positional and Isotropic Displacement (Å²) Parameters for $Rh_3[CH_3N(PF_2)_2]_3Cl_3$ (4) in the C2/c Space Group ^a

$B/{ m \AA}^2$	z	y	x	Atom
2.449(6)	0.31801(2)	0.29074(4)	0.19476(2)	Rh(1)
2.464(6)	0.34005(2)	0.34791(4)	0.36732(2)	Rh(2)
2.585(7)	0.43425(2)	0.40886(4)	0.25356(2)	Rh(3)
3.24(3)	0.31423(7)	0.1597(1)	0.30475(9)	Cl(1)
3.44(3)	0.43896(6)	0.2870(2)	0.36920(9)	Cl(2)
3.24(3)	0.41562(6)	0.2304(1)	0.17685(9)	Cl(3)
2.36(2)	0.22814(6)	0.3145(1)	0.20988(8)	P(1)
2.45(2)	0.25044(6)	0.3925(2)	0.36852(8)	P(2)
2.92(3)	0.36965(6)	0.4990(2)	0.43548(8)	P(3)
2.70(3)	0.45477(6)	0.5628(2)	0.32523(9)	P(4)
2.91(3)	0.43418(7)	0.5051(2)	0.14685(9)	P(5)
2.53(2)	0.32091(6)	0.4099(2)	0.09801(8)	P(6)
3.63(8)	0.1886(2)	0.3832(4)	0.1498(2)	F(1a)
4.20(8)	0.1927(2)	0.1942(4)	0.2052(3)	F(1b)
5.04(9)	0.2310(2)	0.5201(4)	0.3937(3)	F(2a)
5.1(1)	0.2163(2)	0.3219(5)	0.4282(2)	F(2b)
4.73(9)	0.3282(2)	0.5996(4)	0.4611(3)	F(3a)
5.4 (1)	0.3928(2)	0.4649(5)	0.5185(2)	F(3b)
5.2(1)	0.5191(2)	0.5737(5)	0.3523(3)	F(4a)
5.2(1)	0.4496(2)	0.6946(4)	0.2923(3)	F(4b)
5.7(1)	0.4852(2)	0.4755(6)	0.0953(3)	F(5a)
5.7(1)	0.4434(2)	0.6448(4)	0.1447(3)	F(5b)
4.30(9)	0.3129(2)	0.3486(4)	0.0167(2)	F(6a)
4.80(6)	0.8524(2)	-0.1279(2)	-0.0637(3)	F(6b)
4.22(9)	1.1421(3)	-0.0793(2)	0.3561(4)	N(1)
3.4(1)	0.4244(2)	0.5826(6)	0.4085(3)	N(2)
3.5(1)	0.9543(4)	-0.250	-0.0624(5)	N(3)
6.4(2)	1.2193(4)	-0.0138(3)	0.3704(7)	C(1)
5.8(2)	0.4465(4)	0.6820(8)	0.4611(5)	C(2)
4.8(2)	0.9683(6)	-0.250	-0.2109(6)	C(3)

^{*} Anisotropically refined atoms are given in the form of the isotropic equivalent displacement parameter defined as $4/3[a^2B_{11}+b^2B_{22}+c^2B_{33}+ab(\cos\gamma)B_{12}+ac(\cos\beta)B_{13}+bc(\cos\alpha)B_{23}]$.

Table 12. Atomic Positional and Isotropic Displacement (\mathring{A}^2) Parameters for $Rh_3[CH_3N(PF_2)_2]_3Cl_3$ (4') in the Pnma Space Group^a

Atom	x	y	z	$B/ ext{\AA}^2$
Rh(1)	0.22593(3)	-0.15806(2)	0.93327(2)	3.001(5)
Rh(2)	0.44321(5)	-0.250	1.4612(4)	3.288(9)
Cl(1)	0.4634(1)	-0.15253(8)	0.91400(9)	4.05(2)
Cl(3)	0.2093(2)	-0.250	0.7958(1)	3.60(3)
P(1)	0.2500(1)	-0.06797(7)	1.0450(1)	3.61(2)
P(2a)	0.4156(3)	-0.1658(2)	1.1665(2)	3.59(6)
P(2b)	0.4546(2)	-0.1567(1)	1.1535(1)	3.56(4)
P(6)	0.0141(1)	-0.16455(7)	0.94420(8)	3.00(2)
F(1a)	0.1285(3)	-0.0336(2)	1.1032(3)	5.91(7)
F(1b)	0.2985(4)	0.0113(2)	1.0013(3)	5.97(8)
F(2aa)	0.342(1)	-0.1887(5)	1.2632(6)	6.2(2)
F(2ab)	0.5488(9)	-0.1370(6)	1.2203(7)	6.6(2)
F(2ba)	0.4399(7)	-0.1724(3)	1.2705(3)	7.2(2)
F(2bb)	0.5930(5)	-0.1182(4)	1.1613(5)	7.0(1)
F(6a)	-0.0608(3)	-0.1189(2)	1.0294(2)	4.78(6)
F (6b)	-0.0637(3)	-0.1279(2)	0.8524(2)	4.80(6)
N(1)	0.3561(4)	-0.0793(2)	1.1421(3)	4.22(9)
N(3)	-0.0624(5)	-0.250	0.9543(4)	3.5(1)
C(1)	0.3704(7)	-0.0138(3)	1.2193(4)	6.4(2)
C(3)	-0.2109(6)	-0.250	0.9683(6)	4.8(2)

^a Anisotropically refined atoms are given in the form of the isotropic equivalent displacement parameter defined as $4/3[a^2B_{11}+b^2B_{22}+c^2B_{33}+ab(\cos\gamma)B_{12}+ac(\cos\beta)B_{13}+bc(\cos\alpha)B_{23}]$.

Pnma), respectively. Whereas the crystal structure with the space group C2/c possesses no symmetry element, the Pnma space group possesses a crystallographic mirror plane passing through atom Rh(2), Cl(3), N(3), and C(3).

The bond distances and bond angles for 4 are listed in Tables 13 and 14 (C2/c and Pnma), respectively. Because there is only a slight difference between the bond distances and angles for the two crystal structure the crystal structure of 4 with the space group C2/c will be only described in detail.

The ORTEP of 4 is shown in Figure 32. The complex is constructed from a triangle of rhodium atoms, which are linked together by a bridging bidentate $CH_3N(PF_2)_2$ ligand, and a chlorine atom. The average $Rh\cdots Rh$ bond separation is 3.099 Å, and is consistent with Rh_3 trimers $[Rh_3(\mu_3-S)_2(\mu_2-S)(\mu_2-Cl)_2(PEt_3)_6]PF_6^{-149}$ and $[Rh_3(\mu_3-E)_2(CO)_6]^-$ (E = S or Se) 150 (3.202 and 3.050 Å) which do not have a single metal-metal bond. The average bridging Rh-Cl bond distance is 2.402 Å, which is similar to the bridging Rh-Cl distance of 2.38 Å in the Rh(I) dimer of $[RhCl(C_8H_{12})]_2$. The coordination about each rhodium atom is approximately square planar. The average $P-Rh-Cl_{cis}$, $P-Rh-P_{cis}$, and $P-Rh-P_{trans}$ angles (average values 87.21°, 89.88°, 95.59°, and 175.03° respectively) are consistent with the square planar geometry of regular Rh(I) monomers. The Rh atom lies effectively in the RhP_2Cl_2 plane with the average displacement out of the square planar unit RhP_2Cl_2 of only 0.07 Å.

The closest structural analogy to 4 is $Rh_3(\mu-H)_3[P(OPr^i)_3]_6$, where the geometry around each rhodium atom is also square planar. This contrasts 4, in which all the chlorine atoms are on the same side of the Rh_3 plane. Thus the dihedral angles between the square-planar $RhCl_2P_2$

Table 13. Selected Bond Distances (Å) and Bond Angles (deg) for $Rh_3(\mu$ -Cl) $_3[CH_3N(PF_2)_2]_3$ (4) in the C2/c Space Group

			Bon	Bond Distances			
atom 1	atom 2	n 2	distance a	atom 1	atom 2	m 2	distance a
Rh(1)	Rh((2)	3.075(1)	Rh(2)	CI(2	3	2.396(1)
Rh(1)	Rh((3)	3.124(1)	Rh(2)	P(2)		2.143(1)
Rh(2)	Rh((3)	3.098(1)	Rh(2)	P(3)		2.135(2)
Rh(1)	CiC	1)	2.398(2)	Rh(3)	CIC	(2	2.412(2)
Rh(1)	SS	3)	2.402(2)	Rh(3)	3)D	3	2.402(2)
Rh(1)	P(1)	~	2.137(1)	Rh(3)	P(4)		2.143(2)
Rh(1) Rh(2)	P(6) CI(1)	1)	2.135(2) 2.404(2)	Rh(3)	P(5)		2.133(2)
			ğ	Bond Angles			
atom 1	atom 2	atom 3	angle ^a	atom 1	atom 2	atom 3	angle ^a
CI(1)	Rh(1)	CI(3)	90.58(6)	Cl(1)	Rh(1)	P(6)	179.02(6)
CI(1)	Rh(1)	P(1)	84.23(6)	CI(3)	Rh(1)	P(1)	170.93(6)
C1(3)	Rh(1)	P(6)	(9)00.06	CI(2)	Rh(3)	P(4)	87.74(6)
P(1)	Rh(1)	P(6)	95.29(6)	CI(2)	Rh(3)	P(5)	175.20(6)
CI(1)	Rh(2)	CI(2)	88.91(6)	CI(3)	Rh(3)	P(4)	176.81(6)
C](1)	Rh(2)	P(2)	88.98(6)	CI(3)	Rh(3)	P(5)	86.31(6)
CI(1)	Rh(2)	P(3)	171.52(6)	P(4)	Rh(3)	P(5)	92.66(6)
CI(2)	Rh(2)	P(2)	176.68(6)	Rh(1)	CI(1)	Rh(2)	79.63(5)
Cl(2)	Rh(3)	P(3)	85.97(6)	Rh(2)	CI(2)	Rh(3)	80.24(5)
P(2)	Rh(2)	P(3)	95.82(6)	Rh(1)	CI(3)	Rh(3)	81.12(5)
CJ(2)	Rh(3)	CI(3)	90.15(6)				

^a Numbers in parentheses are estimated standard deviations in the least significant digits.

Table 14. Selected Bond Distances (Å) and Bond Angles (deg) for Rh₃(μ-Cl)₃[CH₃N(PF₂)₂]₃ (4") in the Pnma Space Group

			Bond 1	Bond Distances			
atom 1	atom 2	n 2	distance ^a	atom 1	atom 2	n 2	distance ^a
Rh(1)	Rh(2)	3)	3.069(1)	Rh(1)	P(6)		2.137(2)
Rh(1)	CI(1)	(1	2.402(1)	Rh(2)	CI(1)		2.407(2)
Rh(1)	CI(3)	€	2.392(1)	Rh(2)	P(2a)	~	2.149(3)
Rh(1)	P(1)		2.136(1)	Rh(2)	P(2b)	6	2.129(2)
			Bon	Bond Angles			
atom 1	atom 2	atom 3	angle ^a	atom 1	atom 2	atom 3	angle ^a
CI(1)	Rh(1)	CI(3)	91.0(5)	P(1)	Rh(1)	P(6)	96.1(5)
CI(1)	Rh(1)	P(1)	86.0(5)	Cl(1)	Rh(2)	P(2a)	93.7(9)
CI(1)	Rh(1)	P(6)	177.7(4)	CI(1)	Rh(2)	P(2b)	86.6(6)
CI(3)	Rh(1)	P(1)	174.1(5)	CI(1)	Rh(1)	CI(3)	90.6(6)
CI(3)	Rh(1)	P(6)	86.9(5)				

* Numbers in parentheses are estimated standard deviations in the least significant digits.

A perspective ORTEP view and labeling scheme of $Rh_3(\mu-Cl)_3[CH_3N(PF_2)_2]_3$, 4, with the thermal ellipsoids at the 50% probability level. For clarity hydrogen atoms are not shown.

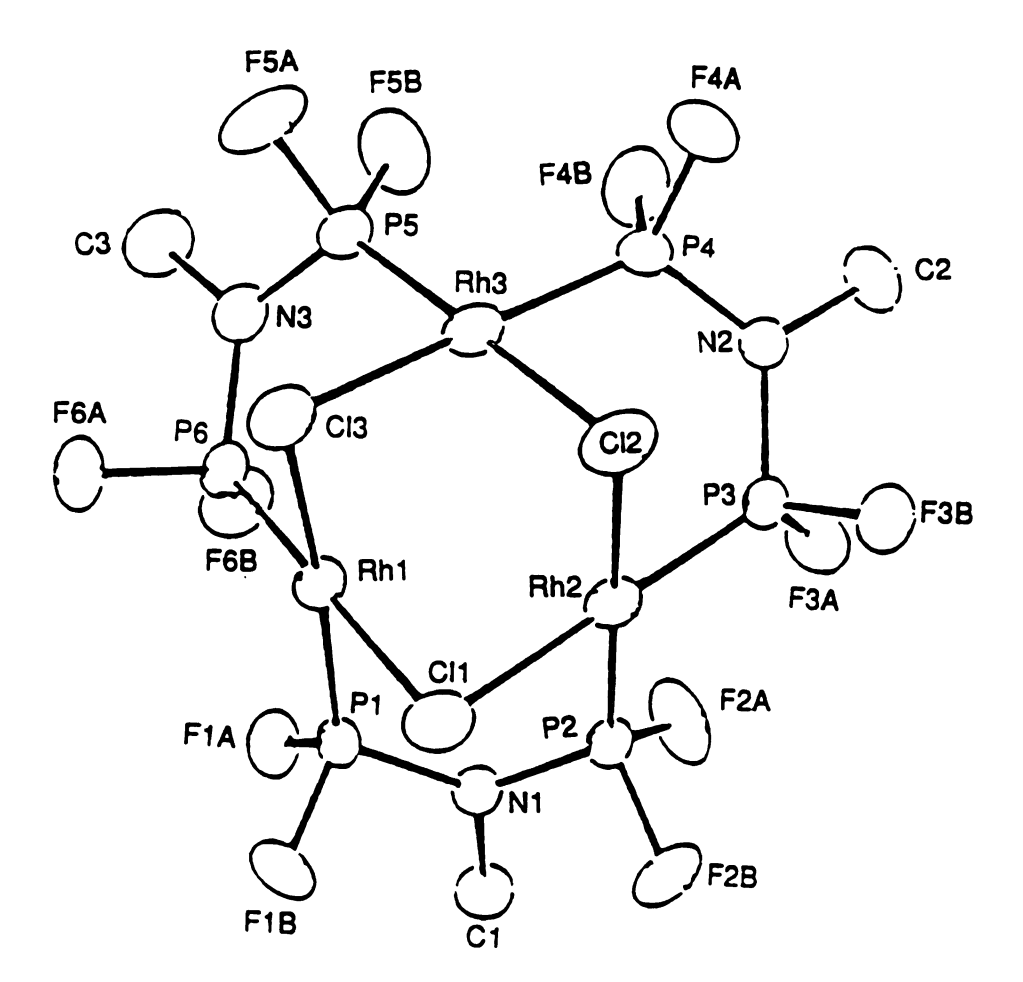


Figure 32

and Rh₃ triangular plane are fairly consistent (120.38(2)°, 120.83(3)°, and 121.04(3)°, respectively) and show little variance.

c. Electronic Absorption and Emission Spectra. The electronic absorption and emission of 4 is shown in Figure 33. The absorption spectrum of 4 displays a pronounced absorption in the ultraviolet spectra region, $\lambda = 266$ nm, $\varepsilon = 1.31 \times 10^4 \text{ M}^{-1} \text{ cm}^{-1}$ and $\lambda = 285 \text{ nm(sh)}$, $\varepsilon =$ $1.10 \times 10^3 \text{ M}^{-1} \text{ cm}^{-1}$, and a broad absorption band in the visible region ($\lambda =$ 415 nm, $\varepsilon = 1.24 \times 10^4 \text{ M}^{-1} \text{ cm}^{-1}$). Since there are no rhodium metal-metal bonds in 4, none of the absorption bands can be ascribed to $\sigma \rightarrow \sigma^*$ transitions centered in the Rh₃ core. Indeed, the absorption spectrum of 4 is similar to the Rh(I) d⁸ monomers. 153-155 The low energy visible absorption band of Rh(CO)Cl(PPh₃)₂¹⁵⁴ and TBA[Rh(P(OPPh₃)₂)mnt] (TBA = tetra-n-butylammonium, $mnt = maleonitriledithiolate)^{155}$ were assigned as metal-to-ligand charge transfer transitions (d $\rightarrow \pi$ and d $\rightarrow \pi^*$), respectively. For the case of square planar dimers Rh(I) dam (dam = bis(diphenylphosphino)methane) and dppm (bis(diphenylphosphino)methane) the assignment is not as clear. Several groups 156,157 initially assigned the low energy absorption as MLCT transition primarily because of their high intensities. Latter the assignment was changed to metalcentered $[\sigma^*(4d_z^2) \rightarrow \sigma(5P_z)]$ transition, ^{158,159} because the low-energy absorption maximum is not greatly affected by replacement of the dppm with dam, by change of environment from solid to solution, or by a change in temperature. In the case of 4 the visible absorption is probably due to a metal-to-ligand transition because there is little or no overlap of the metals 4d_{z2} and 5p_z orbitals.

The emission of 4 is shown in Figure 26. Red luminescence is observed from solids at low temperatures, upon excition with frequencies

Electronic absorption spectrum (——) of 4 dissolved in CH_2Cl_2 at room temperature, and uncorrected emission spectrum (- - -) of crystalline 4 at 77 K.

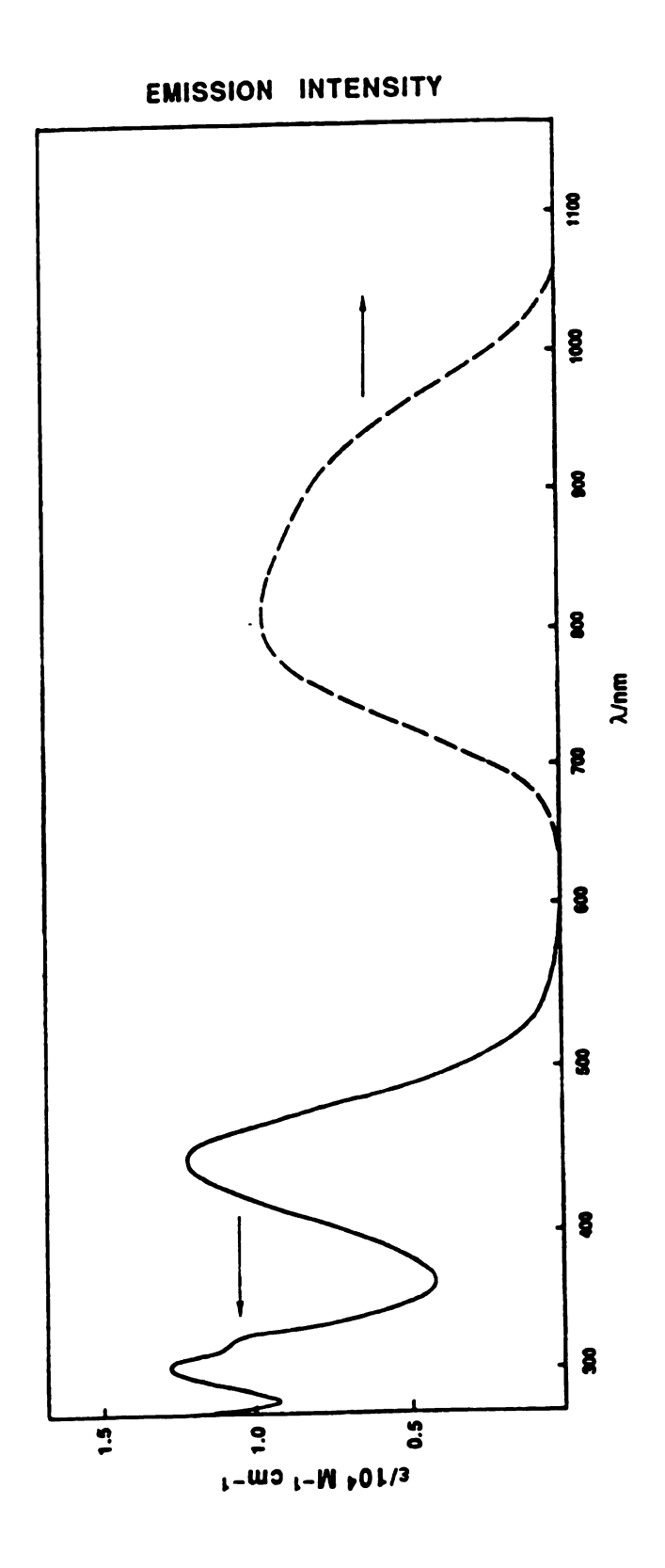


Figure 33

coincident with absorption manifold. The emission is quite broad and is centered at 850 nm. The broading is probably due to the different isomers of Rh₃(μ -Cl)₃[CH₃N(PF₂)₂]₃.

CHAPTER IV

Preparation of Dimolybdenum(V,V) Dimers

A. Background

The study of quadruply bonded dimers is an active area of research in inorganic chemistry. The spectroscopic properties of quadruply bonded dimers have been intensely investigated. $^{33-64}$ A general result to emerge from these studies is that the lowest electronic transition is the $\delta^2 \rightarrow {}^1(\delta \delta^*)$ transition, which typically falls in the visible region ($\lambda = 500-700$ nm). The complexes $[M_2X_8]^{n^-}$ (M = Re, Mo; X = Cl, Br) do not exhibit mirror image absorption and emission spectra. Two possible explanations for this are (1) that the emitting state is not ${}^1A_{2u}$ ($\delta \delta^*$) but rather a 3E_g or ${}^3A_{2g}$ state or (2) the absorption transition in $[M_2X_8]^{n^-}$ produce ${}^1A_{2u}$ ($\delta \delta^*$) MMCT states with eclipsed geometry and the emission originates from ${}^1(\delta \delta^*)$ MMCT states of staggered (D_4 or D_{4d}) geometry.

In support of the second hypothesis are the spectra of $Mo_2X_4(PR_3)_4$ complexes (X = Cl, Br, I; R = alkyl).⁶¹ The emission bands in these molecules are mirror images of their $\delta^2 \to {}^1(\delta\delta^*)$ absorption profiles. The bulky phosphine ligands in these quadruply bonded Mo_2 dimers are believed to create a large steric barrier to rotation about the metal-metal bond. Hence, the ${}^1(\delta\delta^*)$ excited state is likely to retain the eclipsed ground state geometry and produce well-behaved luminescence. Athough knowledge of the luminescence properties is emerging, a reliable synthetic route to quadruple bond complexes possessing long-lived luminescence has not been developed.

Spectroscopic studies during the recent years have demonstrated metal complexes bonded by strong π -acids having low-lying metal-to-ligand charge transfer states which are long-lived and highly emissive. ^{155,160,162} The π -acid ligand 2,2'-bipyridine (bpy) and

maleonitrile dithiolate mnt²⁻ can induce long-lived, low lying metal-to-ligand charge transfer excited states owing to their good electron accepting properties. The metal-to-ligand charge transfer excited state of Ru(bpy)₃²⁺ is at 590 nm with a quantum yield of 0.042 and a lifetime of 580 ns at 25 °C.¹⁶⁰ The metal-to-ligand charge transfer excited state for Pt(PPh₃)₂mnt is at 650 nm with a lifetime of 24 µs at 77 K.¹⁵⁵ Thus we were interested in ascertaining whether the emissive properties of the quadruply bonded dimers could be enhanced by incorporation of lowest energy MLCT states in the excited state manifold of quadruply bonded cores ligated by (bpy) and mnt²⁻.

B. Results and Discussion

1. Reaction of Mnt² with Quadruply Bonded Metal Complexes

A common precursor in the preparation of molybdenum quadruple bonded dimers is $Mo_2(O_2CCH_3)_4$. Substituted complexes are generally synthesized by using Me_3SiCl to remove the acetate ligands. However the reaction of Na_2mnt with $Mo_2(O_2CCH_3)_4$ in the presence of Me_3SiCl yields decomposition products. In the absence of Me_3SiCl , green and orange precipitates form. The electronic and infrared spectra of the green precipitate is shown in Figures 34 and 35, respectively. The absorption spectrum is identical to that of $[(C_4H_9)_4]_2Mo(mnt)_3$. The orange precipitate, which was characterized by infrared, U.V.-visible spectroscopy, elemental analysis, and X-ray crystallography, is unique. Infrared, U.V.-visible spectroscopy, and elemental analysis all support a complex with a $Mo_2(O)(S)(\mu-S)_2$ core.

 ${\bf Electronic\ absorption\ spectrum\ of\ [(C_4H_9)_4]_2Mo(mnt)_3\ dissolved\ in\ CH_2Cl_2}.$

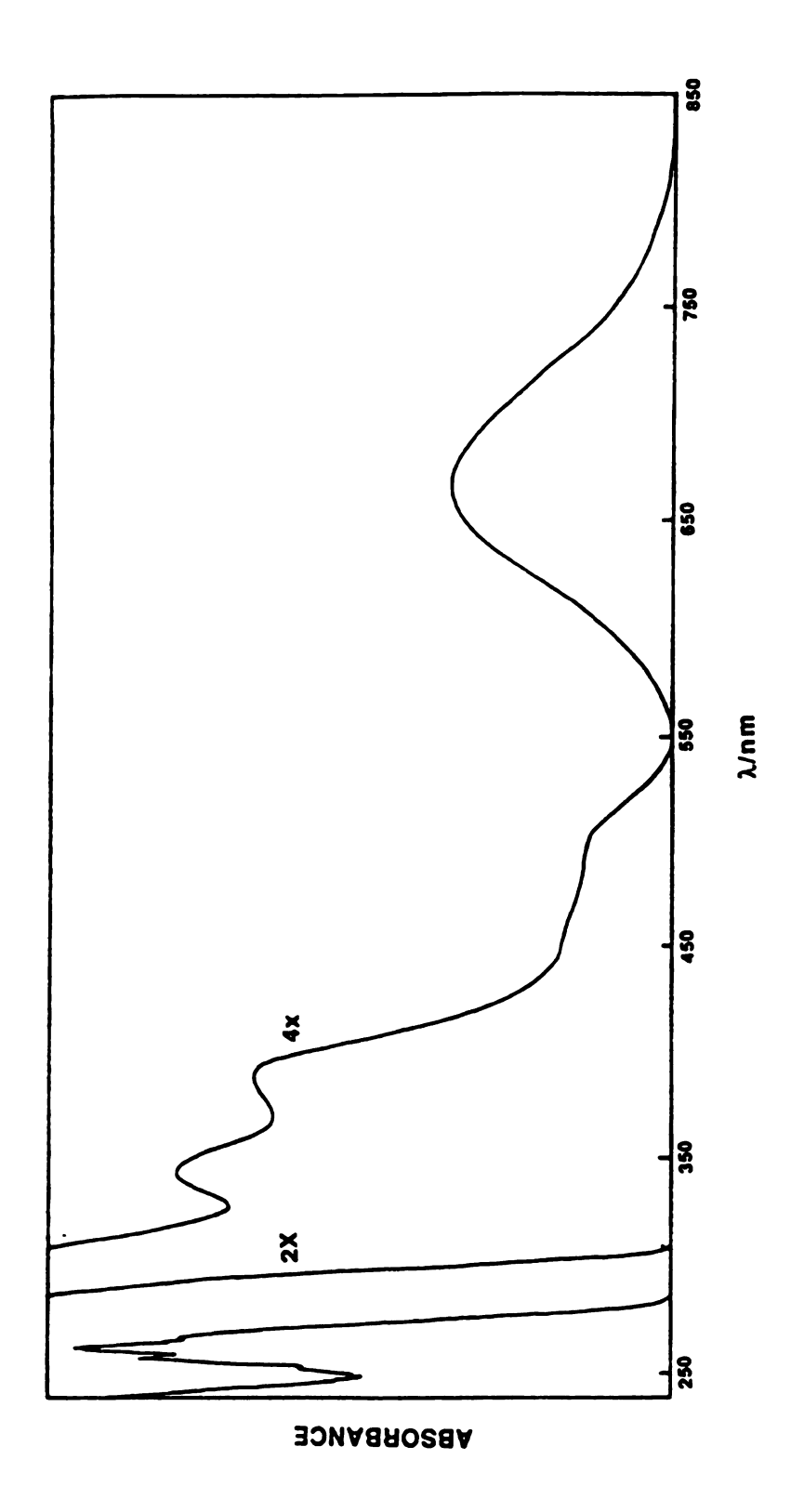


Figure 34

 $\label{eq:mid_likelihood} \mbox{Mid IR spectrum of } [(\mbox{${\rm C}_4$H}_9)_4]_2 \mbox{Mo(mnt)}_3.$

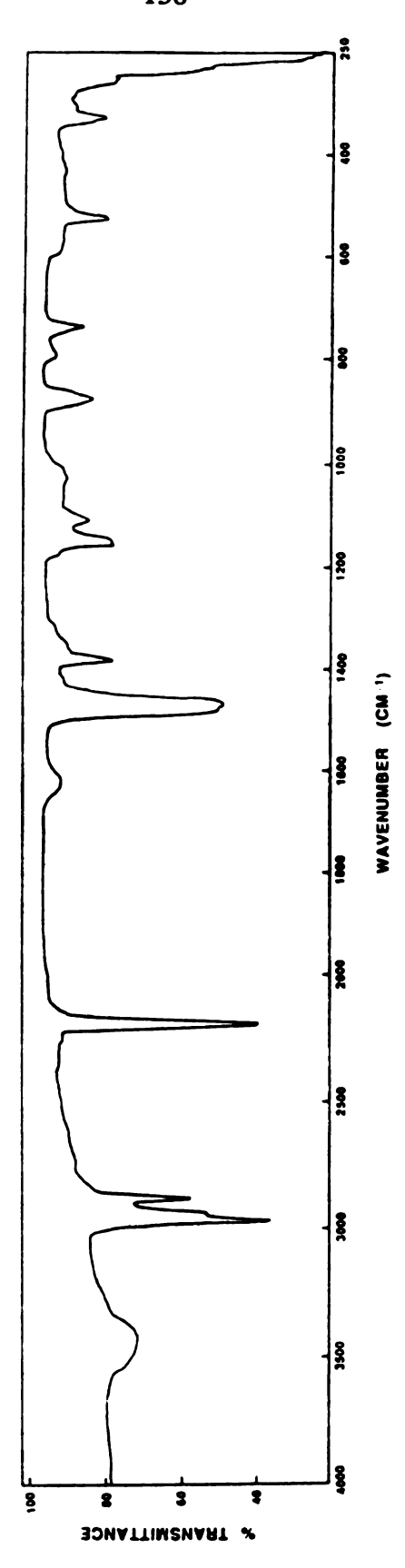


Figure 35

The IR spectrum (Figure 36) shows a band at 955 cm⁻¹ and 530 cm⁻¹, which are typical bands for terminal Mo=O and Mo=S stretching vibrations. A weak band at 470 cm⁻¹ and a band at 340 cm⁻¹ are assigned to the stretching vibration of di-μ-sulfido bridge. The typical stretching vibrations due to the di-μ-sulfido bridge are medium intensity bands at ~ 450 cm⁻¹, and ~ 350 cm⁻¹. 164

The electronic spectrum of the proposed $Mo_2(O)(S)(\mu-S)_2$ species is shown in Figure 37. The spectrum exhibits strong absorption in the ultraviolet region with less intense and unresolved absorption bands in the visible region. The electronic spectrum is similar to other compounds containing a $Mo_2(O)(S)(\mu-S)_2$ core. 166,167

The structure of the complex was unequivocally determined by solving the X-ray crystal structure. The crystal parameters and details of intensity collections are listed Table 15; the positional parameters for the anion and cations are listed in Table 16 and 17, respectively. The ORTEP of the structure is shown in Figure 38. Consistent with spectroscopic data, the compound was determined to be $[(C_4H_9)N]_2[Mo_2(O)(S)(\mu-1)]_2[Mo_2(O)(S)]$ S)₂(mnt)₂]. The structure of the $[Mo_2(O)(S)(\mu-S)_2(mnt)_2]^{2-}$ dianion is very similar to that of the dianion $[Mo_2(O)_2(\mu-S)_2(i-mnt)_2]^{2-}$ reported by Gelder and Enemark. 168 The geometry about each of the molybdenum atoms in [Mo₂(O)(S)(µ-S)₂(mnt)₂]²⁻ is best described as a distorted square pyramid with terminal oxygen and sulfur atoms in the apical positions; the two bridging sulfur atoms and the two sulfur atoms from 1,2-dicyanoethylene-2,2-dithiolate (mnt) ligand form the basal plane of each square pyramid. The bond distances and bond angles of $[Mo_2(O)(S)(\mu-S)_2(mnt)_2]^{2-}$ and the cations are listed in Tables 18 and 19, respectively. A Mo(V)...Mo(V) separation of 2.858(1) Å, is typical of other Mo(V)...Mo(V) dimers and

 $\label{eq:mid_likelihood} \mbox{Mid IR spectrum of } [(\mbox{C_4H}_9)\mbox{N}]_2 [\mbox{Mo_2}(\mbox{$O)$}(\mbox{$S)$}(\mbox{μ-$S)}_2 (\mbox{mnt})_2].$

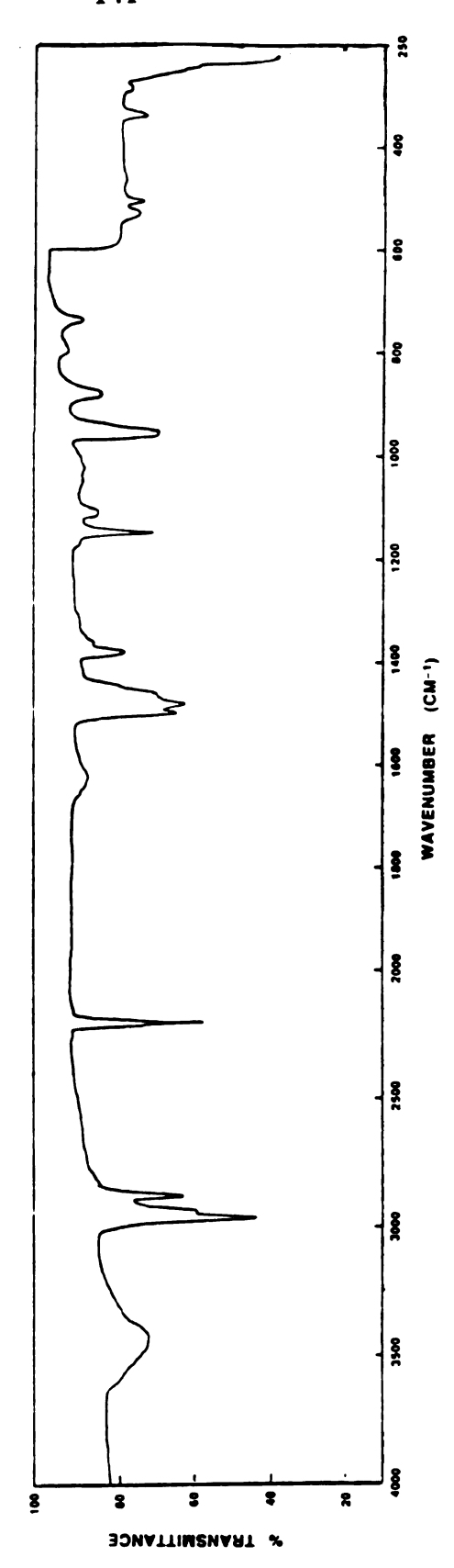


Figure 36

Electronic absorption spectrum of $[(C_4H_9)N]_2[Mo_2(O)(S)(\mu-S)_2(mnt)_2]$ dissolved in CH_2Cl_2 .

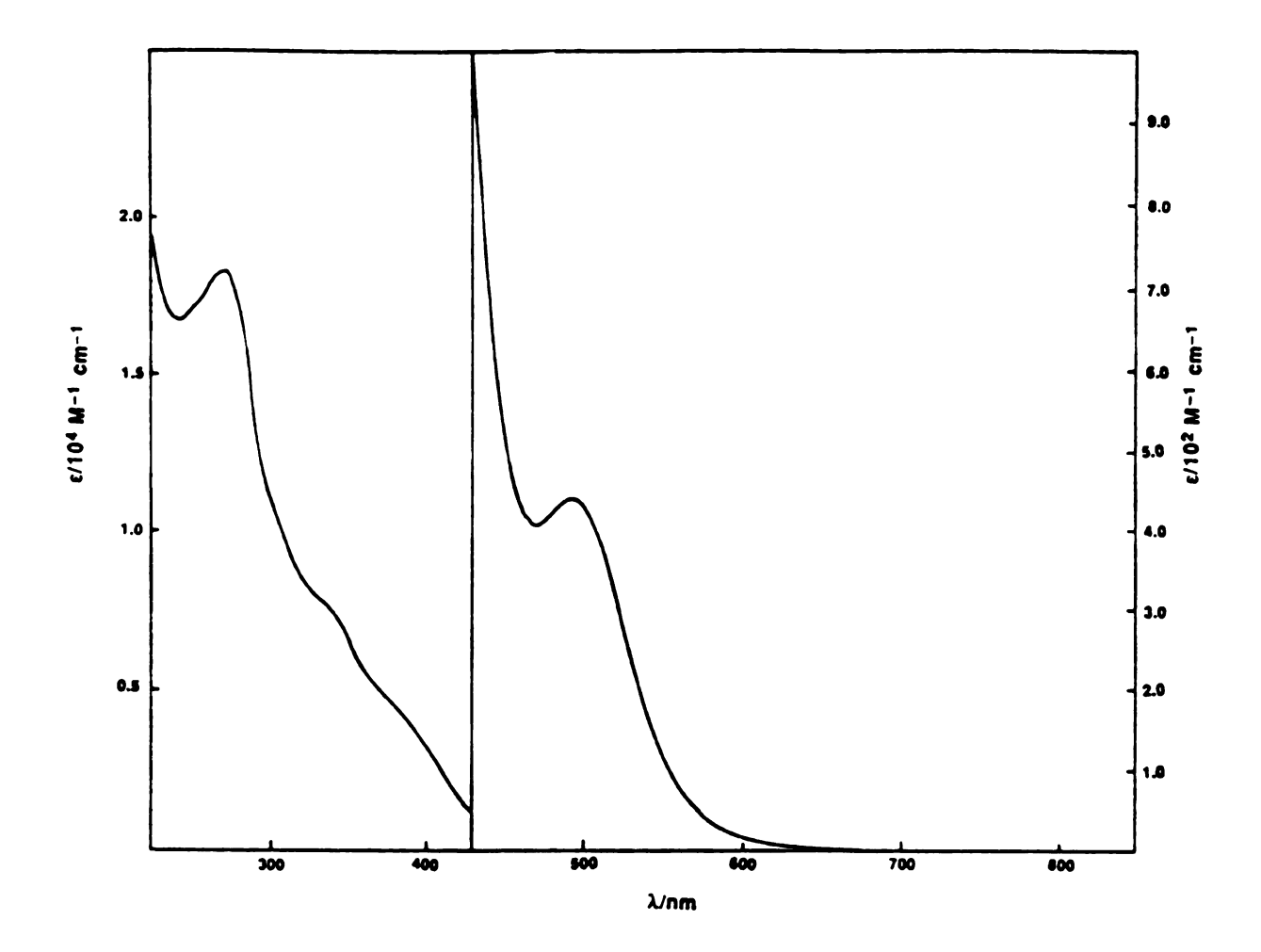


Figure 37

Table 15. Crystal Data for $[Mo_2(O)(S)(\mu-S)_2(mnt)_2]^{2-}$ and $Mo_2O_4Cl_4(dmbpy)_2$

	8	9
formula	$\mathrm{Mo_2N_6OS_7C_{40}H_{72}}$	$\mathrm{Mo_2Cl_2O_4N_4C_{24}H_{24}}$
formula weight	1069.35	695.27
crystal dimensions, mm	$0.11 \times 0.30 \times 0.50$	$0.10 \times 0.15 \times 0.20$
crystal system	monoclinic	trigonal
space group	$P2_{1}/c$	P 3 ₁ 21
unit cell parameters		
a, Å	19.547(4)	16.135(4)
<i>b</i> , Å	15.210(4)	16.135(4)
c, Å	18.754(6)	10.709(3)
α , deg	90	90
$oldsymbol{eta}$, deg	101.69(2)	90
γ, deg	90	120
V , Å 3	5460(2)	2414.4(13)
$oldsymbol{z}$	4	3
$ ho_{ m calcd},~{ m g/cm^3}$	1.24	1.43
$\mu(\text{Mo K}\alpha), \text{ cm}^{-1}$	6.3	9.6
radiation (λ, \dot{A})	Mo Ka(0.71073)	Mo Ka(0.71073)
temp, °C	27(1)	25(1)
scan method	θ - 2θ	θ - 2θ
scan rate, deg min ⁻¹	2	4
no. of unique data, total		
with $F_0^2 > 3\sigma(F_0^2)$	7168, 4834	2109,1243
no. of parameters refined	505	167
transmission factors, min, m	ax 0.844, 0.935	0.877, 0.916
$R^{\mathbf{a}}$	0.046	0.042
$R_{\mathbf{w}}^{\mathbf{b}}$	0.049	0.051
GOF c	3.16	1.68

 $^{{}^{}a}R = \sum ||F_{o}| - |F_{c}||/\sum |F_{o}|| \cdot {}^{b}R_{w} = [\sum w(|F_{o}| - |F_{c}|)^{2}/\sum w|F_{o}|^{2}]^{1/2}; w = 1/\sigma^{2}(|F_{o}|). \quad {}^{c} \text{ Goodness of fit} = [\sum w(|F_{o}| - |F_{c}|)^{2}/(N_{obsd} - N_{parameters})]^{1/2}.$

Table 16. Atomic Positional and Isotropic Displacement (Å²) Parameters for $[Mo_2(O)(S)(\mu-S)_2(mnt)_2]^{2-a}$

Atom	x	y	z	$B/ ext{\AA}^2$
Mo(1)	0.25023(3)	0.12794(5)	0.04924(3)	4.49(1)
Mo(2)	0.39544(3)	0.12021(4)	0.04492(3)	4.28(1)
S(1)	0.1784(1)	0.2575(2)	0.0499(1)	6.29(6)
S(2)	0.19328(1)	0.0852(2)	0.1482(1)	5.91(5)
S(3)	0.3173(1)	0.2341(1)	0.0063(1)	4.56(4)
S(4)	0.3370(1)	0.0463(1)	0.1228(1)	5.19(5)
S(5)	0.4742(1)	0.2407(1)	0.0338(1)	5.18(5)
S(6)	0.4919(1)	0.0782(1)	0.1423(1)	5.35(5)
O(1)	0.2095(3)	0.0630(4)	-0.0249(3)	6.4(1)
S(7)	0.3998(2)	0.0371(3)	-0.0338(2)	2.58(8)
N(1)	0.0143(4)	0.3357(6)	0.0985(6)	11.8(3)
N(2)	0.0378(4)	0.1201(7)	0.2253(5)	10.1(2)
N(3)	0.6599(4)	0.3047(5)	0.0702(5)	9.3(2)
N(4)	0.6833(4)	0.0976(5)	0.2063(5)	8.3(2)
C(1)	0.0604(5)	0.2885(7)	0.1009(6)	8.1(3)
C(2)	0.0757(4)	0.1371(7)	0.1883(5)	7.2(2)
C(3)	0.1172(4)	0.2290(6)	0.1019(5)	5.9(2)
C(4)	0.1242(4)	0.1564(5)	0.1438(4)	5.6(2)
C(5)	0.5561(4)	0.2088(5)	0.0823(4)	5.0(2)
C(6)	0.5627(4)	0.1389(5)	0.1284(4)	5.1(2)
C(7)	0.6145(4)	0.2620(5)	0.0751(5)	6.2(2)
C(8)	0.6303(4)	0.1165(6)	0.1712(5)	6.1(2)

^a Anisotropically refined atoms are given in the form of the isotropic equivalent displacement parameter defined as $4/3[a^2B_{11}+b^2B_{22}+c^2B_{33}+ab(\cos\gamma)B_{12}+ac(\cos\beta)B_{13}+bc(\cos\alpha)B_{23}]$.

Table 17. Atomic Positional and Isotropic Displacement (\dot{A}^2) Parameters for the

Tetrabutylammionium Ionsa

Atom	×	y	z	$B/ ext{\AA}^2$
N(5)	0.3848(3)	0.3007(4)	0.2723(3)	5.2(2)
N(6)	-0.1311(3)	0.2880(5)	0.2379(4)	6.1(2)
C(1)	0.0604(5)	0.2885(7)	0.1009(6)	8.1(3)
C(2)	0.0757(4)	0.1371(7)	0.1883(5)	7.2(2)
C(3)	0.1172(4)	0.2290(6)	0.1019(5)	5.9(2)
C(4)	0.1242(4)	0.1564(5)	0.1438(4)	5.6(2)
C(5)	0.5561(4)	0.2088(5)	0.0823(4)	5.0(2)
C(6)	0.5627(4)	0.1389(5)	0.1284(4)	5.1(2)
C(7)	0.6145(4)	0.2620(5)	0.0751(5)	6.2(2)
C(8)	0.6303(4)	0.1165(6)	0.1712(5)	6.1(2)
C(9)	0.3260(4)	0.3346(6)	0.3070(4)	6.1(2)
C(10)	0.2538(5)	0.3074(8)	0.2719(5)	9.6(3)
C(11)	0.1966(6)	0.3434(9)	0.3065(6)	12.4(4)
C(12)	0.171(1)	0.417(1)	0.2832(9)	27.1(9)
C(13)	0.4530(4)	0.3341(6)	0.3165(4)	6.2(2)
C(14)	0.5182(5)	0.3060(7)	0.2899(5)	8.2(3)
C(15)	0.5824(5)	0.3296(8)	0.3409(7)	10.9(4)
C(16)	0.6481(6)	0.3099(8)	0.3131(8)	13.2(5)
C(17)	0.3752(5)	0.3329(5)	0.1938(4)	6.0(2)
C(18)	0.3760(5)	0.4322(6)	0.1838(4)	7.3(3)
C(19)	0.3644(7)	0.4575(6)	0.1063(5)	9.9(3)
C(20)	0.3656(7)	0.5549(7)	0.0946(6)	11.2(4)

Table 17 (cont).

Atom	x	y	z	$B/ ext{\AA}^2$
C(21)	0.3841(5)	0.2014(5)	0.2695(4)	5.8(2)
C(22)	0.3975(6)	0.1551(6)	0.3432(5)	7.9(3)
C(23)	0.4059(7)	0.0579(6)	0.3363(5)	9.8(3)
C(24)	0.4236(7)	0.0135(8)	0.4060(6)	12.8(5)
C(25)	-0.1155(4)	0.2367(6)	0.1731(5)	6.8(2)
C(26)	-0.1782(5)	0.2051(7)	0.1185(5)	8.9(3)
C(27)	-0.1549(7)	0.1631(8)	0.0550(6)	12.5(4)
C(28)	-0.2099(8)	0.149(1)	-0.0067(7)	17.0(6)
C(29)	-0.1664(4)	0.2299(7)	0.2851(5)	7.7(3)
C(30)	-0.1248(6)	0.1536(7)	0.3211(6)	10.4(4)
C(31)	-0.1634(7)	0.1057(9)	0.3705(7)	14.5(5)
C(32)	-0.126(1)	0.042(1)	0.4169(9)	25(1)
C(33)	-0.1795(4)	0.3651(6)	0.2130(5)	7.0(2)
C(34)	-0.1532(5)	0.4316(6)	0.1661(5)	8.2(3)
C(35)	-0.2091(6)	0.5009(7)	0.1431(6)	10.3(4)
C(36)	-0.1897(8)	0.5699(9)	0.0977(7)	16.3(6)
C(37)	-0.0613(4)	0.3193(5)	0.2794(5)	7.2(3)
C(38)	-0.0642(5)	0.3708(8)	0.3475(6)	10.8(4)
C(39)	0.0173(8)	0.382(1)	0.3905(8)	28.2(7)
C(40)	0.0162(9)	0.424(1)	0.435(1)	33(1)

^a Anisotropically refined atoms are given in the form of the isotropic equivalent displacement parameter defined as $4/3[a^2B_{11}+b^2B_{22}+c^2B_{33}+ab(\cos\gamma)B_{12}+ac(\cos\beta)B_{13}+bc(\cos\alpha)B_{23}]$.

ORTEP drawing and numbering scheme of $[(C_4H_9)N]_2[Mo_2(O)(S)(\mu-S)_2(mnt)_2]$ with 50% probability thermal ellipsoids. For clarity $(C_4H_9)_4N^+$ ions are not shown. Selected bond distance and angles are listed in Table 18.

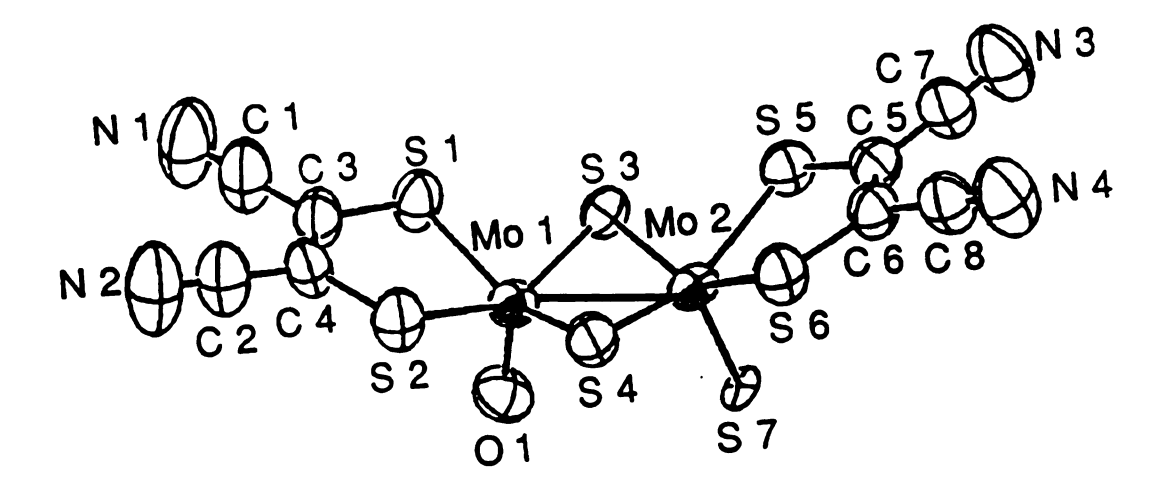


Figure 38

Table 18. Selected Bond Distances (Å) and Bond Angles (deg) for $[Mo_2~(O)(S)(\mu-S)_2(mnt)_2]^{2-}$

			Во	Bond Distances			
atom 1	ato	atom 2	distance ^a	atom 1	atom 2	m 2	distance ^a
Mo(1)	M	Mo(2)	2.858(1)	Mo(2)	S(3)		2.326(2)
Mo(1)	Š	1	2.421(2)	Mo(2)	S(4)	~	2.318(2)
Mo(1)	ŏ	ଛ	2.431(3)	Mo(2)	S(5		2.430(2)
Mo(1)	Š	3)	2.325(2)	Mo(2)	S(6,		2.429(2)
Mo(1)	Š	4	2.318(2)	Mo(2)	S(7)		1.958(4)
Mo(1)	ŏ	(1)	1.759(5)				
			E	Bond Angles			
atom 1	atom 2	atom 3	angle a	atom 1	atom 2	atom 3	angle a
Mo(2)	Mo(1)	S(1)	127.88(6)	Mo(2)	Mo(1)	0(1)	104.4(2)
Mo(2)	Mo(1)	S(2)	128.11(5)	S(1)	Mo(1)	S(2)	81.96(8)
Mo(2)	Mo(1)	S (3)	52.09(5)	S(1)	Mo(1)	S(3)	78.77(8)
Mo(2)	Mo(1)	S(4)	51.95(6)	S (1)	Mo(1)	S(4)	142.00(8)
S(1)	Mo(1)	0(1)	106.9(2)	Mo(1)	Mo(2)	S(7)	104.1(1)
S(2)	Mo(1)	S (3)	145.59(8)	S (3)	Mo(2)	S(4)	100.45(8)
S(2)	Mo(1)	S(4)	78.06(8)	S (3)	Mo(2)	S(5)	78.40(7)
S(2)	Mo(1)	0(1)	104.5(2)	S (3)	Mo(2)	S (6)	142.25(7)
S (3)	Mo(1)	S(4)	100.48(7)	S(3)	Mo(2)	S(7)	111.9(1)
S (3)	Mo(1)	O (1)	108.3(2)	S(4)	Mo(2)	S (5)	145.23(8)
S(4)	Mo(1)	0 (1)	109.2(2)	S(4)	Mo(2)	S(6)	78.78(7)
Mo(1)	Mo(2)	S (3)	52.07(5)	S(4)	Mo(2)	S(7)	105.3(1)
Mo(1)	Mo(2)	S(4)	51.92(5)	S(5)	Mo(2)	S(6)	81.62(7)
Mo(1)	Mo(2)	S(5)	128.45(6)	S(5)	Mo(2)	S(7)	107.2(1)
Mo(1)	Mo(2)	S (6)	127.83(6)	S(6)	Mo(2)	S(7)	104.5(1)
Mo(1)	S (1)	(3) (3)	105.4(3)	Mo(1)	S(4)	Mo(2)	76.13(7)
Mo(1)	S(2)	C(4)	105.7(3)	Mo(2)	S(5)	C(8)	106.1(3)
Mo(1)	S(3)	Mo(2)	75.84(6)	Mo(2)	S(6)	C(6)	105.7(3)

a Numbers in parentheses are estimated standard deviations in the least significant digits.

Table 19. Selected Bond Distances (Å) and Bond Angles (deg) for [N(C₄H₉)₄] tons

		Воп	Bond Distances		•
atom 1	atom 2	distance *	atom 1	atom 2	distance *
N(5)	(6))	1.521(11)	C(15)	C(16)	1.51(2)
N(5)	C(13)	1.507(9)	C(17)	C(18)	1.521(12)
N(5)	C(17)	1.526(9)	C(18)	C(19)	1.476(12)
N(5)	C(21)	1.512(10)	C(19)	C(20)	1.499(14)
N(6)	C(25)	1.526(12)	C(21)	C(22)	1.526(11)
N(6)	C(23)	1.512(12)	C(22)	C(23)	1.496(13)
N(6)	C(33)	1.520(11)	C(23)	C(24)	1.449(15)
N(6)	C(37)	1.503(10)	C(25)	C(26)	1.509(12)
C(1)	C(3)	1.429(12)	C(26)	C(27)	1.50(2)
C(2)	C(4)	1.415(13)	C(27)	C(28)	1.43(2)
C(3)	C(4)	1.347(12)	C(29)	C(30)	1.499(14)
C(5)	C(6)	1.361(11)	C(30)	C(31)	1.50(2)
C(5)	C(1)	1.426(11)	C(31)	C(32)	1.40(2)
C(6)	C(8)	1.441(10)	C(33)	C(34)	1.498(14)
(6))	C(10)	1.491(12)	C(34)	C(32)	1.517(15)
C(10)	C(11)	1.50(2)	C(35)	C(36)	1.45(2)
C(11)	C(12)	1.27(2)	C(37)	C(38)	1.51(2)
C(13)	C(14)	1.522(13)	C(38)	C(39)	1.64(2)
C(14)	C(15)	1.461(13)	C(39)	C(40)	1.06(3)

Table 19 (cont.)

Bond Angles

atom 1	atom 2	atom 3	angle ^a	atom 1	atom 2	atom 3	angle *
(6) <u>)</u>	N(5)	C(13)	108.1(6)	C(25)	N(6)	C(37)	105.5(6)
(6) (6)	N(5)	C(17)	110.3(6)	C(29)	N(6)	C(33)	107.5(6)
(6))	N(5)	C(21)	110.5(6)	C(29)	N(6)	C(37)	110.9(6)
C (13)	N(5)	C(17)	110.2(6)	C(33)	N(6)	C(37)	110.9(7)
C(13)	N(5)	C(21)	110.9(6)	N(5)	C(6)	C(10)	116.6(7)
C(17)	N(5)	C(21)	106.8(5)	C (6)	C(10)	C(11)	115.4(9)
C(25)	N(6)	C(29)	110.8(7)	C(10)	C(11)	C(12)	116.0(1)
C(25)	N(6)	C(33)	111.2(6)	N(5)	C(13)	C(14)	115.6(7)
C(13)	C(14)	C(15)	112.4(8)	C(26)	C(27)	C(28)	114.0(1)
C(14)	C(15)	C(16)	114.0(1)	N(6)	C(29)	C(30)	116.5(8)
N(5)	C(17)	C(18)	115.8(6)	C(29)	C(30)	C(31)	111.0(1)
C(17)	C(18)	C(19)	112.2(7)	C(30)	C(31)	C(32)	117.0(1)
C(18)	C(19)	C(20)	113.5(8)	N(6)	C(33)	C(34)	115.8(7)
N(5)	C(21)	C(22)	115.6(6)	C(33)	C(34)	C(32)	108.9(9)
C(21)	C(22)	C(23)	112.3(7)	C(34)	C(32)	C(36)	114.0(1)
C(22)	C(23)	C(24)	113.1(9)	N(6)	C(37)	C(38)	114.7(7)
N(6)	C(25)	C(36)	115.9(7)	C(37)	C(38)	C(33)	105.6(9)
C(25)	C(26)	C(27)	109.8(9)	C(38)	C(39)	C(40)	106.0(2)

^a Numbers in parentheses are estimated standard deviations in the least significant digits.

indicative of a single Mo-Mo bond. An average Mo- S_b -Mo (S_b = bridging sulfur) bond angle of 75.99°, an average bond distance of 2.322 Å, and an average S_b -Mo- S_b angle of 100.47° are in the range of those observed for other compounds with Mo₂(S)₂ bridges. 165-170 Dihedral angles between the two $Mo(S_b)_2$ planes, the two $Mo(S_b)_2$ triangles, and the two basal planes of the dimer are 148.43(11)°, 25.51(11)°, and 154.60(10)°, respectively. Each molybdenum atom is 0.707 Å above the basal plane towards the axial atoms. Similar values were observed for previously reported examples of complexes with $[Mo_2XY(\mu-S)_2]^{2+}$ (X,Y = O and/or S) cores, as illustrated in Table 20 and $21.^{165,166,170}$ Despite these similarities, the apical Mo=X (X = O,S) distances of the $[Mo_2(O)(S)(\mu-S)_2(mnt)_2]^{2-}$ dimer are different from typical $[Mo_2XY(\mu-S)_2]^{2+}$ cores. The observed $Mo_1-O_1 = 1.759(5)$ Å, $Mo_2-S_2 = 1.759(5)$ 1.958(4) Å) are much shorter then average Mo-O and Mo-S bond distance of 1.687 Å and 2.111 Å, respectively. The good π -accepting properties of the mnt²⁻ ligand will accept electron density from the metal thereby enhancing the Mo-O and M-S π -donating interaction. This synergistic effect between the π -accepting and terminal π -donor ligands may well explain the short terminal bond distances.

The origins of the bridging sulfur and terminal sulfur and oxygen atoms are not resolved. An unidentified intermediate could be oxidized with molecular oxygen to form the terminal oxygen bond. However, when the reaction was performed under strict air free condition, a small amount of $[Mo_2(O)(S)(\mu-S)_2(mnt)_2]^{2-}$ still formed indicating that the oxygen for the molybdenum oxo bond may be delivered upon oxidation of the acetate ligand of the starting complex. Similarly the bridging and terminal sulfur must come from the oxidation of the Na₂mnt ligand. The solution of Mo(mnt)₃²and $[Mo_2(O)(S)(\mu-S)_2(mnt)_2]^2$ do not interconvert

Table 20. Relevant angles for complexes with $Mo_2(\mu-S)_2XY$ (X, Y = O, S) cores

Compound	Mo-S _b -Mo, S _b -Mo-S _b , deg ^a	S _b -Mo-S _b , deg ^a	Dihedral angle of basal plane, deg	Dihedral angle Mo(S _b) ₂ plane, deg ^a	Dihedral angle triangle, deg Ref.	Ref.
$[(\eta^2\text{-}S_2)\text{MoO}(\mu\text{-}S)_2\text{MoS}(S_4)]^2$	75.6(1)					166
$[M_{02}O(S)(\mu-S)_2(S_2)_2]^2$	74.8(1)	102.45	142.9		28.3	170
$[\mathrm{Mo_2}(\mathrm{O})(\mathrm{S})(\mu\mathrm{-S})_2(\mathrm{dtc})_2]^2$	75.2	101.6		149.4		165
$[\mathrm{Mo_2}(\mathrm{O}(\mathrm{S})(\mu ext{-S})_2(\mathrm{mnt})_2]^2$ -	75.99	100.47	154.60(10)	148.43	25.51 thi	this work
$[\mathrm{Mo_2(O)_2(\mu\text{-}S)_2(i\text{-}\mathrm{mnt})_2}]^{2 ext{-}}$	75.8(1)	101.6(1)		153.1		168
$[M_{02}O_{2}(\mu-S)_{2}(SC_{2}H_{4}S)_{2}]^{2}$	75.5(4)	100.5(4)		144.5		167
syn -[$Mo_2(S)_4(SC_2H_4S)_2$] ² -	76.2(1)	100.6(1)		147.2		167
$[(\eta^2-S_2)MoS(\mu-S)_2MoS(S_4)]^2$	75.5(1)	102.1(4)		153.2(2)		169

 8 $S_{\rm b}$ = bridging sulfur

Table 21. Relevant bond distances for complexes with $Mo_2(\mu - S)_2XY$ (X, Y = O, S) cores^a

Compound	Мо-Мо	Mo=Ot	Mo-Mo Mo=O _t Mo-S _b	Mo=St	Mob	Ref
$[(\eta^2-S_2)M_0O(\mu-S)_2M_0S(S_4)]^{2-}$	2.850(1)	2.014(5)	2.350	1.862(7)		166
$[Mo_2O(S)(\mu-S)_2(S_2)_2]^2$	2.811(1)	1.945(6)	2.314	1.986(6)	0.783	170
$[\mathrm{Mo_2}(\mathrm{O})(\mathrm{S})(\mu\mathrm{-S})_2(\mathrm{dtc})_2]^2$	2.826(3)	1.82(2)	2.317	1.98(1)	0.7	165
$[\mathrm{Mo_2}(\mathrm{O}(\mathrm{S})(\mu\text{-}\mathrm{S})_2(\mathrm{mnt})_2]^{2}.$	2.858(1)	1.759(5)	2.322	1.9858(4)	0.707	this work
$[\mathrm{Mo}_2(O)_2(\mu\text{-S})_2(i\text{-mnt})_2]^2$	2.821(2)	1.664(7)	2.300(4)		0.72	168
$[Mo_2O_2(\mu-S)_2(SC_2H_4S)_2]^{2-}$	2.866(3)	1.659(3)	2.341(9)			167
$syn ext{-}[\mathrm{Mo}_2(\mathrm{S})_4(\mathrm{SC}_2\mathrm{H}_4\mathrm{S})_2]^{2 ext{-}}$	2.855(1)		2.515(2)	2.103(2)		167
$[(\eta^2\text{-}S_2)\text{MoS}(\mu\text{-}S)_2\text{MoS}(S_4)]^2$	2.3837(1)		2.32(2)	2.110(2)	0.74(2)	169

^a All distances given in Å. ^bMo displacement from the basal plane, Å.

and, therefore it is unlikely that they are produced along a concerted reaction pathway.

To avoid oxygen addition to the quadruple bonded metal core $Mo_2(O_2CCH_3)_4$ was replaced by $Mo_2Cl_4(dppm)_2$ as a precursor complex. The reaction of $Mo_2Cl_4(dppm)_2$ with Na_2mnt yields a dark green solid which has not been identified. The mid IR spectrum of this unknown solid is shown in Figure 39. A band at 2200 cm⁻¹ is assigned to the C=N stretching vibration. The far IR spectrum of the compound is shown in Figure 40. No Mo-Cl stretching vibration or bands due to Mo-O, Mo-O, Mo-S, or Mo-S stretching vibrations are observed.

The absorption spectrum of the product is shown in Figure 41, and is similar to $Mo_2Cl_4(dppm)_2$. The band at 634 nm (ϵ = 2490 M⁻¹cm⁻¹) in $Mo_2Cl_4(dppm)_2$, which is attributed to the $\delta^2 \rightarrow \delta\delta^*$ transition, is red shifted to 650 nm (ϵ = 1307 M⁻¹cm⁻¹). Higher energy bands are not as well defined as in $Mo_2Cl_4(dppm)_2$. Nevertheless, these data suggest that the quadruple bond core is preserved and mnt appears to be attach to the core.

2. Reaction of Bipyridine with Quadruply Bond Metal Complexes.

Reaction of bypyridine with Mo₂Cl₄(CH₃CN)₄ leads to the generation of insoluble products. To this end, we turned our attention to dmbpy with the goal of inducing greater solubility. The preparation followed procedures similiar to those for the preparation of Mo₂Cl₄(bpy)₂. Although the coumpound is believed to be Mo₂Cl₄(dmbpy)₂, it was not fully characterized. The compound was very susceptible to oxidation and refluxing in o-dichlorobenzene led to the formation of a red solution from which crystalline red solid is isolated. A single X-ray quality crystal was

Mid IR spectrum of the green compound isolated from the reaction of ${
m Mo_2Cl_4(dppm)_2}$ with ${
m Na_2(mnt)}$.

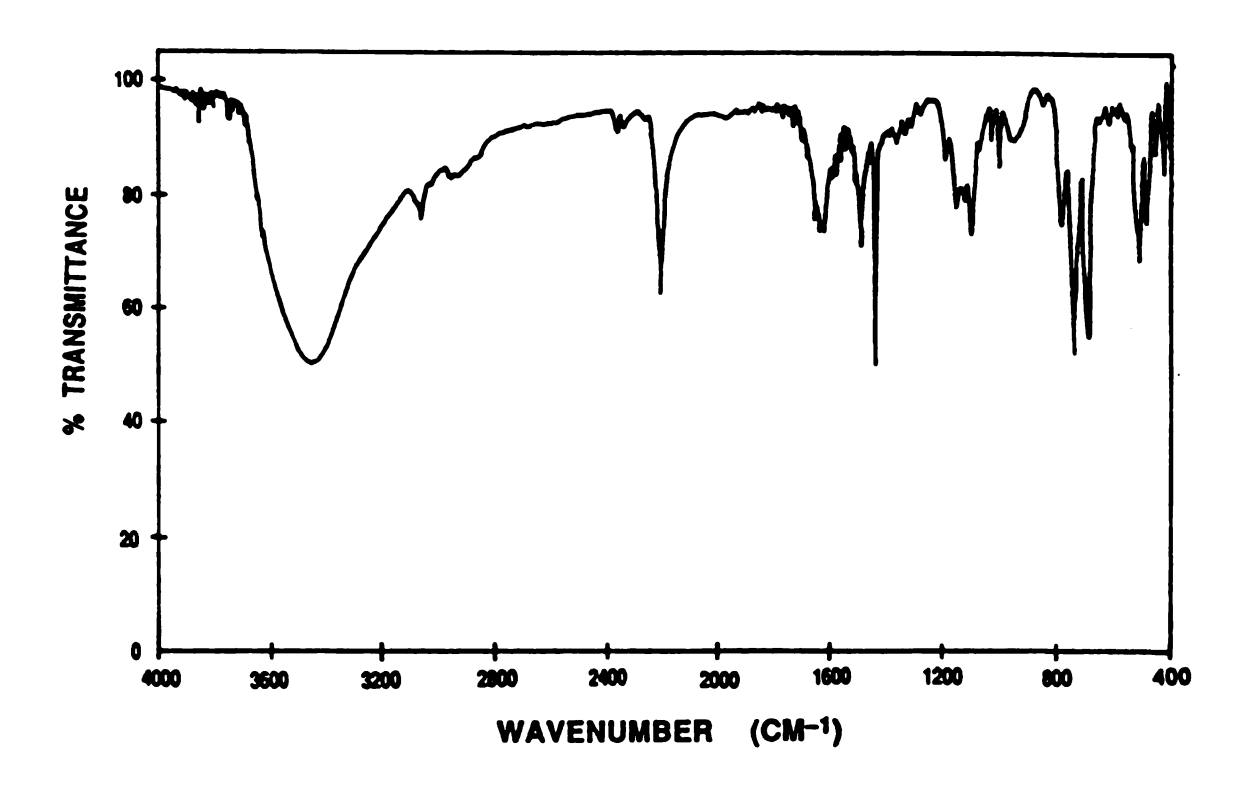


Figure 39

Far IR spectrum of the green compound isolated from the reaction of ${\rm Mo_2Cl_4(dppm)_2}$ with ${\rm Na_2(mnt)}$.

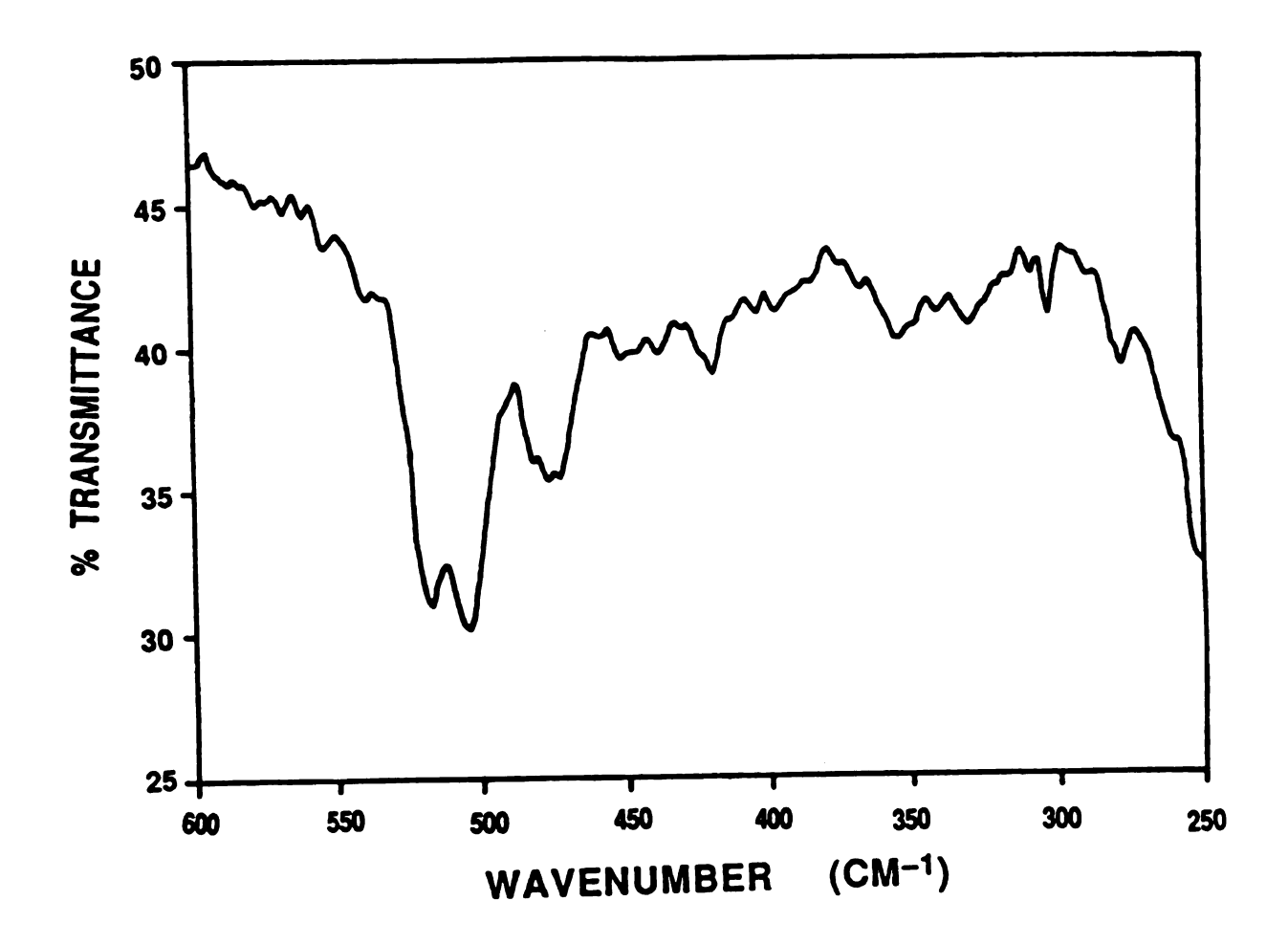


Figure 40

 $\label{eq:continuous} \text{Electronic absorption spectrum of } \text{Mo}_2(\text{dppm})_2(\text{mnt})_2 \text{ dissolved in } \text{CH}_2\text{Cl}_2.$

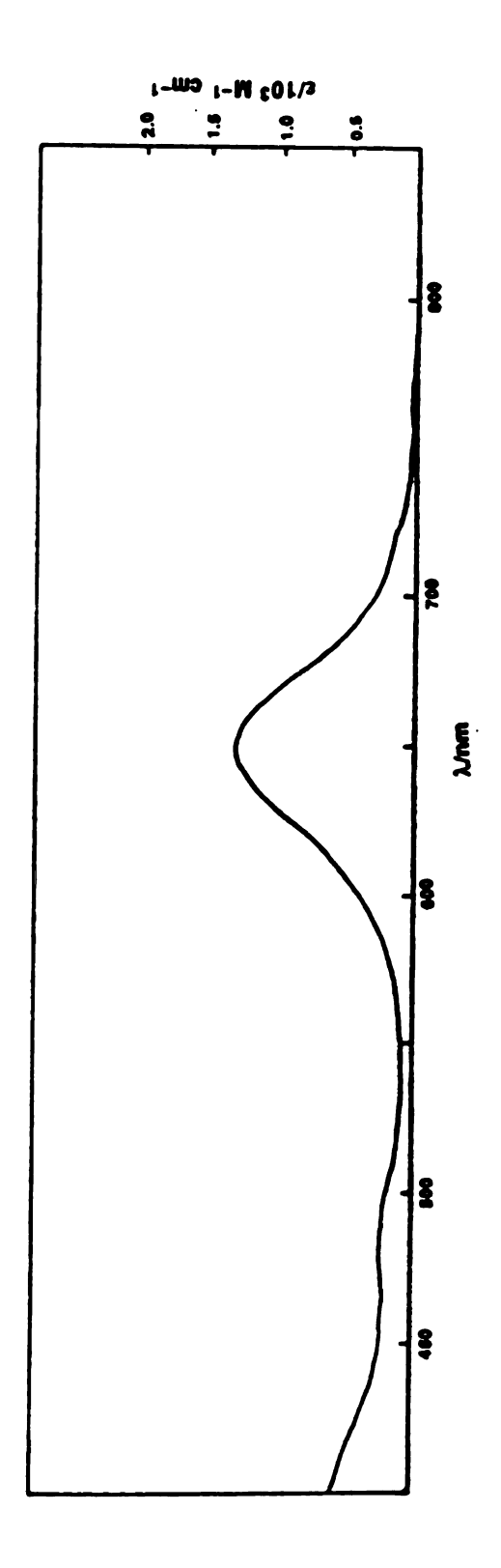


Figure 41

cr

ar

sh

tw for

co

Th Ta

ha

2.

bo an

0 X

re

di:

ea (F

vi

an res

sh

c01

шо шо

obtained, and was characterized as Mo₂O₂Cl₂(µ-O)₂(dmbpy)₂. The crystallographic data is listed in Table 15, and the positional parameters are listed in Table 22. The ORTEP diagram of $Mo_2O_2Cl_2(\mu-O)_2(dmbpy)_2$ is shown in Figure 42. The Mo₂O₄ core of the dinuclear complex consists of two terminal oxo ligands in a cis-arrangement and two bridging oxygen forming a non-planar ring. The coordination around each Mo atom is completed by a Cl atom and a chelating 4,4'-dimethyl-2,2'-bipyridyl ligand. The bond lengths and bond angles for Mo₂O₂Cl₂(µ-O)₂(dmbpy)₂, listed in Table 23, compare favorably to the complex Mo₂O₂Cl₂(µ-O)₂(bpy)₂ which has been prepared by several methods. 171-173 The Mo-Mo bond distance of 2.562(2) Å in $Mo_2O_2Cl_2(\mu-O)_2(dmbpy)_2$ indicates a strong Mo-Mo single bond. 173 The Mo-O_b-Mo (O_b = bridging oxygen) angle (83.2°) and O_b-Mo-O_b angles (91.7°) are similar to $Mo_2Cl_4(bpy)_2$, as are the MoO_t (O_t = terminal oxygen) and MoCl bond distances of 1.682(7) Å, and 2.451(4) Å, respectively.¹⁷³ The dihedral angle between the two Mo(O_b)₂ planes of the dimer is 144.89°(30) between that of the two $Mo(O_b)_2$ triangles is 35.11°(30).

With this x-ray structure, the infrared and absorption spectra are easily interpreted. The infrared spectrum of $Mo_2O_2Cl_2(\mu-O)_2(dmbpy)_2$ (Figure 43) shows a band at 965 cm which is typical of Mo=O stretching vibration. The bands at 760 cm⁻¹ and 440 cm⁻¹ are due to the antisymmetric and symmetric stretching vibration of the Mo- (O_b) bond, respectively. The electronic spectrum for $Mo_2O_2Cl_2(\mu-O)_2(dmbpy)_2$ is shown in Figure 44 and is similar to compounds containing a Mo_2O_4 core. 171,172

There has been a great interest in coordination compounds of molybdenum, because of their possible relationship to redox-active molybdo- enzymes for which there is evidence that two molybdenum

Table 2

for Mo_2

Atom

Mo(1)

Cl(1)

0(1)

0(2)

N(1)

N(10)

C(2)

C(3)

C(4) C(5)

C(5a

C(6)

C(7)

C(8)

C(9)

C(10

C(41)

C(71)

a Ani equiv

ab(cos

Table 22. Atomic Positional and Isotropic Displacement (Å²) Parameters for $Mo_2(O)_2Cl_2(\mu-O)_2(dmbpy)_2^a$

Atom	x	y	z	$B/{ m \AA}^2$
Mo(1)	0.56661(7)	0.61177(7)	-0.1041(1)	3.37(2)
Cl(1)	0.5769(3)	0.5762(3)	-0.3242(4)	7.1(1)
O(1)	0.6588(5)	0.7238(6)	-0.1224(9)	5.4(3)
O(2)	0.6070(5)	0.5212(5)	-0.0647(8)	3.6(2)
N(1)	0.4168(7)	0.4853(7)	-0.140(1)	4.5(3)
N(10)	0.4645(6)	0.6653(6)	-0.1456(9)	3.3(2)
C(2)	0.400(1)	0.3989(9)	-0.150(2)	6.8(5)
C(3)	0.313(1)	0.328(1)	-0.173(2)	8.1(6)
C(4)	0.2328(8)	0.3370(8)	-0.179(1)	4.4(3)
C(5)	0.2508(9)	0.4279(8)	-0.168(1)	4.3(4)
C(5a)	0.3419(8)	0.501(1)	-0.151(1)	3.7(3)
C(6)	0.3040(8)	0.6384(8)	-0.153(1)	4.0(3)
C(7)	0.3353(8)	0.7331(7)	-0.153(1)	3.2(3)
C(8)	0.4319(7)	0.7944(8)	-0.154(1)	3.5(3)
C(9)	0.494(1)	0.7586(9)	-0.148(1)	4.3(4)
C(10a)	0.3681(8)	0.6018(9)	-0.145(10	3.5(3)
C(41)	0.134(1)	0.254(1)	-0.189(2)	8.3(6)
C(71)	0.2651(7)	0.7667(9)	-0.160(1)	5.1(4)

^a Anisotropically refined atoms are given in the form of the isotropic equivalent displacement parameter defined as $4/3[a^2B_{11}+b^2B_{22}+c^2B_{33}+ab(\cos\gamma)B_{12}+ac(\cos\beta)B_{13}+bc(\cos\alpha)B_{23}]$.

ORTEP drawing and numbering scheme of $Mo_2O_2Cl_2(\mu-O)_2(dmbpy)_2$ with 50% probability ellipsoids. For clarity hydrogen atoms are not shown. Selected bond distances and angles are listed in Table 23.

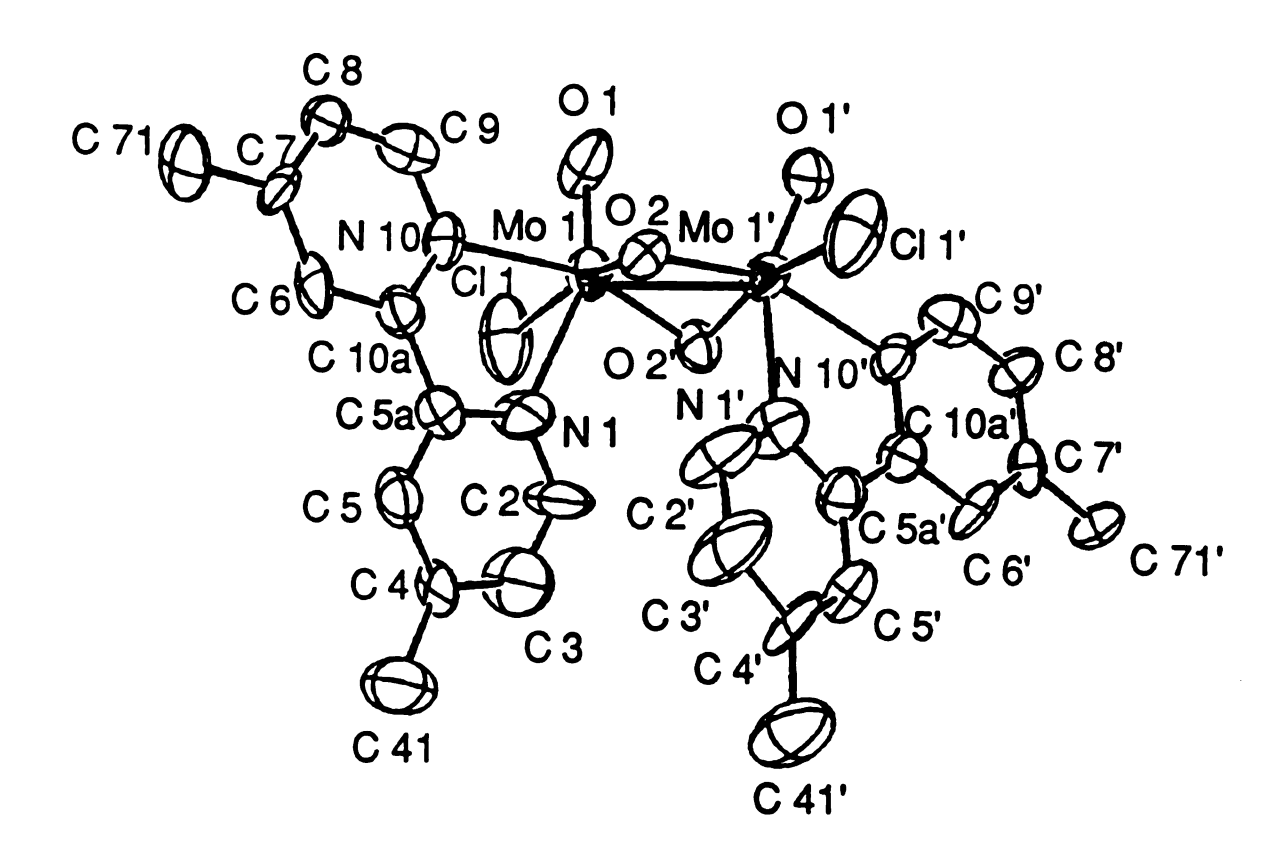


Figure 42

Table 23. Selected Bond Distances (Å) and bond Angles (deg) for $Mo_2O_2Cl_2(\mu-O)_2(dmbpy)_2^{\Delta}$

			Bond D	Bond Distances			
atom 1	atom 2	n 2	distance ^b	atom 1	atom 2	n 2	distance ^b
Mo(1) Mo(1) Mo(1) Mo(1)	Mo(1)' CI(1) O(1) O(2)	(1), 1) 1)	2.562(2) 2.451(4) 1.682(7) 1.921(10)	Mo(1) Mo(1) Mo(1)	O(2)' N(1) N(10)) (0)	1.937(8) 2.284(8) 2.253(12)
			E	Bond Angles			
atom 1	atom 2	atom 3	angle ^b	atom 1	atom 2	atom 3	angle ^b
Mo(1)'	Mo(1)	CI(1)	135.1(1) 100.5(4)	0(1)	Mo(1)	O(2)	91.7(4) 155.8(5)
Mo(1)'	Mo(1)	0 (2)	48.7(2)	O(1)	Mo(1)	N(10)	89.3(4)
Mo(1)'	Mo(1)	0(3),	48.1(3)	0(1)	Mo(1)	0(2),	105.4(4)
Mo(1)'	Mo(1)	N(1)	102.5(3)	0(2)	Mo(1)	N(1)	88.1(4)
Mo(1)'	Mo(1)	N(10)	130.3(3)	0(3)	Mo(1)	N(10)	157.8(3)
CI(1)	Mo(1)	Q 1)	90.7(4)	(1) (1)	Mo(1)	0(2)	112.9(4)
CI(1)	Mo(1)	(2)	86.8(3)	N(1)	Mo(1)	N(10)	70.1(4)
<u>CI(1)</u>	Mo(1)	0(3).	163.0(2)	N(1)	Mo(1)	0(3),	84.9(4)
<u>CI(1)</u>	Mo(1)	N(1)	78.2(3)	N(10)	Mo(1)	0(2),	82.2(4)
CI(1)	Mo(1)	N(10)	92.7(3)	Mo(1)	0(3)	Mo(1)'	83.2(4)

^a Atoms designated by the prime (') symbol are at Y, X, -Z.

^b Numbers in parentheses are estimated standard deviations in the least significant digits.

 $\label{eq:mid_loss} \mbox{Mid IR spectrum of $Mo_2O_2Cl_2(\mu$-O)_2(dmbpy)_2$.}$

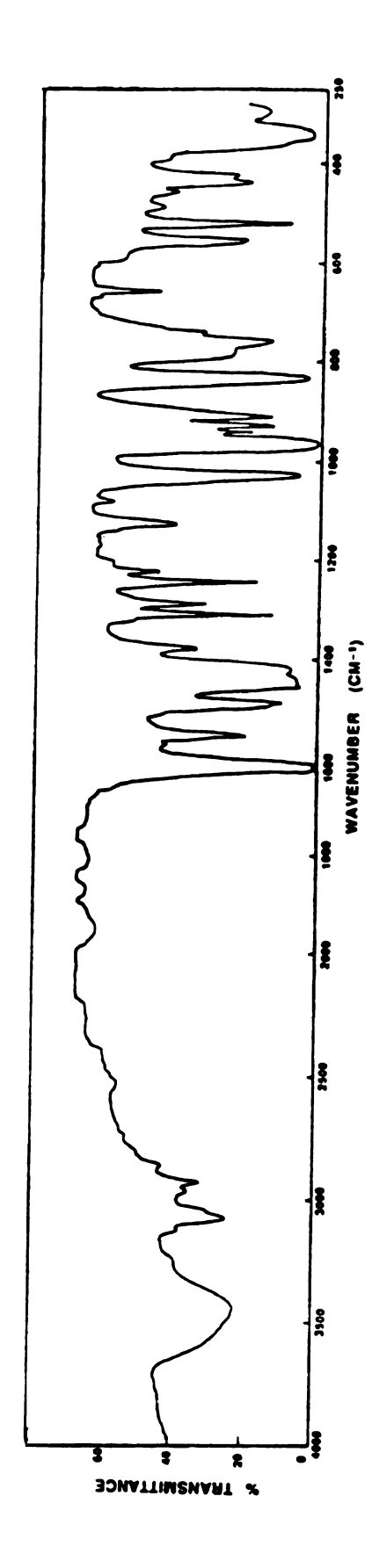


Figure 43

Electronic absorption spectrum of $\text{Mo}_2\text{O}_2\text{Cl}_2(\mu\text{-O})_2(\text{dmbpy})_2$ dissolved in CH $_3\text{CN}.$

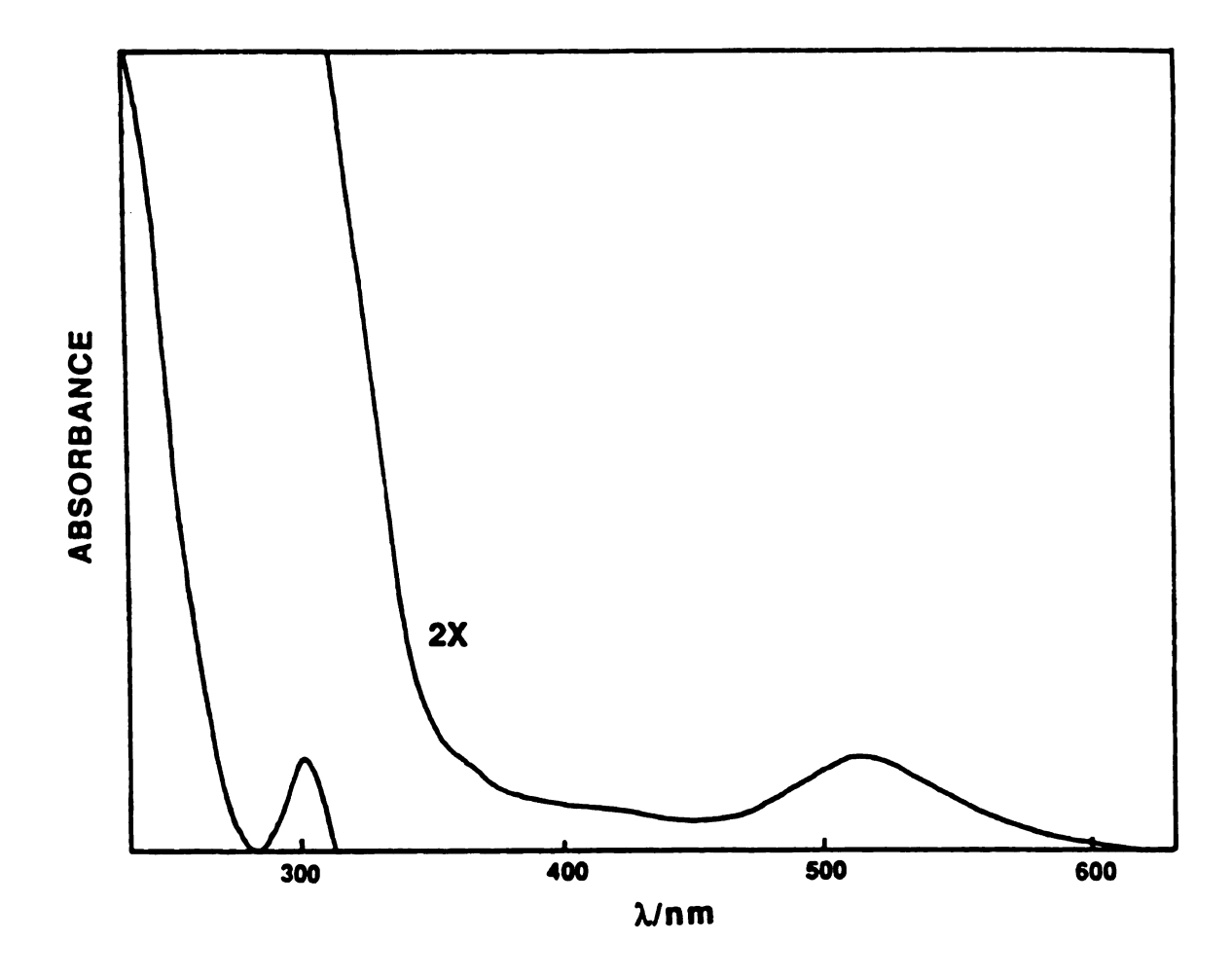


Figure 44

atoms are at the active site. ¹⁷⁴ The Mo(V) dimers $(MoYL)_2X_2$ $(Y = O, X_2 = O_2, S_2, OS)$ and Y = X = S) are of interest as models for such enzymes. There are few general synthetic designs to prepare these $Mo_2(V,V)$ dimers. Initial preparations employed Mo(V) monomers $MoCl_5$ and $(NH_4)_2Mo(S)_4$ as starting reagents under inert atmosphere to form sulfur bridging complexes. ¹⁷⁵ Oxygen bridge complexes also have relied on the monomer $MoCl_5$ upon addition of large excess of chelating compounds such as sodium N_1N_2 -dialkyldithiocarbamates (Na(dtc)) to yield $Mo_2O_3(dtc)_4$. ¹⁷⁶ A problem with using molybdenum monomers as starting reagents is the preoponderance of different side reactions competing with dimer formation. In this respect the synthetic design using molybdenum quadruple bond dimers as starting reagents is useful because the dimetallic core acts as a template.

The reaction of quadruple bond $Mo_2(II,II)$ cores to $Mo_2(V,V)$ is unique. Although the $Mo_2(II,II)$ core can be oxidized while maintaining the bimetallic core, the formal oxidation state of the core is $Mo_2(III,III)$. The quadruple bonded molybdenum, tungsten, and rhenium dimers have been shown to oxidatively add acids (HCl, HBr) and/or halogens. In most cases, extensive ligand rearrangements occurs with concomitant reduction of bond order. In the reaction of alkyl and aryl disulfides edge sharing bioctahedra are obtained. The conversion of $Mo_2(II,II)$ to $Mo_2(V,V)$ (MoYL)₂X₂ (Y = O, X₂ = O₂, S₂, OS and Y = X = S) cores is without precedent and provides a convenient route to the preparation of these interesting biological model compounds.

APPENDIX

Nuclear Magnetic Resonance Spectra

 $^{31}P\{^{1}H\}$ NMR spectrum of $Rh_{2}[CH_{3}N(PF_{2})_{2}]_{3}(PF_{3})_{2}$, 1. NMR spectrum was not reference to an external standard.

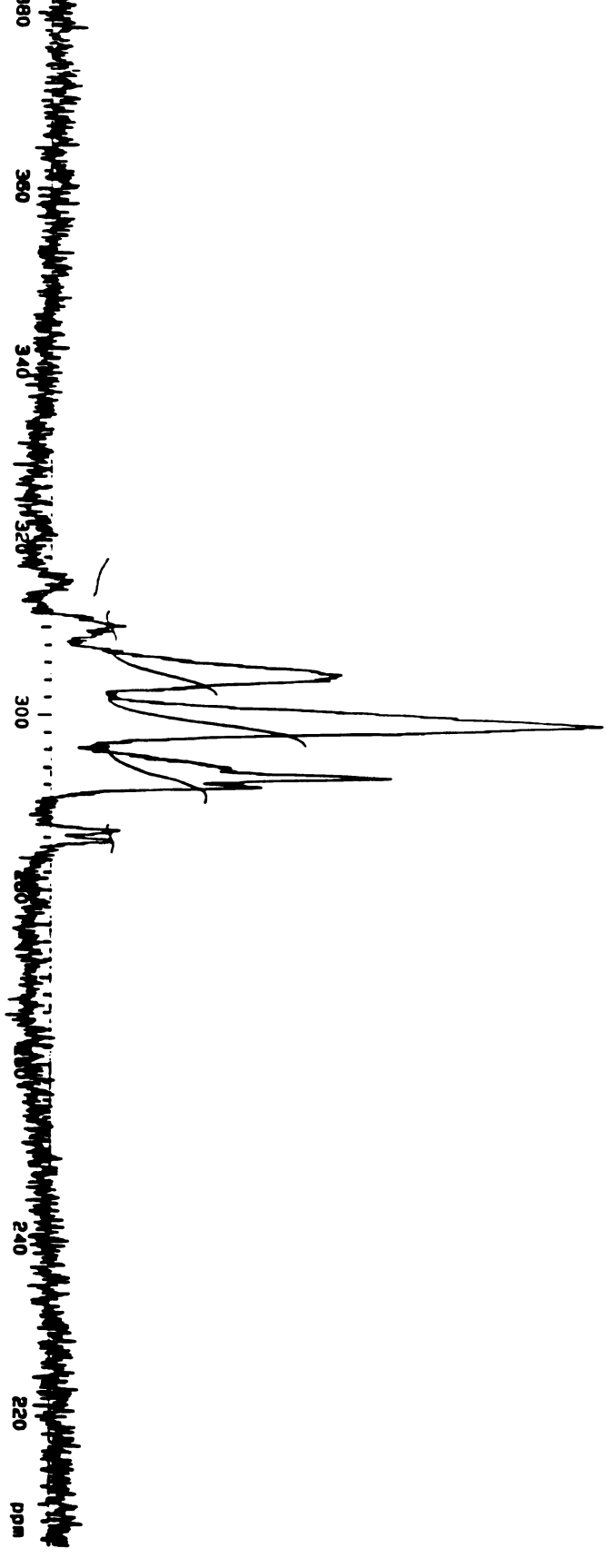


Figure 45

 $^{31}\rm{P}\{^1\rm{H}\}$ NMR spectrum of $\rm{Rh}_2[\rm{CH}_3N(\rm{PF}_2)_2]_3(\rm{PF}_3)Cl_2$, 2 prepared by method i of Section II.A.2c.

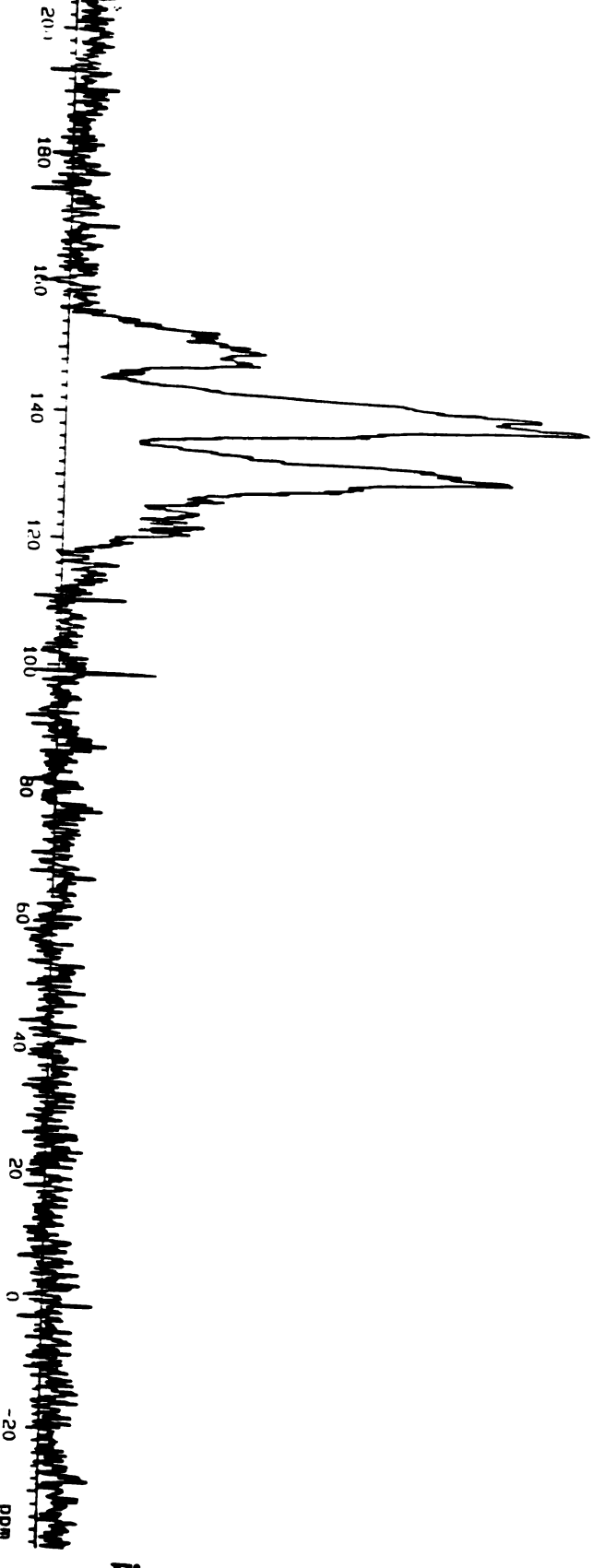


Figure 46

 $^{31}\mathrm{P}(^{1}\mathrm{H})$ NMR spectrum of $\mathrm{Rh_{2}[CH_{3}N(PF_{2})_{2}]_{3}Cl_{4}},$ 3.

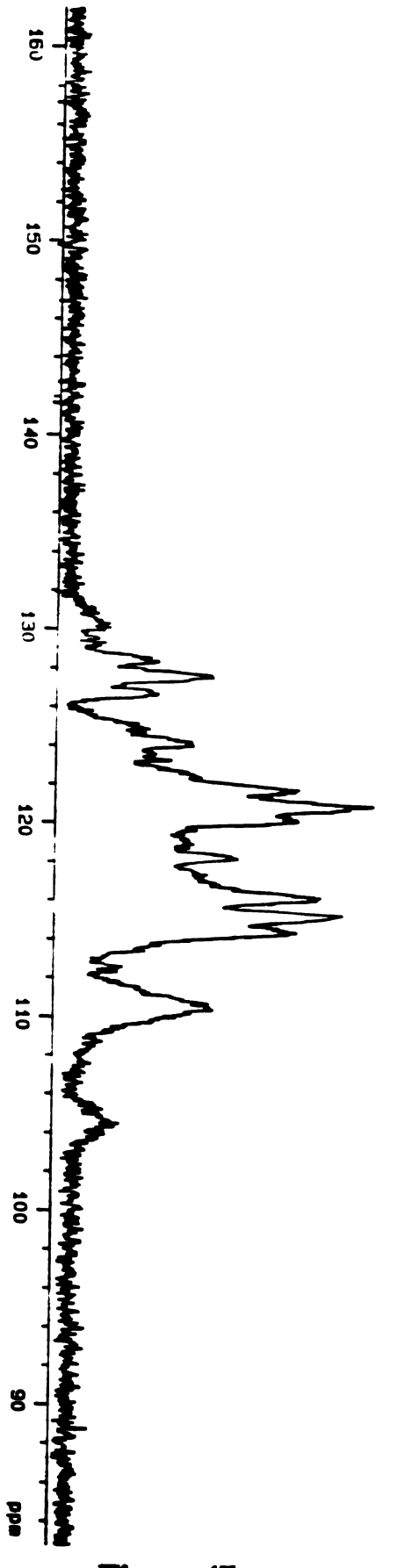


Figure 47

 $^{19}\mathrm{F}$ NMR spectrum of $\mathrm{Rh_2[CH_3N(PF_2)_2]_3(PF_3)_2},\,\mathbf{1}$

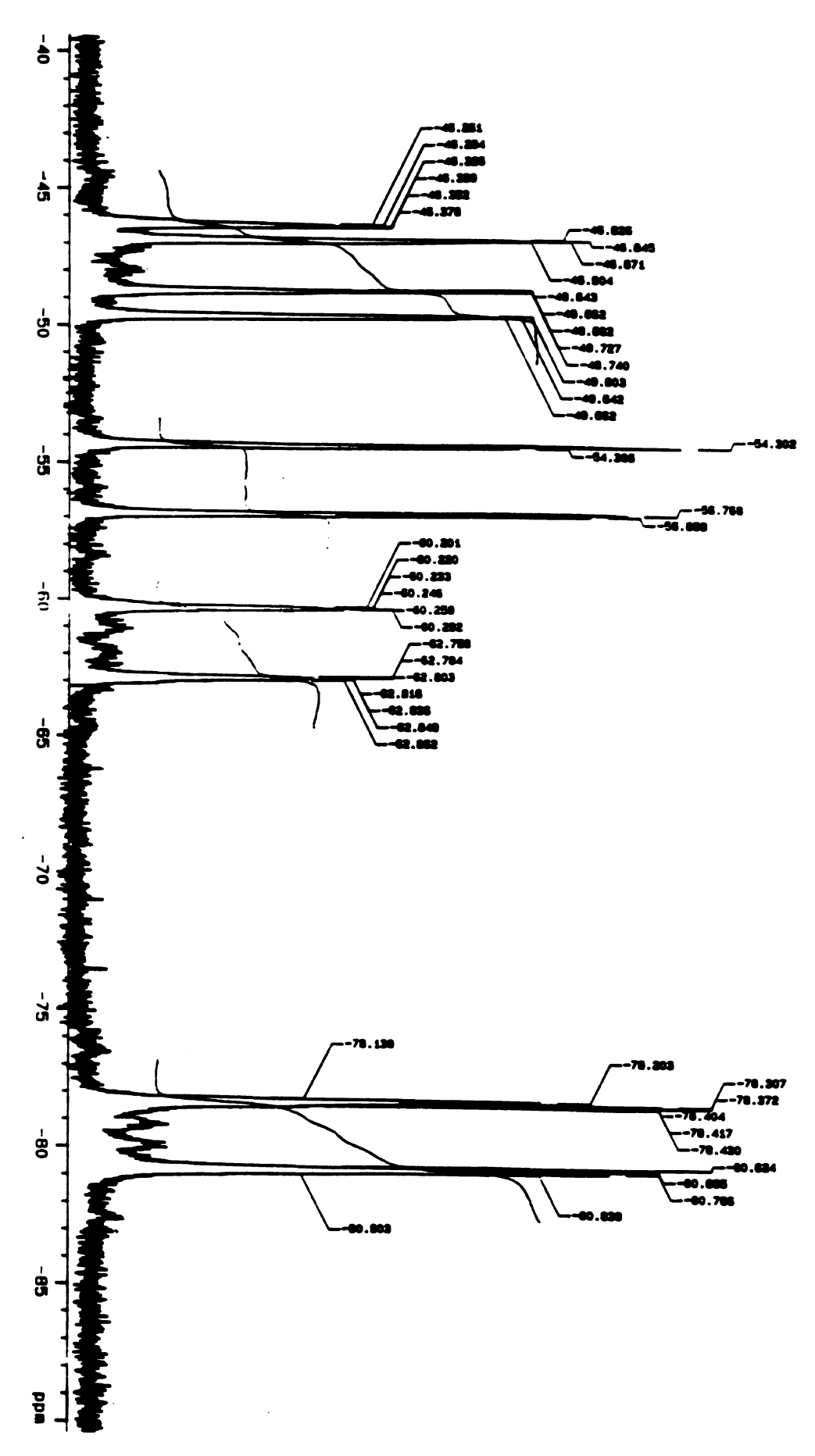


Figure 48

 $^{19}{\rm F}$ NMR spectrum of ${\rm Rh_2[CH_3N(PF_2)_2]_3(PF_3)Cl_2}$, 2 prepared by method i of Section II.A.2.c.

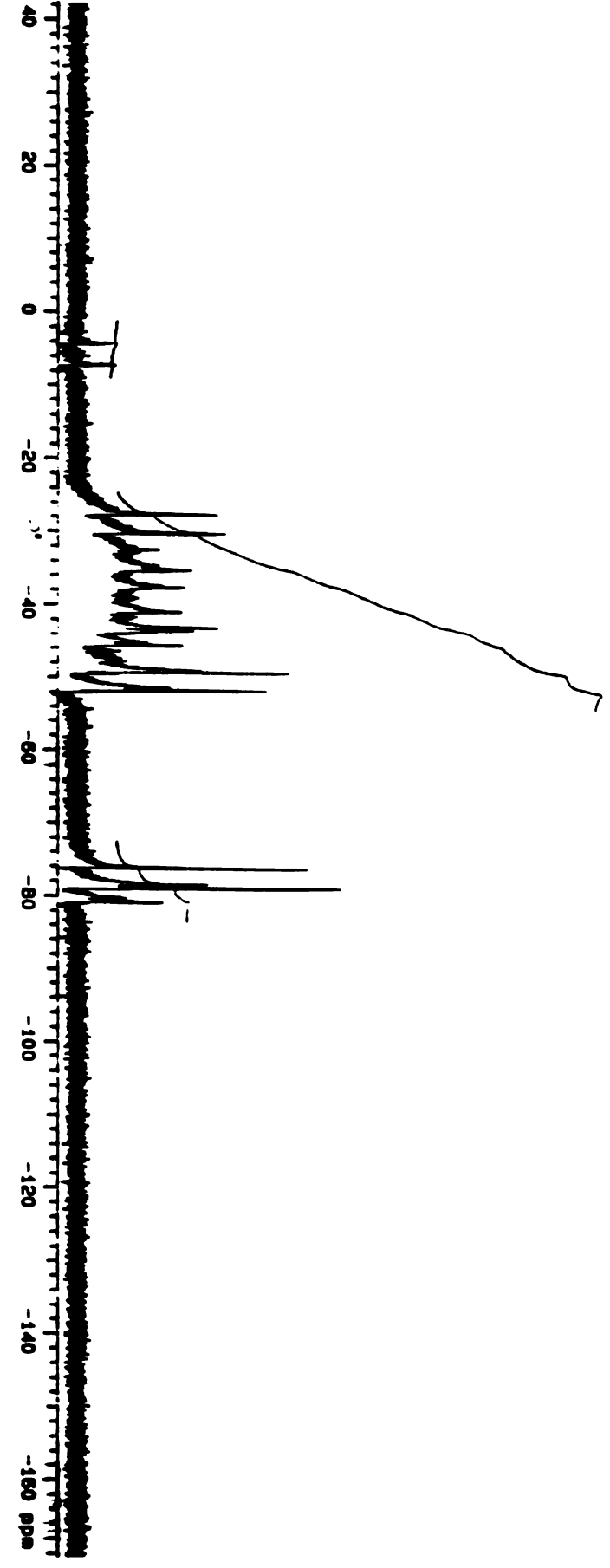


Figure 49

 $^{19}\mathrm{F}$ NMR spectrum of $\mathrm{Rh_2[CH_3N(PF_2)_2]_3Cl_4}$, 3.

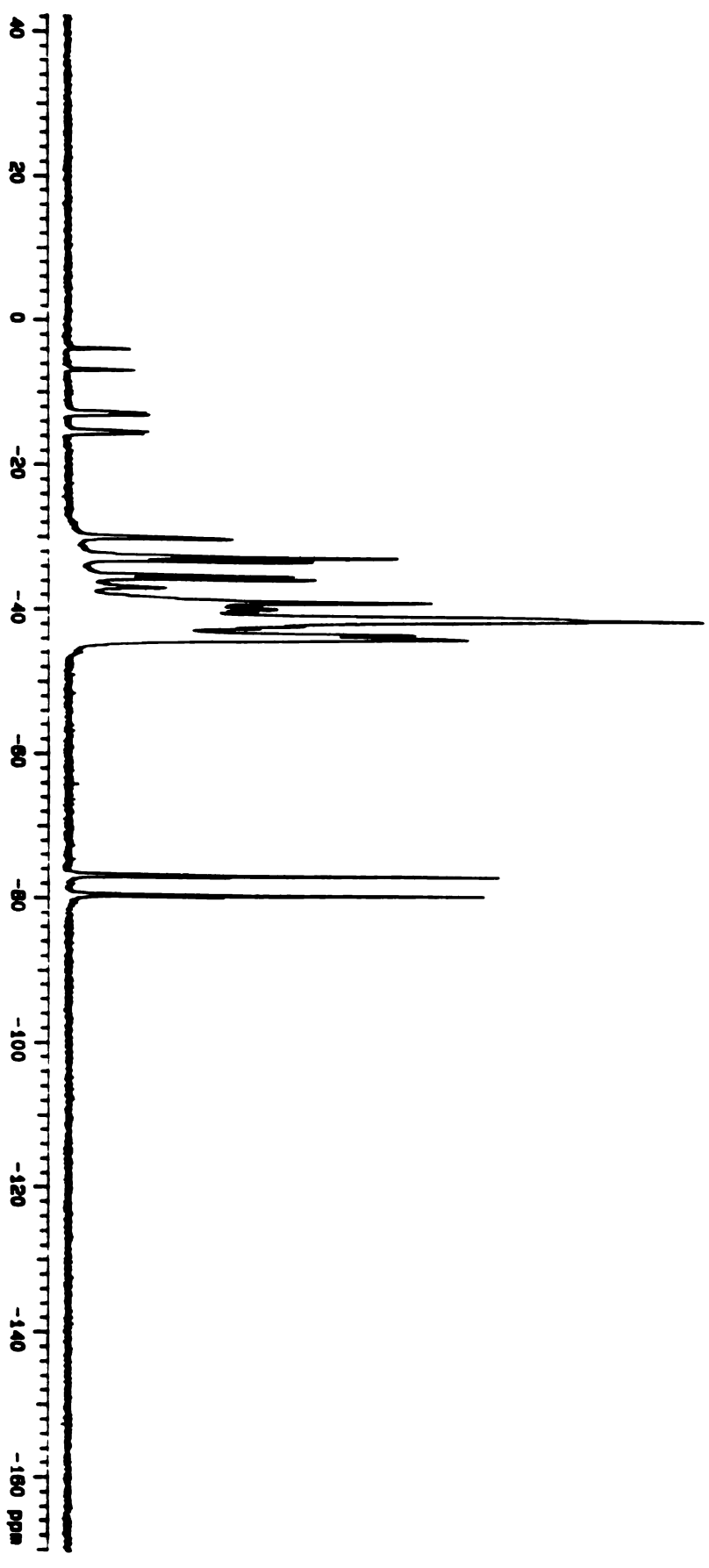


Figure 50

 $^{19}\rm{F}\{^{31}\rm{P}\}$ NMR spectrum of $\rm{Rh}_2[\rm{CH}_3N(\rm{PF}_2)_2]_3(\rm{PF}_3)Cl_2$, 2 prepared by method i of Section II.A.2.c.

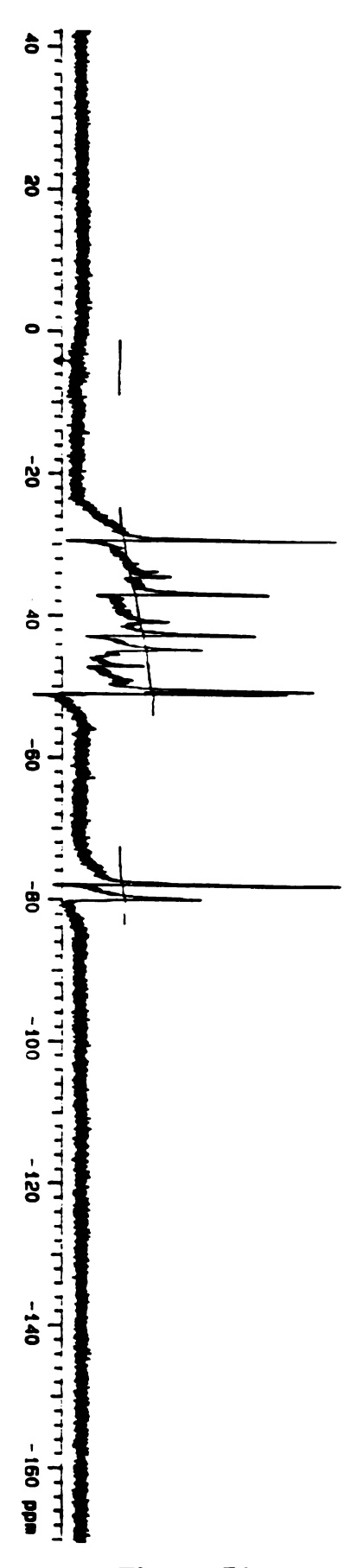
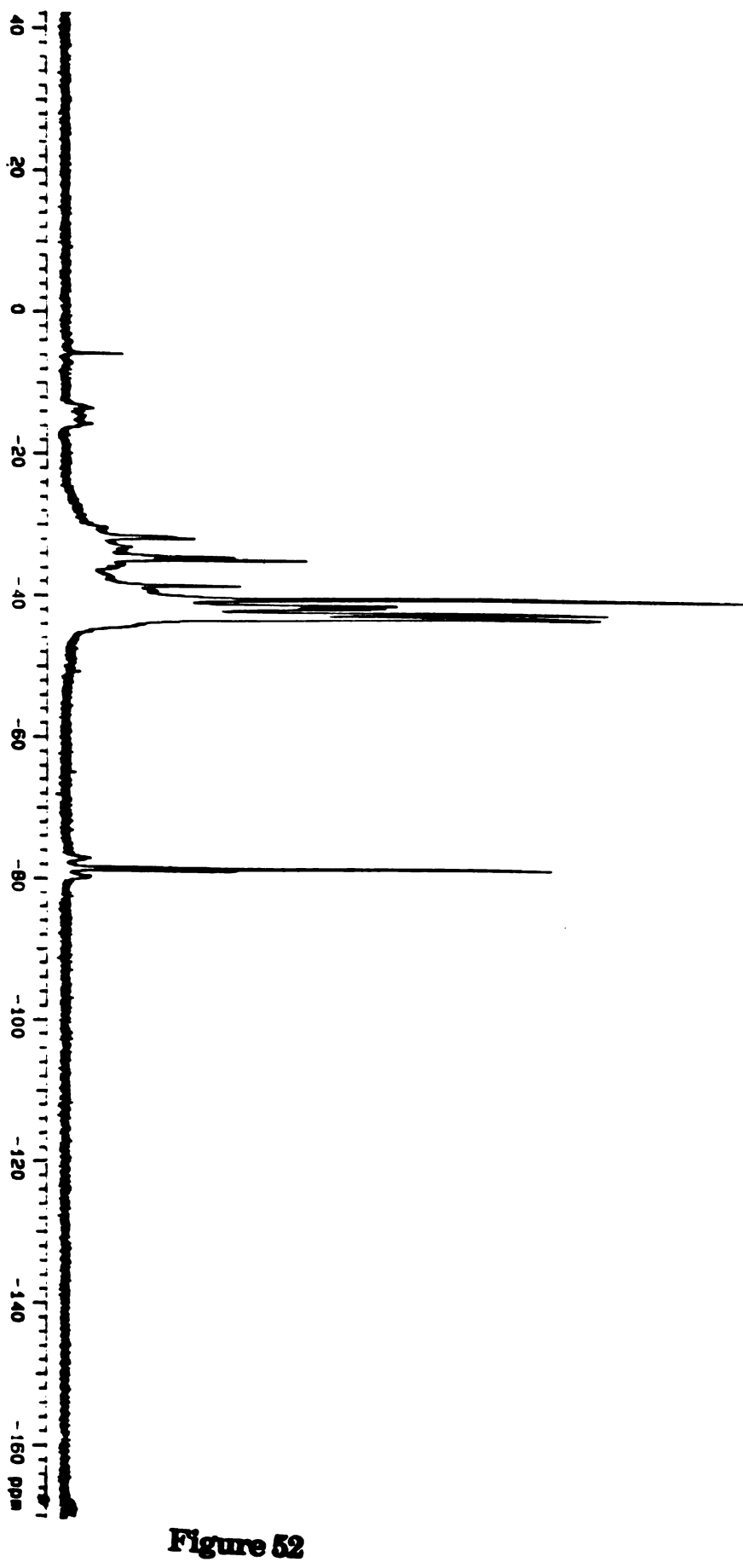
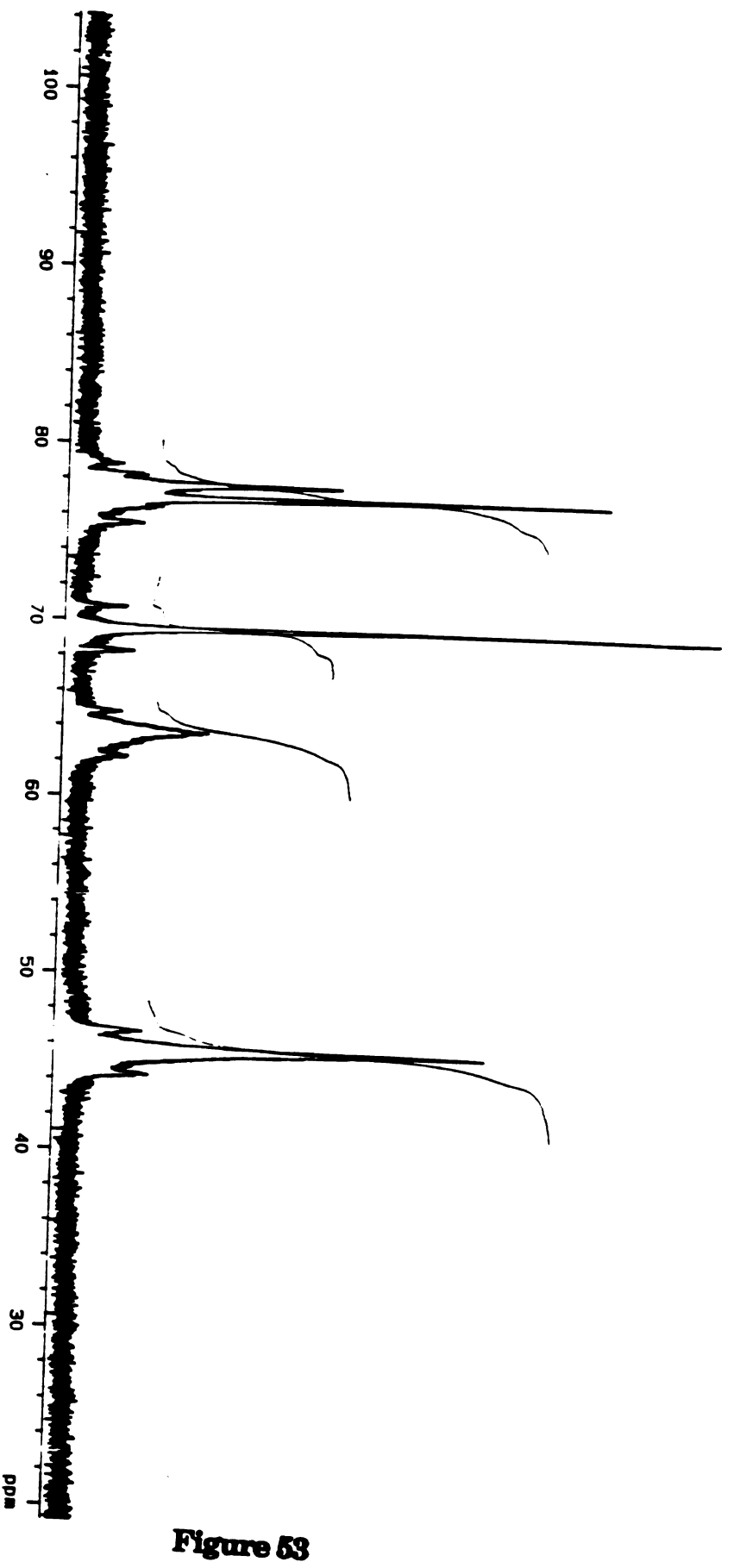


Figure 51

 $^{19}\rm{F}\{^{31}\rm{P}\}$ NMR spectrum of $\rm{Rh}_2[\rm{CH}_3N(\rm{PF}_2)_2]_3(\rm{PF}_3)Cl_2$, 2 prepared by method i of Section II.A.2.c.



 $^{19}\rm{F}\{^{31}\rm{P}\}$ NMR spectrum of $\rm{Rh_2[CH_3N(PF_2)_2]_3Cl_4}$, 3. NMR spectrum was not reference to an external standard



 $^{31}\mathrm{P\{1H\}}$ NMR spectrum of $\mathrm{Rh_3(\mu\text{-}Cl)_3[CH_3N(PF_2)_2]_3},\,\mathbf{1}$

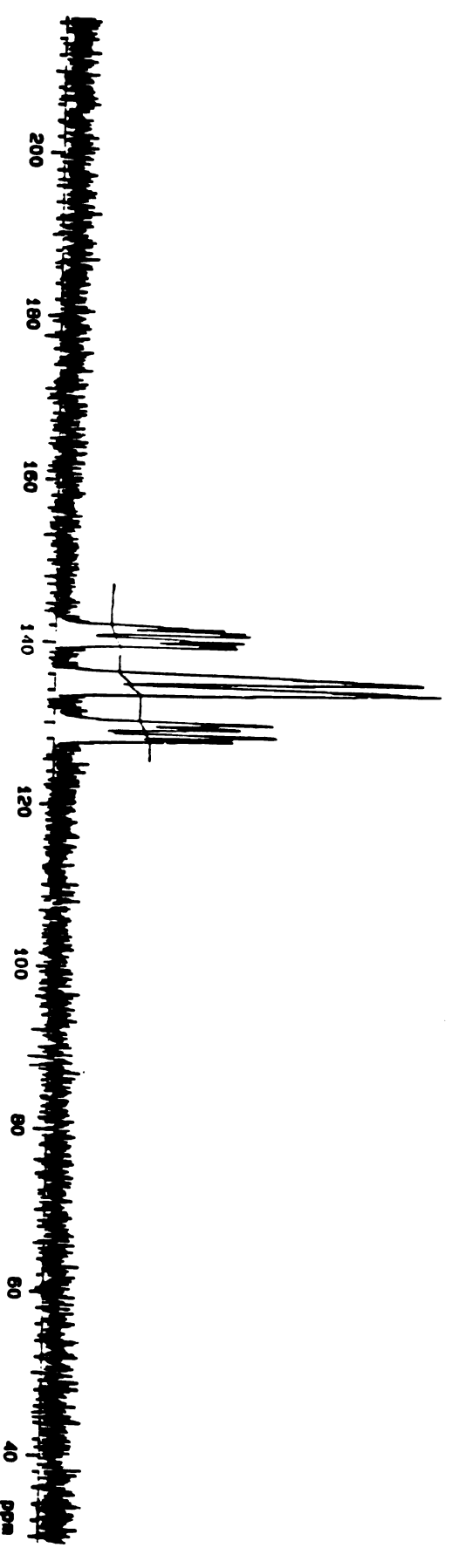
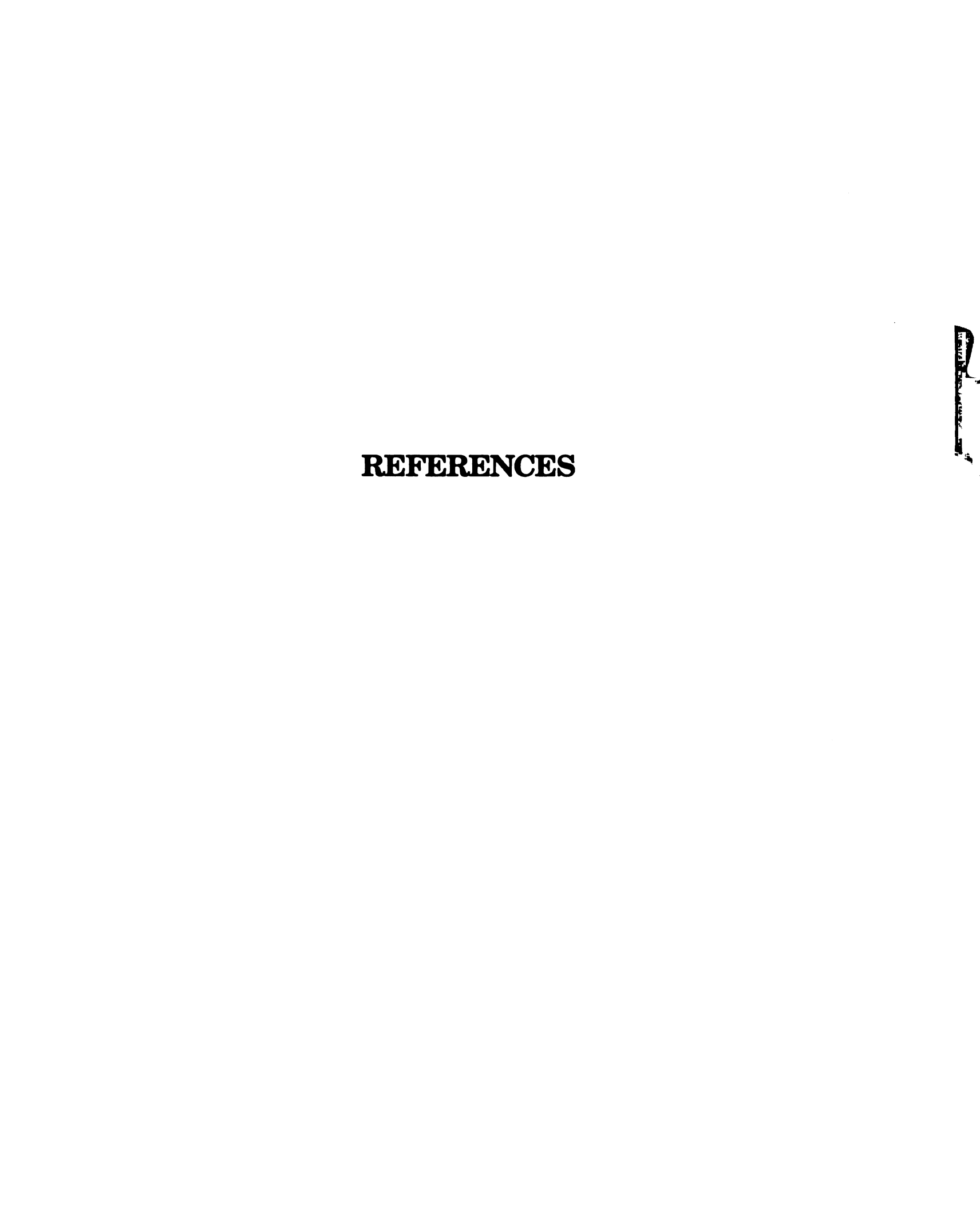


Figure 54



- 1. Photoinduced Electron Transfer; Fox, M. A., Chanon, M., Eds.; Elsevier: Amsterdam, 1988.
- 2. Juris, A.; Balzani, V.; Barigelletti, F.; Campagna, S.; Belser, P.; von Zelewsky, A. Coord. Chem. Rev. 1988, 84, 85 277.
- 3. Photochemistry and Photophysics of Coordination Compounds; Yersin, H., Vogler, A., Eds.; Springer-Verlag: Berlin, 1987.
- 4. Adamson, A. W. J. Chem. Ed. 1983, 60, 797-802.
- Porter, G. B. In Concepts of Inorganic Photochemistry; Adamson,
 A. W. Fleischauer, P. D., Eds.; Wiley: New York, 1975.
- 6. Kavarnos, G. J.; Turro, N. J. Chem. Rev. 1986, 86, 401-449.
- 7. Balzani, V.; Sabbatini, N.; Scandola, F. Chem. Rev. 1986, 86, 319-337.
- 8. Energy Resources through Photochemistry and Catalysis; Grätzel M., Ed.; Academic Press: New York, 1983.
- 9. Gray, H. B.; Maverick, A. W. Science 1981, 214, 1201-1205.
- Photochemical Conversion and Storage of Solar Energy; Connolly,
 J. S., Ed.; Academic Press: New York, 1981.
- (a) Roundhill, D. M.; Gray, H. B.; Che, C.-M. Acc. Chem. Res. 1989,
 22, 55-61. (b) Marshall, J. L.; Steigman, E.; Gray, H. B. In Excited
 States and Reactive Intermediates; A. B. P. Lever, Ed.; ACS
 Symposium Series 307; American Chemical Society: Washington,
 DC, 1986, pp 166-176 and references therein. (c) Caspar, J. V.;
 Gray, H. B. J. Am. Chem. Soc. 1984, 106, 3029-3030.
- (a) Rodman, G. S.; Daws, C. A.; Mann, K. R. Inorg. Chem. 1988,
 27, 3347-3353. (b) Rodman, G. S.; Mann, K. R. Inorg. Chem. 1985,
 24, 3507-3508.

- (a) Hill, C. L.; Bouchard, D. A.; Kadkhodayan, M.; Williamson, M.
 M.; Schmidt, J. A.; Hilinski, E. F. J. Am. Chem. Soc. 1988, 110, 5471-5479.
 (b) Hill, C. L.; Bouchard, D. A. J. Am. Chem. Soc. 1985, 107, 5148-5157.
- (a) Chang, I.-J.; Nocera, D. G. J. Am. Chem. Soc. 1987, 109, 4901-4907.
 (b) Chang, I.-J.; Nocera, D. G. Inorg. Chem. 1989, 28, 4309-4311.
 (c) Partigianoni, C. M.; Chang, I.-J.; Nocera, D. G. Coord. Chem. Rev. 1990, 97, 105-107.
- 15. Caspar, J. V. J. Am. Chem. Soc. 1985, 107, 6718-6719.
- 16. Pierson, B.K.; Olson, J.M. In New Comprehensive Biochemistry; Amesa, J. D.; Elsevier: Dordrecht, 1987; Vol 15, 21-42.
- 17. Meyer, T. J. Acc. Chem. Res. 1989, 22, 163-170.
- Moore, T. A.; Gust, D.; Mathis, P.; Mialocq, J. C.; Chachaty, C.;
 Bensasson, P. A.; Land, E. J.; Doizi, D.; Liddell, P. A.; Lehman, W.
 R.; Nemeth, G. A.; Moore, A. L. Nature 1984, 307, 630-632.
- Gust, D; Moore, T. A.; Moore, A. L.; Makings, L. R.; Seely, G. R.;
 Ma, X.; Trier, T. T.; Gao, F. J. Am. Chem. Soc. 1988, 110, 7567-7569.
- Danielson, E.; Elliott, C. M.; Merkert, J. W.; Meyer, T. J. J. Am.
 Chem. Soc. 1987, 109, 2519-2520.
- 21. (a) Barber, J. In Photosysthesis in Relation to Model System;
 Elsevier: New York, 1979. (b) Clayton, R. K. In Photosythesis:
 Physical Mechanisms and Chemical Patterns; Cambridge
 University Press: London, 1980.
- (a) Bock, C. R.; Meyer, T. J.; Whitten, D. G. J. Am. Chem. Soc.
 1974, 96, 4710-4712. (b) Young, R. C.; Meyer, T. J.; Whitten, D. G. J.
 Am. Chem. Soc. 1975, 97, 4781-4782.

- 23. Lin, C. -T.; Bottcher, W.; Chou, M.; Creutz, C.; Sutin, N. J. Am. Chem. Soc. 1976, 98, 6536-6544.
- 24. Pichat, P.; Fox, M. A. In *Photoinduced Electron Transfer*; Fox, M. A.; Chanon, M., Eds.; Elsevier: Amsterdam, 1988; Part D.
- 25. Gerischer, H. In *Photoelectrochemistry, Photocatalysis, and Photoreactors*; Schiavello, M. Ed.; D. Reidel Plublishers: Dordrecht, 1985.
- Baral, S.; Fendler, J. H. In Photoinduced Electron Transfer; Fox,
 M. A.; Chanon, M., Eds.; Elsevier: Amsterdam, 1988; Part B.
- 27. Tsuchida, E.; Kaneko, M.; Hoshino, M. J. Phys. Chem. 1986, 90, 2283-
- Baral, S.; Zhao, X. K.; Rolandi, R.; Fendler, J. Phys Chem. 1987, 91, 2701-2704.
- 29. Rabani, J. In Photoinduced Electron Transfer; Fox, M. A.; Chanon,M., Eds.; Elsevier: Amsterdam, 1988; Part B.
- 30. Gratzel, M. E. In Energy Resources Through Photochemisty and Cataysis; Academic Press: New York, 1983.
- 31. Gard, D. R.; Brown, T.L. J. Am. Chem. Soc. 1982, 104, 6340-6347.
- 32. Freedman, A.; Bersohn, R. J. Am. Chem. Soc. 1978, 100, 4116-4118.
- 33. Rothberg, L. J.; Cooper, N. J.; Peters, K. S.; Vaida, V. J. Am. Chem. Soc. 1982, 104, 3536-3537.
- 34. Morse, D. L.; Wrighton, M. S. J. Am. Chem. Soc. 1976, 98, 3931-3934.
- 35. Lee, K.-W.; Pennington, W. T.; Cordes, A. W.; Brown, T. L. Organometallics 1984, 3, 404-413.
- 36. Lee, K.-W.; Pennington, W. T.; Cordes, A. W.; Brown, T. L. J. Am. Chem. Soc. 1985, 107, 631-641.

- 37. Lee, K.-W.; Brown, T. L. Organometallics. 1985, 4, 1030-1036.
- 38. Lee, K.-W.; Hanckel, J. M.; Brown, T. L. J. Am. Chem. Soc. 1986, 108, 2266-2273.
- 39. Chaudret, B.; Delavaux, B.; Poilblanc, R. Coord. Chem. Rev. 1988, 86, 191-243.
- Stiegman, A. E.; Miskowski, V. M. J. Am. Chem. Soc. 1988, 110, 4053-4054.
- Stiegman, A. E.; Miskowski, V. M.; Gray, H. B. J. Am. Chem. Soc.
 1986, 108, 2781-2782.
- 42. Shin, Y.-G. K.; Miskowski, V. M.; Nocera, D. G. accepted for publication in *Inorg. Chem*.
- 43. Mortola, A. P.; Moskowitz, J. W.; Rosch, N.; Cowman, C. D.; Gray,
 H. B. Chem. Phy. Lett. 1975, 32, 283-286.
- 44. Norman, J. G., Jr.; Kolari, H. J. J. Am. Chem. Soc. 1975, 97, 33-37.
- 45. Hay, P. J. J. Am. Chem. Soc. 1982, 104, 7007-7017.
- 46. Mathisen, K. B.; Wahlgren, U.; Pettersson, L. G. M. Chem. Phys. Lett. 1984, 104, 336-342.
- 47. Stromberg, A.; Petersson, L. G. M.; Wahlgren, U. Chem. Phys. Lett. 1985, 118, 389-394.
- 48. Hall, M. B. Polyhedron 1987, 6, 679-684.
- 49. Ziegler, T.; Tschike, V.; Becke, A. Polyhedron 1987, 6, 685-693.
- 50. Bursten, B. E.; Clark, D. L. Polyhedron, 1987, 6, 695-704.
- 51. (a) Cowman, C. D.; Gray, H. B.; Gray, H. B. J. Am. Chem. Soc.
 1973, 95, 8177-8178. (b) Cowman, C. D.; Togler, W. C.; Gray, H. B.
 Isr. J. Chem. 1977, 15, 308-310. (c) Miskowski, V. M.; Goldbeck, R.
 A.; Kliger, D. S.; Gray, H. B. Inorg. Chem. 1979, 18, 86-89.
- 52. Trogler, W. C.; Gray, H. B. Acc. Chem. Res. 1978, 11, 232-239.

- 53. (a) Cotton, F. A.; Martin, D.S.; Fanwick, P. E.; Peters, T. J.; Webb, T. R. J. Am. Chem. Soc. 1976, 98, 4681-4682. (b) Fanwick, P. E.; Martin, D. S.; Cotton, F. A.; Webb, T. R. Inorg. Chem. 1977, 16, 2103-2106. (c) Trogler, W.C.; Cowman, C. D.; Gray, H. B.; Cotton, F. A. J. Am. Chem. Soc. 1977, 99, 2993-2996.
- Rice, S. F.; Wilson, R. B.; Solomon, E. I. Inorg. Chem. 1980, 19, 3425-3421.
- 55. (a) Manning, M. C.; Trogler, W. C. Inorg. Chem. 1982, 21, 2797-2800. (b) Manning, M. C.; Trogler, W. C. J. Am. Chem. Soc. 1983, 105, 5311-5320.
- Martin, D. S.; Newman, R. A.; Fanwick, P. E. Inorg. Chem. 1982,
 21, 3400-3406.
- 57. Fraser, I. F.; Peacock, R. D. Chem. Phys. Lett. 1983, 98, 620-623.
- 58. Clark, R. J. H.; Stead, M. J. Inorg. Chem. 1983, 22, 1214-1220.
- Lichtenberger, D. L.; Blevins, C. H. J. Am. Chem. Soc. 1984, 106, 1636-1641
- 60. Robbins, G. A.; Martins, D. S. Inorg. Chem. 1984, 23, 2086-2093.
- 61. (a) Martin, D. S.; Huang, H.-W.; Newman, R. A. Inorg. Chem.
 1984, 23, 699-701. (b) Huang, H.-W.; Martin, D. S. Inorg. Chem.
 1985, 24, 96-101.
- 62. (a) Fanwick, P. E. Inorg. Chem. 1985, 24, 258-263. (b) Fanwick, P. E.; Bursten, B. E.; Kaufmann, G. B. Inorg. Chem. 1985, 24,1165-1169.
- 63. Dallinger, R. F. J. Am. Chem. Soc. 1985, 107, 7202-7204.
- Morris, D. E.; Sattelberger, A. P. Woodruff, W. H. J. Am. Chem.
 Soc. 1986, 108, 8270-8271.

- (a) Zietlow, T. C.; Hopkins, M. D.; Gray, H. B. J. Solid State Chem.
 1985, 57, 112. (b) Hopkins, M. D. Gray, H. B.; Miskowski, V. M.
 Polyhedron 1987, 6, 705-714. (c) Hopkins, M. D.; Schaefer, W. P.;
 Bronikowski, M. J.; Woodruff, W. H.; Miskowski, V. M.; Dallinger,
 R. F.; Gray, H. B. J. Am. Chem. Soc. 1987, 109, 408-416. (d) Hopkins,
 M. D.; Miskowski, V. M.; Gray, H. B. J. Am. Chem. Soc. 1988, 110,
 1787-1793.
- Cotton, F. A.; Daniels, L. M.; Powell, G. L.; Kahaian, A. J.; Smith,
 T. J.; Vogel, E. F. Inorg. Chim. Acta 1988, 144, 109-117.
- 67. Winkler, J. R.: Nocera, D. G.; Netzel, T. L. J. Am. Chem. Soc. 1986, 108, 4451-4458.
- Erwin, D. K.; Geoffroy, G. L.; Gray, H. B.; Hammond, G. S.;
 Solomon, E. I.; Trogler, W. L.; Zagars, A. A. J. Am. Chem. Soc.
 1977, 99, 3620-3625.
- Trogler, W. C.; Erwin, D. K.; Geoffroy, G. L.; Gray, H. B. J. Am.
 Chem. Soc. 1978, 100, 1160-1163.
- (a) Cotton, F. A.; Kalbacher, B. J. Inorg. Chem. 1976, 15, 522-524. (b)
 Bino, A.; Cotton, F. A. J. Am. Chem. Soc. 1979, 101, 4150-4154.
- (a) Nocera, D. G.; Gray, H. B. Inorg. Chem. 1984, 23, 3686-3688. (b)
 Nocera, D. G.; Gray, H. B. J. Am. Chem. Soc. 1981, 103, 7349.
- 72. Che, C.-M.; Butler, L. G.; Gray, H. B. J. Am. Chem. Soc. 1981, 103, 7796-7797.
- (a) Rice, S. F.; Gray, H. B. J. Am. Chem. Soc. 1983, 105, 4571-4575.
 (b) Rice, S. F.; Gray, H. B. J. Am. Chem. Soc. 1981, 103, 1593-1595.
 (c) Rice, S. F.; Mildeer, S. J.; Gray, H. B.; Goldbeck, R. A.; Kliger, D. A. Coord. Chem. Rev. 1982, 43, 349-354

- Marshall, J. L.; Stobart, S. R.; Gray, H. B. J. Am. Chem. Soc. 1984, 106, 3027-3029.
- 75. Stein, P.; Dickson, M. K.; Roundhill, D. M. J. Am. Chem. Soc. 1983, 105, 3489-3494.
- Che, C.-M.; Butler, L. G.; Gray, H. B.; Crooks, R. M.; Woodruff, W. H. J. Am. Chem. Soc. 1983, 105, 5492-5494.
- 77. Dallinger, R. F.; Miskowski, V. M.; Gray, H. B.; Woodruff, W. H. J. Am. Chem. Soc. 1981, 103, 1595-1596.
- 78. Brummer, J.G.; Crosby, G.A. Chem. Phys. Let. 1984, 112, 15-19.
- 79. Harvey, P.D.; Gray, H.B. J. Am. Chem. Soc. 1988, 110, 2145-2147.
- 80. Harvey, P.D.; Dallinger, R.F.; Woodruff, W.H.; Gray, H.B. *Inorg. Chem.* 1989, 28, 3057-3059.
- 81. Che, C.-M.; Lee, W.-M. J. Chem. Soc. Chem. Commun. 1986, 512-513.
- 82. Vlcek, A., Jr.; Gray, H. B. J. Am. Chem. Soc. 1987, 109, 286-287.
- 83. Harvey, P.D.; Gray, H. B. New Journal of Chem. 1987, 11, 595-596.
- 84. Che, C.-M.; Mak, T. C. W.; Miskowski, V. M.; Gray, H. B. J. Am. Chem. Soc. 1986, 108, 7840-7841.
- 85. Roundhill, D. M. J. Am. Chem. Soc. 1985, 107, 4354-4356.
- 86. Mann. K. R.; Lewis, N. S.; Miskowski, V. M.; Erwin, D. K.; Hammond, G.S.; Gray, H.B. J. Am. Chem. Soc. 1977, 99, 5525-5526.
- 87. Rice, S. F.; Miskowski, V. M.; Gray, H. B. *Inorg. Chem.* 1988, 27, 4704-4708.
- 88. Winkler, J. R.; Marshall, J. L. Natzel, T. L. Gray, H. B. J. Am. Chem. Soc. 1986, 108, 2263-2266.
- Fox, L. S.; Marshall, J. L.; Gray, H. B. J. Am. Chem. Soc. 1987, 109,
 6901-6902.

- 90. Che, C.-M.; Lee, W.-M.; Cho, K.-C. J. Am. Chem. Soc. 1988, 110, 5407-5411.
- 91. Harvey, E. L.; Stiegman, A. E.; Vlcek, A., Jr.; Gray, H. B. J. Am. Chem. Soc. 1987, 109, 5233-5235.
- 92. Bennett, M. A.; Patmore, D. J. Inorg. Chem. 1971, 10, 2387-2395
- 93. Nixon, J. F. J. Chem. Soc. A. 1968, 2689-2692.
- 94. Lucas, H. J.; Kennedym E. R. In Organic Syntheses; Horning, E. C., Ed.; John Wiely: New York, 1955; Vol 3, pp. 482-483.
- 95. Rempel, G. A.; Legzdine, P.; Smith, H.; Wilkinson, G. *Inorg. Syntheses*, **1972**, *13*, 90-91.
- 96. Herde, J. L.; Jenoff, C. V. Inorg. Nucl. Chem. Lett. 1971, 7, 1029-1031.
- 97. Brencic, J. V.; Cotton, F. A. Inorg. Chem. 1970, 9, 436-440.
- 98. Davison, A.; Holm, R. H. Inorg. Syntheses 1967, 10, 11-13.
- 99. Lanton, D.; Mason, R. J. Am. Chem. Soc. 1965, 87, 921.
- Best, S. A.; Smith, T. J.; Walton, R. A. Inorg. Chem. 1978, 17, 99-104.
- San Fillipo, J., Jr.; Sniadoch, H. J.; Grayson, R. L. Inorg. Chem.
 1974, 13, 2121-2130.
- Newsham, M. D.; Giannelis, E. P.; Pinnavaia, T. J.; Nocera, D. G.
 J. Am. Chem. Soc. 1988, 110, 3885-3891.
- Mussell, R. D.; Nocera, D. G. J. Am. Chem. Soc. 1988, 110, 2764-2772.
- 104. Frenz, B. A. In Computing in Crystallography; Schenk, H., Olthof-Hazelkamp, R., Vankonigsveld, H., Bassi, G. C., Eds; Delft University Press: Delft, Holland; 1978; pp. 64-71.

- Orpen, A. G.; Connelly, N. G. J. Chem. Soc., Chem. Commun.
 1985, 1310-1311.
- 106. Marynick, D. S. J. Am. Chem. Soc. 1984, 106, 4064-4065.
- Xiao, S.-X.; Trogler, W. C.; Ellis, D. E.; Berkovitch-Yellin, Z. J. Am.
 Chem. Soc. 1983, 105, 7033-7037.
- 108. Avanzino, S. C.; Chen, H.-W.; Donahue, C. J.; Jolly, W. L. *Inorg. Chem.* 1980, 19, 2201-2205.
- Corderman, R. R.; Beauchamp, J. L. Inorg. Chem. 1978, 17, 1585 1588.
- 110. Savariault, J.-M.; Serafini, A.; Pelissier, M., Cassoux, P. *Theor. Chim. Acta.* 1976, 42, 155-161.
- 111. Nixon, J. F. Adv. Inorg. Chem. Radiochem. 1985, 29, 41-141.
- 112. King, R. B. Acc. Chem. Res. 1980, 13, 243-248.
- 113. Newton, M. G.; Pantaleo, N. S.; King, R. B.; Lotz, T. J. J. Chem. Soc., Chem. Commun. 1978, 514-515.
- 114. Chaloyard, A.; El Murr, N.; King, R. B. J. Organometal. Chem.1980, 188, C13-C15.
- 115. King, R. B.; Gimeno, J. Inorg Chem. 1978, 17, 2390-2395.
- Newton, M. G.; King, R. B.; Chang, M.; Gimeno, J. J. Am. Chem.
 Soc. 1977, 99, 2802-2803.
- 117. Kruck, T.; Sylvester, G.; Kunau, I.-P. Angew. Chem., Int. Ed. Eng.1971, 10, 725.
- 118. (a) Halper, J. Acc. Chem. Res. 1982, 15, 238-244. (b) Connors, J. A.; Zaforani-Moattor, M. T.; Bickerton, J.; Saied, N. I.; Suradi, S. Carson, R.; Ghassan, A. T.; Skinner, H. A. Organometallics 1982, 1, 1166-1174.
- 119. Norton, J. R. Acc. Chem. Res. 1979, 12, 139-145.

- (a) Roberts, D. A.; Geoffroy, G. L. J. Organomet. Chem. 1981, 214,
 221-231. (b) Gree, M. A.; Haffman, J. C.; Caulton, K. G. J. Am.
 Chem. Soc. 1981, 103, 695-696.
- Mague, J. T.; Johnson, M. P. Lloyd, C. L. J. Am. Chem. Soc. 1989,
 111, 5012-5013.
- 122. McLafferty, F. W. In Interpretation of Mass Spectrum 3^{rd.} ed.University Science Books: Mill Vally, Calf. 1980, pp 17.
- 123. Watson, J, T. In *Introduction To Mass Spectrometry 2nd Ed.* Raven Press: New York, 1985.
- 124. (a) Sutherland, B. R.; Cowie, M. Inorg. Chem. 1984, 23, 1290-1297.(b) Cowie, M.; Dwight, S. K. Inorg. Chem. 1979, 18, 2700-2706.
- 125. Kubiak, C. P.; Eisenberg, R. J. Am. Chem. Soc. 1980, 102, 3637-3639.
- 126. Jenkins, J. A.; Ennett, J. P.; Cowie, M. Organometallics 1988, 7, 1845-1853.
- (a) Gibson, J. A. E.; Cowie, M. Organometallics 1984, 3, 984-996. (b)
 Cowie, M.; Dwight, S. K. Inorg. Chem. 1980, 19, 209-216.
- 128. Fair, J. P.; Olmstead, M. M.; Balch, A. L. *Inorg, Chem.* 1983, 22, 1229-1235 and references therein.
- 129. Gibson, J. A. E.; Cowie, M. Organometallics 1984, 3, 722-731.
- 130. Tortorelli, L. J.; Tucker, C. A.; Woods, C.; Bordner, *Inorg. Chem.*1986, 25, 3534-3537.
- 131. Boyar, E. R.; Robinson, S. D. Coord. Chem. Rev. 1983, 50, 109-208.
- 132. Felthouse, T. R. Prog. Inorg. Chem. 1982, 29, 73-166.
- 133. Cotton, F. A.; Walton, R. A. Multiple Bonds Between Metal Atoms; Wiley-Interscience: New York, 1982; Chapter 7.
- 134. Cotton, F. A.; Eagle, C. T.; Price, A. C. Inorg. Chem. 1988, 27, 4362-4368.

- 135. Balch, A. L.; Oram, D. E. J. Organomet. Chem. 1988, 349, 245-256.
- (a) Cowie, M.; Dickson, R. S. Inorg. Chem. 1981, 20, 2682-2688. (b)
 Cowie, M.; Dickson, R. S. Inorg. Chem. 1981, 20, 2682-2688. (c)
 Cowie. M. Inorg, Chem. 1979, 18, 286-292 and references therein.
- 137. King, R. B.; Chang, M.; Newton, M. G. J. Organomet. Chem. 1985, 296, 15-30.
- 138. Lever, A. B. P. Inorganic Electronic Spectroscopy; Elsevier: New York, 1984; Chapter 7.
- 139. Miskowski, V. M.; Gray, H. B. In *Understanding Molecular Properties*; Avery, J., Dahl, J. P., Hansen, A. E., Eds.; Reidel: Dordrecht, Holland; 1987.
- 140. (a) Che, C.-M.; Butler, L. G.; Grunthaner, P. J.; Gray, H. B. Inorg.
 Chem. 1985, 24, 4662-4665. (b) Miskowski, V. M; Smith, T. P.;
 Loehr, T. M.; Gray, H. B. J. Am. Chem. Soc. 1985,107, 7925-7934.
- Stiegman, A. E.; Miskowski, V. M. J. Am. Chem. Soc. 1988, 110, 4053-4054.
- 142. Harvey, P. D.; Butler, I. S.; de C. Barreto, M.; Coville, N. J.; Harris,G. W. *Inorg. Chem.* 1988, 27, 639-642.
- 143. Jackson, R. A.; Poë, A. Inorg. Chem. 1978, 17, 997-1003.
- 144. Wrighton, M. S.; Ginley, D. S. J. Am. Chem. Soc. 1975, 97, 2065-2072.
- 145. Albright, T. A.; Burdett, J. K.; Whangbo, M.-H. Orbital Interactions in Chemistry; Wiley-Interscience: New York, 1985; Chapters 15-19.
- 146. Geoffroy, G. L.; Wrighton, M. S. Organometallic Phototchemistry;
 Academic Press: New York, 1979.

- 147. Abrahamson, H. B.; Frazier, C. C.; Ginley, D. S.; Gray, H. B.; Lilienthal, J.; Tyler, D. R.; Wrighton, M. S. *Inorg. Chem.* 1977, 16, 1554-1556.
- 148. Levenson, R. A.; Gray, H. B. J. Am. Chem. Soc. 1975, 97, 6042-6047.
- 149. Ibers, J. A.; Snyder, R. G. Acta Cryst. 1962, 15, 923-930.
- Gall, D.; Garlaschelli, L.; Ciani, G.; Fumagalli, A.; Martinengo,S.; Sironi, A. J. Chem. Soc. Dalton Trans. 1984, 55-61.
- 151 Cecconi, F.; Ghilardi, C. A.; Midollini, S.; Orlandini, A.; Vacca, A.; Ramirez, J. A. Inorg. Chim. Acta. 1989, 155, 5-6
- 152. Brown, R. K.; Williams, J. M.; Sivak, A.J.; Muetterties, E. L. Inorg. Chem. 1980, 19, 370-374.
- 153. Balch, A. L. J. Am. Chem. Soc. 1976, 98, 8049-8054.
- Brady, R.; Flynn, B. R.; Geoffroy, G. L.; Gray, H.B.; Peone, J., Jr.;
 Vaska, L. *Inorg. Chem.* 1976, 15, 1485-1488.
- 155. Johnson, C.E.; Eisenberg, R.; Evans, T.R.; Burberry, M.S. J. Am. Chem. Soc. 1983, 105, 1795-1802.
- 156. Kubiak, C. P.; Eisenberg, R. Inorg. Chem. 1980, 19, 2726-2732.
- Balch, A. L.; Labakie, J. W.; Delker, G. Inorg, Chem. 1979, 18, 1224 1227.
- 158. Inga, M.; Kenney, S.; Kenney, J. W. III.; Crosby, G. A.; Organometallics. 1986, 5, 230-234.
- 159. Fordyce, W.A.; Crosby, G. A. J. Am. Chem. Soc. 1983, 104, 985-988.
- 160. Van Houten, J.; Watts, R. J. J. Am. Chem. Soc. 1976, 98, 4853-4858.
- 161. Persaud, L.; Langford, C. H.; Inorg. Chem. 1985, 24, 3562-3567.
- 162. Cotton, F. A.; Dunbar, K. R.; Verbruggen, M. G. J. Am. Chem. Soc. 1987, 109, 5498-5506.

- 163. Stiefel, E. T.; Bennett, L. E.; Dori, Z.; Crawford, T. H.; Sime, L.; Gray, H.B. *Inorg. Chem.* 1970, 9, 281-286.
- 164. Ueyaa, N.; Nakato, M.; Araki, T.; Nakamura, A.; Yamashita, S.;
 Yanashita, T. Chem. Lett. 1979, 421-424.
- Newton, W. E.; McDonald, J. W.; Yamanouchi, K.; Enemark, J. H.
 Inorg. Chem. 1979, 18, 1621-1626.
- Xin, X.; Morris, N. L.; Jameson, G. B.; Pope, M. T. Inorg. Chem.
 1985, 24, 3482-3485.
- 167. Hsieh, T.-C.; Gebreyes, K.; Zubieta, J. Transition Met. Chem. 1985, 10, 84-89.
- 168. Gelder, J. I.; Enemmark, J. H. Inorg. Chem. 1976, 15, 1839-1843.
- Clegg, W.; Christon, G.; Garner, C. D.; Sheldrick, G. M. Inorg.
 Chem. 1981, 20, 1562-1566.
- 170. Coucovanis, D.; Koo, S.-M. Inorg. Chem. 1989, 28, 2-5.
- 171. Mitchell, P. C. H. J. Inorg. Nucl. Chem. 1963, 25, 963-970.
- 172. Saha, H. K.; Halker, M. C. J. Inorg. Nucl. Chem. 1971, 33, 3719-3731.
- 173. Beck, J.; Hiller, W.; Schweda, E.; Strahle, J. Z. Naturforsch. 1984, 39b, 1110-1113.
- 174. Molybdenum Enzyme; Spiro, T. G., Ed.; Wiley: New York, 1985.
- 175. Pan, W.-H.; Chandler, T.; Enemark, J. H.; Stiefel, E. I. *Inorg. Chem.* 1984, 23, 4265-4269.
- 176. Newton, W. E.; Corbins, J. L.; Bravaid, D. C.; Searles, J. E.; McDonald, J. W. *Inorg. Chem.* 1974, 13, 1100-1104.

- 177. (a) Cotton, F. A.; Kalbacher, B. J. Inorg. Chem. 1976, 15, 522-524.
- (b) Bino, A.; Cotton, F. A. Angew. Chem., Int. Ed. Engl. 1979, 18, 332-334.
 (c) Bino, A. Cotton, F. A. J. Am. Chem. Soc. 1979, 101, 4150-4154.
- 178. Cotton, F. A.; Extine, M. W.; Niswander, R. H. *Inorg. Chem.* 1978, 17, 692-696.
- 179. Cotton, F. A.; Powell, G. L. J. Am. Chem. Soc. 1984, 106, 3371-3372.
- 180. Bereman, R. D.; Baird, D. M.; Moreland, C. G. Polyhedron 1983, 2, 59-61.

MICHIGAN STATE UNIV. LIBRARIES 31293006259406